

I. SYSTEMATIC EXAMINATION OF
THE AIR AT WINNIPEG FOR
NATURAL AND ARTIFICIAL
RADIOACTIVE MATERIALS

II. CONSTRUCTION AND TESTING OF A
SEMICIRCULAR β -RAY SPECTROGRAPH
FOR PHOTOGRAPHIC RECORDING

A Thesis In Two Parts
Presented To
The Faculty of Graduate Studies
University of Manitoba

In Partial Fulfillment
of the Requirements for the Degree
Master of Science

by
Walter Cram Patterson

October 1959



ABSTRACT

Part I of the thesis describes development of a new scintillation counter technique, permitting the simultaneous determination of concentrations of all three measurable components of airborne radioactivity. Details of the design and construction of mechanical and electronic apparatus involved are given, with emphasis upon automatic data-recording features. Data yields for the concentrations of airborne activities values of the order of 10^{-4} $\mu\mu\text{c}/\text{cc}$ of air for radium active deposit, and 10^{-6} $\mu\mu\text{c}/\text{cc}$ of air for thorium active deposit and for fallout. Daily and long-term variations of these concentrations are compared with related phenomena and possible correlations suggested.

Part II of the thesis describes the construction and calibration of a fixed-field semicircular β -ray spectrograph for photographic recording of the internal conversion spectra of γ -rays emitted by radionuclides. Design considerations and operational techniques are outlined. Alignment and calibration of the spectrograph, to permit measurements at high resolving power of electron momenta and conversion-line intensities using accepted values for Ir^{192} as a standard, are discussed in detail. Resolution of 0.4 per cent has been obtained.

PREFACE

The work herein described was performed at the University of Manitoba during 1958-59. Both projects were under the direction of Dr. R. D. Connor.

The author wishes to express his deep gratitude to Dr. Connor for his patient guidance, generous assistance, and unfailing encouragement; to Dr. Ian Fairweather for many helpful suggestions; to Thor Jacobson for lightening the burden of data analysis for Part I; to C. J. Kubin and John Schouten for their painstaking work in mechanical construction of apparatus for Part II; and to George Epp for service far beyond the call of duty. Thanks are also extended to Dr. F. Terentiuk and Dr. J. L. Wolfson for their helpful cooperation in regard to air sampling for Part I, to the staff of the Pure Chemistry section of the National Research Council for their hospitality and assistance in data analysis for Part II, and to the Dominion Public Weather Office at Winnipeg for preparation of meteorological data for Part I.

This work has been carried out with funds granted by the National Research Council, without which the studies could not have been undertaken. Their support is gratefully acknowledged.

TABLE OF CONTENTS

CHAPTER	PAGE
PART I	
I. INTRODUCTION	1
II. DESCRIPTION OF THE APPARATUS	4
Sampling Unit	4
Detector Head	6
Electronics	9
Print-Out Unit	10
Technical Problems and Solutions	12
III. DATA PROCESSING	15
IV. RESULTS AND TABULATION OF RELATED DATA	25
V. ANALYSIS OF DATA AND CONCLUSIONS	32
PART II	
I. INTRODUCTION	37
II. DESCRIPTION OF THE SPECTROGRAPH	43
Magnet	43
Vacuum Chamber and System	49
Source Assembly	52
Plate Holder and Assembly	56
III. OPERATION OF THE SPECTROGRAPH	62
Preparation of the Plate	62
Exposure of the Plate	63
Processing of the Plate	64
IV. CALIBRATION OF THE SPECTROGRAPH	65
Theoretical Background	65
Calibration Procedures	72

CHAPTER	PAGE
V. CONCLUSIONS	81
BIBLIOGRAPHY	83

LIST OF PLATES

PLATE	PAGE
I. Air sampler installation on the roof of the Science building, University of Manitoba	5
II. Filter-activity counter	7
III. Sample page of processed tape record	17
IV. Spectrograph front view	45
V. Spectrograph rear view	46
VI. End of vacuum box with access panel removed	51
VII. Source mounting plug	54
VIII. Plate holder components	59
IX. The four photographic plates analyzed	66

LIST OF FIGURES

FIGURE	PAGE
1. Cross-section of detector head of filter- activity counter	8
2. Characteristic form of decay curve for activity on filter sample	8
3. Danysz' design for an early β -ray spectrograph . .	39
4. Three elevations of spectrograph magnet	47
5. Three elevations of vacuum box	50
6. Source mounting, two elevations	55
7. Various views of plate holder	58
8. Microphotometer traces of conversion line and step function	67
9. Geometry of source-slit-plate arrangement	71
10. Calibration of the notches with respect to $H\alpha$. . .	73
11. Energy-sensitivity calibration curve for Ilfex film in the spectrograph	80

LIST OF TABLES

TABLE	PAGE
I. The Relations Between Filter Activity and Airborne Activity	23
II. Conversion Factors from Raw Data to Airborne Concentration	23
III. Key to Code for Meteorological Data	26
IV. Daily Data	27
V. Manufacturer's Specifications for Magnet	48
VI. Performance of the Spectrograph	74
VII. Energies and Momenta of Ir ¹⁹² Conversion Lines Used in This Work	76
VIII. Absolute Intensities of Ir ¹⁹² Conversion Lines Used in This Work	76
IX. Microphotometer Data	77
X. Consolidated Data	79

PART I

CHAPTER I

INTRODUCTION

In each of the three chains of natural radio-activity which descend from the long-lived parents U^{238} , U^{235} , and Th^{232} there occurs an isotope of an element with $Z=86$, which is gaseous at normal temperatures. Initially recorded in the radium series as radium emanation, it received the name radon. With the discovery of corresponding isotopes in the actinium and thorium series, this element received the more general symbol Em, for emanation. Isotopes Em^{222} , Em^{220} , and Em^{219} now bear the names radon, thoron, and actinon respectively.

Studies indicate the presence in soil of one part in 10^{12} of radium and varying amounts of thorium and actinium, from which evolve these three Em isotopes, which diffuse upward through the soil. Radon has a half-life of 3.8 days, thoron one of 54.5 seconds, and actinon one of 3.9 seconds; thus a radon atom has a much higher probability than a thoron or actinon atom of diffusing into the open air before decaying. Indeed actinon has not yet been successfully determined in the atmosphere.

The elements resulting from the decay of emanation are solids at normal temperatures, and so are adsorbed onto aerosols, primarily those with diameters 0.001 to 0.04 microns (W52). These solids, known as radium, thorium, and actinium active deposit respectively, are also of course

active; thus there is present in the air a distribution of radioactive particles having their origin in natural activity in the soil.

Since the first large-scale open-air fission of heavy elements began in 1945, a measurable amount of artificial activity in the form of β -active isotopes of the medium-mass elements has accumulated in the atmosphere. The long-lived man-made radioactive fission products thus generated have been christened "fallout" by the popular press. Thus a given volume of the atmosphere contains radioactive material of both natural and artificial origin, whose concentrations may vary with height, terrain, meteorological conditions, and the occurrence of recent nuclear weapons tests.

Previous investigators since the turn of the century concerned themselves with airborne radioactivity and related phenomena. They were confronted however with two interacting difficulties. If the active solids were to be removed from the air for analysis, the low specific activity of air necessitated the processing of large volumes to get usefully measurable amounts of radioactivity. However the short half-lives of the natural components meant that if time-consuming radiochemical separations were made, large initial amounts of these activities were required to compensate for decay during processing. This in turn called for large-scale processing of huge volumes of air.

This report describes development of a new technique for examination of airborne radioactivity, by means of which it is possible with apparatus of small dimensions to distinguish between and measure simultaneously the concentrations of radium active deposit, thorium active deposit, and fallout. Radioactive aerosols are collected on a small filter paper whose activity is then monitored in a scintillation counter and recorded continuously, giving a decay curve for the activity on the filter which can be analysed into three components identified by their half-lives as radium active deposit, thorium active deposit, and fallout, each of whose concentration in the air can then be calculated.

CHAPTER II

DESCRIPTION OF THE APPARATUS

I. SAMPLING UNIT

The unit used to obtain samples of airborne activity was initially installed at the University of Manitoba by the X-Rays and Nuclear Radiations Group of the National Research Council as part of Canada's contribution to the International Geophysical Year. The IGY Project was interested exclusively in monitoring long-lived activities remaining in measurable quantities on samples which were to be sent to Ottawa for processing. It was decided to attempt to measure the short-lived natural radioactivities also present initially, by a non-destructive technique in order to avoid interference with the Ottawa group's determinations. The form of the sample suggested the technique described herein.

Plate I shows the sampler installation on the roof of the Science building, at a height above ground level of approximately sixty-five feet. All data listed refers to air at this location. The sampler was a commercial unit, manufactured by the Staplex Co., New York, under the designation Type TF1A. It was essentially a vacuum cleaner assembly able to draw air at an average rate of about twenty cubic feet per minute through a five-inch filter supported on a wire grid mounted over its air intake. A

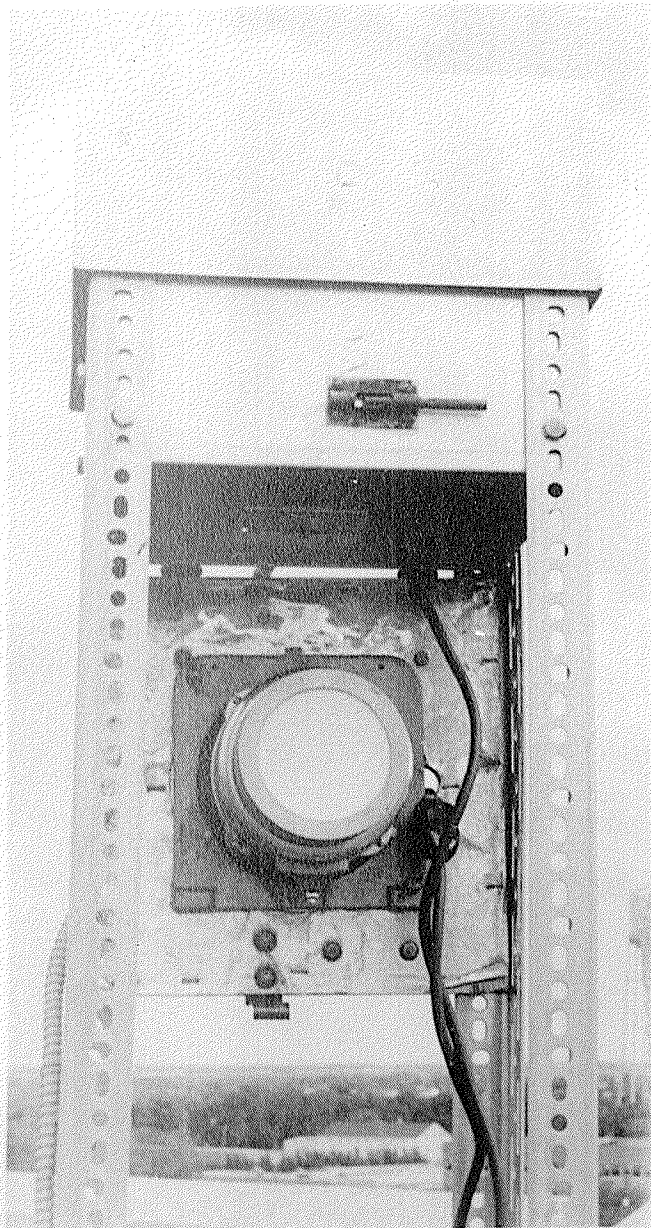


PLATE I

Air sampler installation on the roof of the Science building, University of Manitoba. In operation the hinged base supporting the sampler proper swings forward and upward through ninety degrees and is locked into place with the bolt visible just above center, completely enclosing the input end of the unit, shown here. Air enters through the narrow spaces around the housing into which the Dexion frame extends; this keeps rain, snow, and other macroscopic matter from depositing on the filter.

pitot gauge on the outlet side calibrated in cubic feet per minute monitored the instantaneous air flow rate.

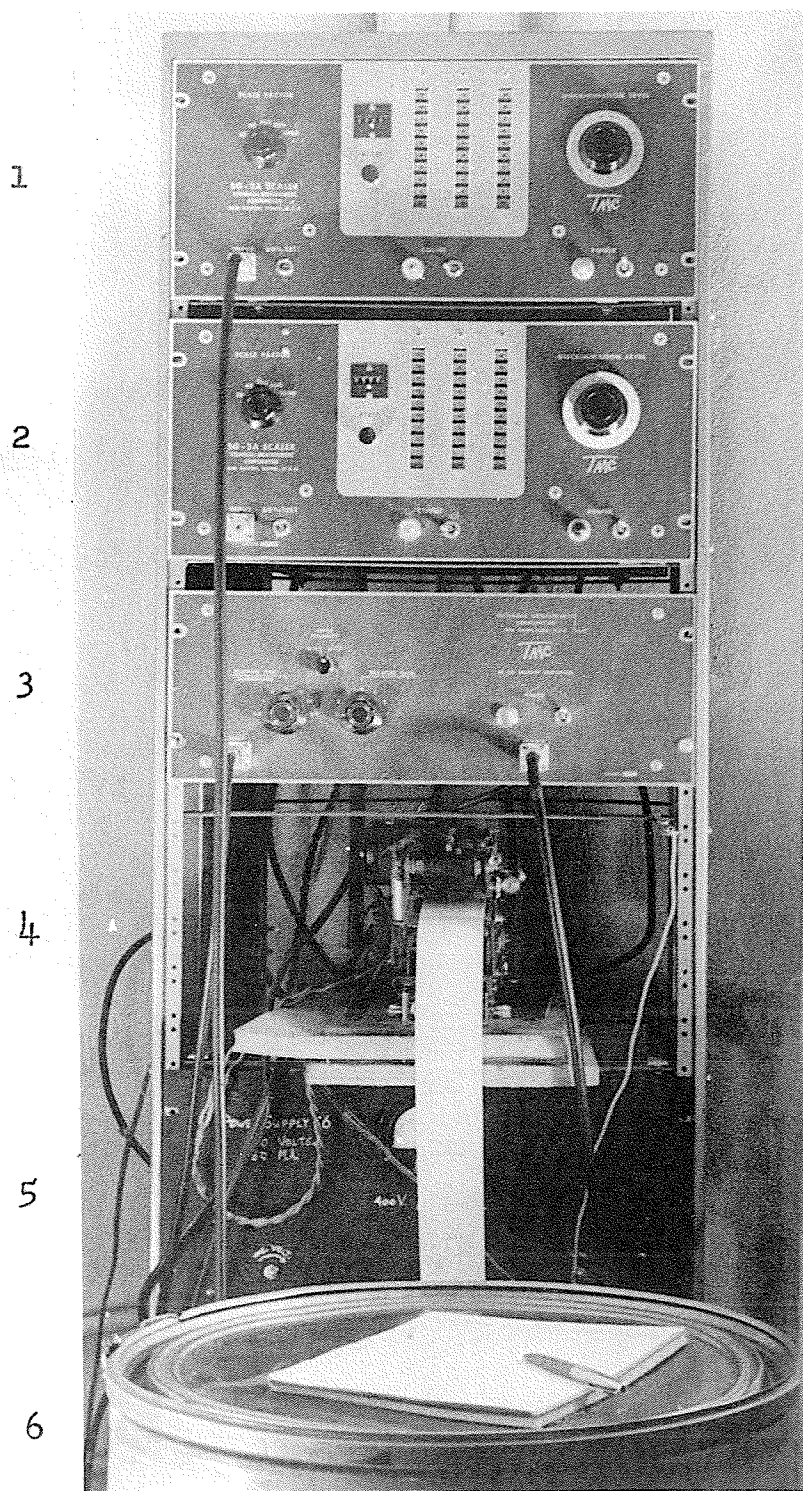
The filter used was manufactured by H. Reeve Angel and Co. Ltd., New York, designated Glass Fibre 934-AH, 10.5 cm. circle, and rated at better than ninety-eight per cent efficiency for aerosols in the activity-bearing size range.

In use, a clean filter was exposed for approximately twenty-four hours, removed in the early afternoon and inserted within three minutes of removal into the detector head of the filter-activity counter described below. The airflow rate at the beginning and end of exposure was recorded, to yield an average flow rate over the exposure. The time of beginning and end of an exposure was also noted; thus the total volume of air processed in a given run could be calculated.

II. DETECTOR HEAD

Fig. 1 shows a cross-section of the detector head of the filter-activity counter. It consisted of a 1/8" thick disc of polyvinyl toluene NE102 plastic scintillator optically coupled with Dow-Corning 10⁶ centistoke silicone fluid to the photocathode of a Dumont 6364 5" photomultiplier tube mounted in an upright position on a weighted cathode-follower base and enclosed in a large light-tight box (see Plate II).

PLATE II



Filter-activity counter: 1. first scaler; 2. second scaler; 3. amplifier; 4. printing timer (note record tape feeding out); 5. power supplies; 6. light-tight box containing detector head.

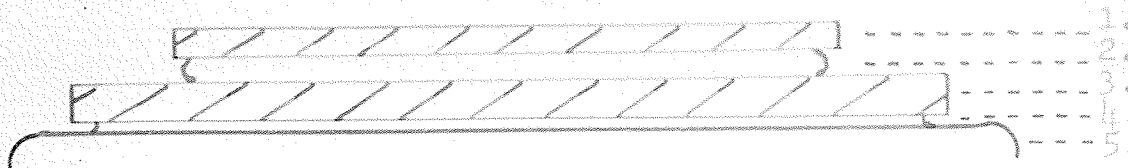


Fig. 1. Cross-section of detector head of filter-activity counter: 1. glass cover disc; 2. filter sample (active side down); 3. plastic scintillator disc; 4. silicone fluid bond; 5. photocathode of photomultiplier tube.

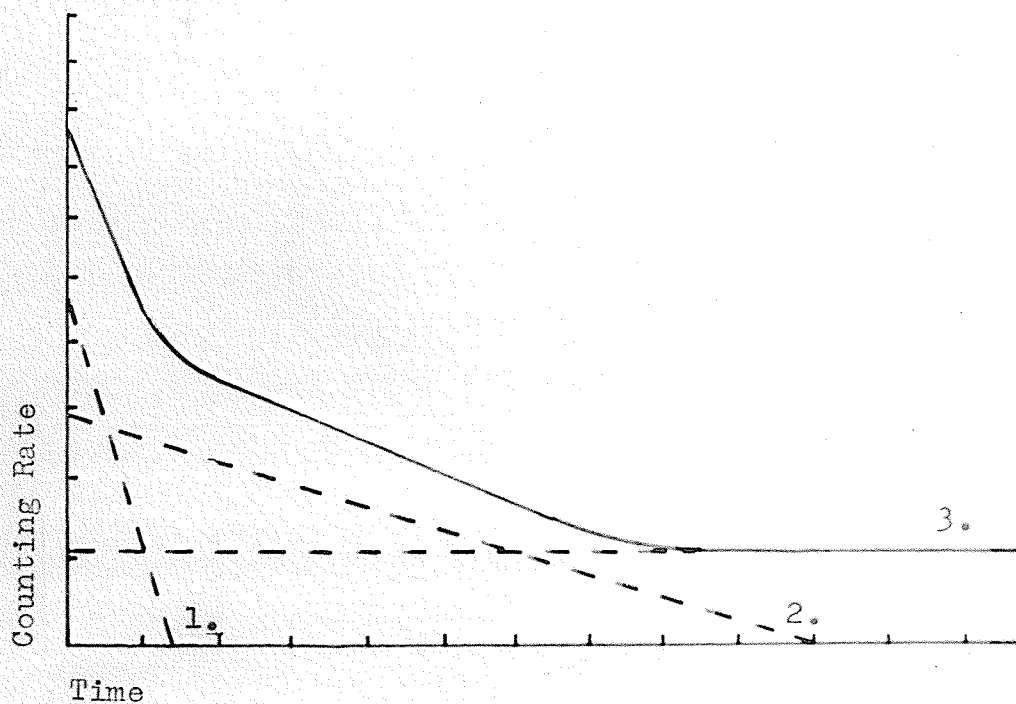


Fig. 2. Characteristic form of decay curve for activity on filter sample, shown here as a solid line and made up of three straight-line decay curves as indicated: 1. radium active deposit; 2. thorium active deposit; 3. long-lived activity ("fallout").

The filter sample was placed active side down on the scintillator disc and covered with a glass disc to ensure uniform positive contact. The box was closed and high tension (1150 volts) applied to the photomultiplier. The resulting pulses were fed through a standard cathode follower to standard electronic equipment described below.

Prior to each filter-count tests were run to measure background and system constants (gain and timer stability). The background counting rate was recorded with no sample on the scintillator but all other settings as usual. This background was later subtracted from the total measured counting rate to give the actual rate due to filter activity. A system gain test was run by placing a standard Cs¹³⁷ source in a prearranged geometry atop the scintillator and noting the resulting counting rate, which would show variations if system gain changed. The other test will be described below.

III. ELECTRONICS

Pulses from the cathode follower were fed to a standard pulse amplifier, Technical Measurements Corporation Model AL-2A, and thence to the input of a three-decade electronic scaler, TMC Model SG-3A. A selection switch made it possible to use one, two or all three neon decades before the mechanical register on the scaler. The pulse normally used to kick over the mechanical register was fed to the input of a second exactly similar scaler. The register pulse from this scaler was employed to close a

relay actuating the print-out unit described below. The use of two scalars in cascade thus permitted actuation of the print-out unit at any powers of ten counts received, from one hundred to one million, to suit the counting rate from the detector. Plate II shows the scalars, the amplifier, and the print-out unit as arrayed for operation. Bias levels were set high enough to exclude almost all spurious counts, the high gain of the amplifier permitting this without undue discrimination against actual counts.

III. PRINT-OUT UNIT

A feature of the technique that called for considerable thought was the means of recording data and the final form in which it would be produced for processing and storage. After several avenues were explored and discarded it was decided to employ a commercial printing timer, Simplex Model WDG-28 CPR.

In this unit the chronometer is an AC motor, which by a ratchet assembly drives a row of coaxial discs with raised numerals on their circumferences, similar to a common odometer but actuated in steps of one hundredth of a minute. When a solenoid circuit is closed, a rubber hammer moving upward forces a strip of paper tape against an inked ribbon, and so against the odometer numerals, leaving on the tape the imprint of the time setting of the odometer at the instant of actuation of the solenoid. For the purpose of this present application, leads from this "print" circuit

of the timer were run to a heavy-duty relay actuated by the register pulse from the second scaler, as referred to in section III above. Thus at the instant the mechanical register of the second scaler would normally have kicked over, the "print" circuit was closed and the time recorded.

In use, the timer was started from zero at the instant the count was begun. With for example four decades lit the ten-thousandth pulse tripped the timer which stamped the time per ten thousand pulses on the paper tape. The filter activity was counted thus for forty-eight (later twenty-four) hours, giving a record of the filter's activity in the form of a succession of times stamped on a paper tape (see Plate II). Subtraction of each time from the following gave a series of time increments, each of whose reciprocal times the appropriate power of ten represented the average counting rate in the corresponding time interval. This counting rate was related by a constant factor to the average activity of the filter in the time interval; the filter-activity counter thus monitored the decay of the activity on the filter.

As a test of the timer, the sixty-cycle test input of the first scaler was used to provide a constant pulse rate. With this pulse generator the time interval taken to record ten thousand pulses is 2.77 minutes. Any recorded departure from this interval served to pinpoint timer trouble.

V. TECHNICAL PROBLEMS AND SOLUTIONS

At one time or another every stage and unit in the counter presented problems. At this point it seems appropriate to discuss their occurrence and solutions, with reference to the previous sections of this chapter.

It is felt that specific reference to troubles arising merely from flaws in apparatus employed in this investigation can be confined to mention of potential trouble spots; their elimination is in most cases obvious. It was necessary to guard against high voltage shorting in the dynode resistor chain, ungrounded cable shields, loss of emission in electron tubes (especially important for comparison of data over many months when the installation has a twenty-four-hour per day duty cycle), and microphonics in input stages (because of the mechanical jar from the timer punch). Problems peculiar to this type of experimental array will now be discussed in detail.

The first difficulty arose at an early stage when it was attempted to use a shallow clear dish of liquid scintillator as the primary detector, placing the filter disc in this dish which was in the position in the detector head later occupied by the plastic scintillator. The liquid scintillator was replaced by the plastic disc when it was found impossible to get consistent and reasonable results because of the uncertain dependence of the liquid's efficiency on moisture, temperature, optical clouding et cetera. The

plastic substitute proved a most satisfactory replacement, fulfilling experimental requirements with unexpected simplicity and reproducibility.

It was found necessary to avoid as much as possible exposing the photocathode of the photomultiplier to light. After such exposure, even to the low level of illumination provided by the pilot lights and heaters of the electronic equipment, the resulting photoelectric excitation of the photocathode contributed many spurious pulses to the count immediately following. This threatened distortion of the beginning of a filter-count decay curve, immediately prior to which the light-tight box had of course to be opened. The filter-counter was therefore installed in a small closet; the closet light was turned off and an opaque plastic sheet was used to cover the relay rack during any interval when the light-tight box was open.

A baffling problem arose at one stage, when apparent jumps in counting rate began to occur. It was then fortuitously noted that on the instant the timer punched, the first decade on the second scaler frequently recorded up to five "counts" (usually of course as the "thousands" digit for a given count), which resulted in a much too short interval before the following punch, i. e. a "jump" in counting rate. The input bias was raised to fifteen volts, and this seemed successful in excluding what was apparently radiative pickup from the hot spark at the mains relay actuating the timer punch.

The timer itself gave more trouble than all other units. The general standard of workmanship in its construction was disappointing, and electrical and mechanical difficulties occurred repeatedly. There is little point in cataloguing them, since almost every subassembly in the unit developed malfunctions. At length it became possible to expect no further trouble, principally because all these subassemblies had been serviced and their weaknesses minimized.

CHAPTER III

DATA PROCESSING

A given filter sample produced a tape record of i a short sixty-cycle test; ii a sensitivity or system gain test; iii a background test; iv the activity-count proper. The further processing of this data will now be described, with reference to Plate III.

Tests i and ii did not call for further processing, merely for comparison to see that the time sequence in each case was approximately the same as that of previous runs. Test iii was processed in the same fashion as the activity-count proper, as the following example demonstrates.

Plate III shows a sample page of processed tape. Each stamped time was subtracted from the one following, yielding the series of time intervals that are listed in the second column here. The tape shown was produced with a total of four decades on the two scalars lit; each time interval therefore represented the time in minutes per ten thousand counts. Inverting this relation by taking reciprocals and multiplying by ten thousand gave the number of counts per minute. These average counting rates are listed in the third column.

However, they include as well as genuine counts from filter activity also those from background. When therefore the above procedure had been carried out on the

background test record (iii) to yield an average background counting rate (constant within a few per cent) this background counting rate was subtracted from the total to yield a series of figures dependent only on filter activity, the fourth column in Plate III.

Since the average counting rate thus obtained referred to an interval between two punched times it seemed reasonable to assign it to the midpoint of the interval; (it was always arranged that intervals be much smaller than the half-lives of the activities being measured). These midpoints were listed in the fifth column for convenience. The data in this form was then transferred to a graph in the form of a long semilog grid with abscissa a linear time axis and ordinate a logarithmic activity axis. The resulting activity curve qualitatively resembled Fig. 2.

As indicated in the figure, the long-lived tail was produced to $t=0$ and subtracted from the remaining activity. The straight tail of this new curve was then produced to $t=0$ and subtracted, leaving one more curve which also appeared straight. In order, the three straight-line curves represented the long-lived component of activity on the filter, the thorium active deposit, and the radium active deposit. (The latter two could be identified by their half-lives.) The $t=0$ intercepts of these three curves gave the counting rate due to each component at the instant the count was begun. Since this time was usually about three minutes after removal of the filter from the sampler, the

PLATE III

0.5000	30.68	3240	2820	614	
0.5000	29.95	3340	2900	581	
0.5000	29.12	3440	3000	554	
0.5000	28.49	3500	3060	525	
0.5000	28.02	3560	3120	497	
0.5000	27.30	3660	3220	469	
0.48805	26.81	3720	3280	442	
0.42302	26.33	3800	3360	416	
0.40274	25.66	3890	3450	390	
0.37703	25.04	4000	3560	367	
0.35204	24.66	4060	3620	340	
0.32739	24.15	4140	3700	315	
0.30323	23.61	4240	3800	291	
0.27852	23.26	4300	3860	268	
0.25530	22.60	4420	3980	245	
0.23275	22.26	4490	4050	223	
0.21111	21.81	4580	4140	201	
0.1	1	2	3	4	5

Sample page of processed tape record: 1. strip of tape; 2. differences between successive punched times; 3. total average counting rates corresponding to time intervals; 4. average counting rates with background subtracted; 5. times in minutes after $t = 0$, corresponding to mid-points of intervals, at which average counting rates are to be plotted.

curve for the short-half-life radium active deposit had to be produced to a point three minutes before $t=0$ to give its initial activity on the filter; the decay of the other two components during this interval could be considered negligible. These initial counting rates could now be related to airborne concentrations of the components.

It would be well at this point to observe that a considerable improvement in statistical quality of results took place after changeover to the amplifier specified, in midMay 1959. A major breakdown at this time resulted in several changes and replacements; all descriptions are of the new, more satisfactory equipment. Results prior to this changeover are also listed, but though calibration tests gave the same results with the chosen settings on the new equipment comparison of the old and new data must be made with caution.

Further, the quality of decay curves given by the new equipment was so high as to permit twenty-four-hour counts. Forty-eight-hour counts had been taken to allow the natural components to die away, leaving a flat long-lived tail which could be extrapolated to $t=0$. Now, however, it became possible to find the long-lived constant counting rate arithmetically, without plotting, by applying the definition of half-life to the thorium active deposit region. Two points from this region, total counting rates C_1 and C_2 at times 10.6 hours apart, were taken; a long-lived counting rate X was assumed. Since $C_1 - X$ was the thorium active

deposit counting rate at time t_1 and $C_2 - X$ that 10.6 hours or one half-life later,

$$2 \cdot (C_2 - X) = C_1 - X$$

or
$$X = 2C_2 - C_1$$

allowing arithmetical determination of X . This value could then be subtracted from the total filter-activity counting-rate points before plotting, speeding up data processing considerably.

When initial counting rates from the filter sample due to each of the three components had been determined, the final step was to relate these counting rates to airborne concentrations of the components over the time interval of sampling. The differential equation for a single airborne activity being collected on a filter is

$$\frac{dN}{dt} = n - \lambda N$$

where N is the number of active atoms on the filter, n the number of active atoms in the volume of air processed per second, and λ the decay constant of the activity. Therefore

$$\frac{dN}{n - \lambda N} = dt$$

and integrating gives

$$-\frac{1}{\lambda} \ln (n - \lambda N) = t + c$$

c a constant. At $t=0$ $N=0$ and therefore

$$c = -\frac{1}{\lambda} \ln n$$

With this substitution the equation becomes

$$\ln \left(\frac{n}{n - \lambda N} \right) = \lambda t \quad \text{or} \quad n - \lambda N = n e^{-\lambda t}$$

Eventually

$$\frac{n}{N} = \frac{\lambda}{1 - e^{-\lambda t}}$$

For λ very small, i. e. activity long-lived, expansion of the exponential leads to $n = N/t$ as might be expected. Also, for λ large, $e^{-\lambda t}$ vanishes after a reasonable time and $n = \lambda N$. The activity in the volume of air processed per second is λn . These considerations give the three equations used here to relate filter activity to airborne activity. The equations are listed in Table I.

These relations make it possible to deduce airborne concentrations of the three components from their activities as collected on a filter. But before this deduction can be made it is necessary to know the relation between the filter activity (see Table I) and the counting rate which this activity produces in the filter-counter. The detector geometry of 2π meant that only one-half of the emitted particles struck the detector, introducing a factor of two. More difficult to determine however, was the overall detection efficiency apart from the geometric factor. It was necessary to estimate what fraction of the total number of particles emitted from the sample and striking the scintillator actually appeared as counts in the final record.

By the time the active filter was placed in the counter it was reasonable to assume that the RaA and the ThA would rapidly become negligible because of their short half-lives. Hence the natural components would consist of

the $B \rightarrow C + C'$ or $B \rightarrow C + C''$ chains, in each of which one α and two β 's are emitted before the nucleus arrives at a relatively stable state. Thus one radon or thoron atom initially present in the sampled air would give rise to three theoretically detectable particles plus a certain number of conversion electrons. In practice, experimental conditions, in particular the input bias, impose a lower limit on the energy of particles detectable; this lower limit had here to be determined to estimate the fraction of the total number of emitted particles lost.

Nuclear Enterprises' NE102 plastic scintillator has an efficiency of approximately one hundred per cent for β 's above 0.025 Mev, and the response of the scintillator increases linearly with energy for such β 's. A 6-Mev α -particle produces the same pulse height in NE102 as a 0.025 Mev β -particle. With reference to this information, a filter was treated with a drop of solution containing C^{14} , a pure β -emitter with end-point 0.158 Mev, allowed to dry, and placed in the detector head of the counter. The resulting counting rate was determined as a function of the bias setting on the first scaler, after subtraction of background at each bias setting. Extrapolation of the resulting curve allowed identification of the cut-off bias with the end-point of the C^{14} spectrum, establishing an approximately linear energy-bias correspondence. With the working bias used it was determined that all β 's above 0.040 Mev were recorded. In the β -spectrum of thorium active deposit according to Flammersfeld (F39) about ninety per cent of the total continuum lies above 0.040 Mev.

No radium active deposit spectrum was readily available in the literature, but the similarity of the decays suggested the assumption of the same figures for both radium and thorium active deposits, i.e. about 1.8 recorded β -particles per radon or thoron parent. Since the α 's from the natural C' daughters are greater than 6 Mev they were recorded one hundred per cent. Interposition of a 1/4" Perspex disc between filter and scintillator discs, thereby intercepting all but a very few of the highest energy β 's and all the α 's, reduced the recorded counting rate to less than one per cent of its original value. The γ contribution to the recorded counting rate was therefore negligible, because of the low stopping power of the thin detector.

It was noted that in the radium active deposit could be expected a total conversion electron intensity of about 0.15 electrons per parent, and in the thorium active deposit one of 0.35 (since the 0.024 Mev A-line was not detected). Thus each radon parent gave rise to $1.8 + 1 + 0.15 = 2.95$ detected particles, and each thoron parent $1.8 + 1 + 0.35 = 3.15$ detected particles. Consequently to get the radon and thoron concentrations in the sampled air it was necessary to divide the recorded counting rate by the corresponding correction factor as derived here.

Because of its uncertain composition the long-lived activity had to be considered purely on the basis of one emitted particle per initial atom, and no correction for chain decay was made to arrive at a figure for airborne concentration of this activity.

TABLE I

THE RELATIONS BETWEEN FILTER ACTIVITY AND AIRBORNE ACTIVITY

Component	n	λn	Airborne Activity
radium active deposit	λN	$\lambda(\lambda N)$	$\lambda(\text{filter activity})$
thorium active deposit	$\frac{\lambda N}{1 - e^{-\lambda t}}$	$\frac{\lambda(\lambda N)}{1 - e^{-\lambda t}}$	$\frac{\lambda(\text{filter activity})}{1 - e^{-\lambda t}}$
long-lived activity	$\frac{N}{t}$	$\frac{(\lambda N)}{t}$	$\frac{1}{t}(\text{filter activity})$

TABLE II

CONVERSION FACTORS FROM RAW DATA TO AIRBORNE CONCENTRATION

Component	$\lambda \text{ sec.}^{-1}$	f	Conversion Factor $\frac{2Cab(X)}{fR}$
radium active deposit	3.8×10^{-4}	2.95	$2.45 \times 10^{-7} \left(\frac{X}{R}\right) \mu\mu \text{ curies/cm}^3$
thorium active deposit	1.8×10^{-5}	3.15	$1.39 \times 10^{-8} \left(\frac{X}{R}\right) \mu\mu \text{ curies/cm}^3$
long-lived activity	-	1	$2.21 \times 10^{-8} \left(\frac{X}{R}\right) \mu\mu \text{ curies/cm}^3$

C--proportionality constant from Table I

f--factor correcting for chain decay

a--conversion factor from disintegrations/minute to $\mu\mu$ curies

b--conversion factor from cubic feet/minute to $\text{cm}^3/\text{second}$

X--recorded initial counting rate in counts/minute

R--average airflow during sampling, in cubic feet/minute

t--(see Table I above) time of sampling in seconds

With these considerations it followed that the activity on the filter was twice the recorded initial counting rate divided by the chain-decay factor for each component. Using the appropriate λ 's and these values for filter activity in the relations listed in Table I, the proportionality constants listed in Table II were derived, by which it was possible to convert from counting rate to airborne concentration in one multiplicative step. The concentration, so far derived in terms of the volume processed per second, was divided by this volume to give the concentration as activity per unit volume. Using the definition of the curie as 3.7×10^{10} disintegrations per second, the final constants in Table II include a factor to make the airborne concentrations appear as micromicro-curies per cubic centimeter of air. It should here be emphasized that the above procedure yields the actual airborne concentrations of the gaseous thoron and radon activities (not of their solid daughter products), under the assumption that the gaseous parent and the solid daughter products are in radioactive equilibrium.

CHAPTER IV

RESULTS AND TABULATION OF RELATED DATA

The following pages are a tabulation of figures obtained by analysis of data as described in Chapter III. As well as giving the concentrations of the three components of airborne activity for each day listed, the table includes a coded breakdown of meteorological conditions prevailing during the time of sampling. This latter data was prepared by the Basic Weather section of the Dominion Public Weather Office at Winnipeg International Airport. The key to the code is given in Table III which reproduces the salient part of the report form filled in by the Weather Office.

The asterisks in May indicate the major overhaul mentioned in Chapter II, after which the data became much more satisfactory. (Errors will be discussed below.) From this point F, T, and R will be used to designate the components due to long-lived activity, thorium active deposit, and radium active deposit respectively. The figures in columns F and T are given in 10^{-6} micromicrocuries per cubic centimeter of air, and those in column R in 10^{-4} micromicrocuries per cubic centimeter of air. The dates listed are those on which sampling began and ended, in each case shortly after noon local time. Note occasional 48-hour samples, with the corresponding double weather reports. "Neg." implies a negligible amount of the component in the period, "uctn." an amount not necessarily negligible but of uncertain magnitude.

TABLE III

KEY TO CODE FOR METEOROLOGICAL DATA

A. WEATHER TYPE	B. PRECIPITATION	C. TIME (GCT) OF PRECIPITATION	D. WIND DIRECTION	E. WIND SPEED	
				Description	Miles/hr
0. Clear	1. None	1. 1230 to 1830	05. NE	0. Calm	0 - 1
1. Partly cloudy	2. Trace	2. 1830 to 0030	09. E	1. Light Air	1 - 3
2. Cloudy	3. .01" - .03"	3. 0030 to 0630	14. SE	2. Light Breeze	4 - 7
3. { Dust-storm Blowing snow	4. .04" - .10"	4. 0630 to 1230	18. S	3. Gentle Breeze	8 - 12
	5. .11" - .30"		23. SW	4. Moderate Breeze	13-18
4. Fog, smoke, haze	6. .31" - 1.00"		27. W	5. Fresh Breeze	19-24
5. Drizzle	7. 1.01" - 3.00"		32. NW	6. Strong Breeze	25-31
6. Rain	8. 3.01" - 5.00"		36. N	7. Moderate Gale	32-38
7. { Snow Rain & snow	9. 5.01" or over		99. Variable	8. Fresh Gale	39-46
				9. Strong Gale	47-54
8. Showers				10. Whole Gale	55-63
9. Thunder-storm					

TABLE IV
DAILY DATA

DATES	AIRBORNE CONCENTRATIONS			METEOROLOGICAL DATA				
	F	T	R	A	B	C	D	E
Dec. 14-15	1.37	.115	.593	7	2	12	18	4
Dec. 16-17	1.23	.110	1.42	7	4	1234	18	3
Dec. 24-25	1.67	.462	4.28	3	2	4	18	4
Dec. 26-27	2.12	.389	1.52	7	2	234	36	3
Dec. 28-29	2.47	.240	4.13	7	2	4	36	5
Dec. 30-31	2.57	1.00	5.20	1	1	-	18	4
Jan. 1-2	2.17	.136	.684	7	4	2	32	6
Jan. 3-4	3.44	neg.	3.82	1	1	-	99	4
Jan. 5-6	2.92	neg.	1.54	2	2	4	14	4
Jan. 7-8	2.65	.117	1.18	1	2	134	99	3
Jan. 9-10	3.30	neg.	.876	2	1	-	14	4
Jan. 11-12	2.54	.324	1.84	7	2	2	18	5
Jan. 13-14	4.01	neg.	1.37	7	2	134	32	4
Jan. 15-16	3.09	neg.	1.62	7	2	3	32	3
Jan. 18-19	4.68	neg.	1.69	1	1	-	27	4
Jan. 20-21	3.77	.405	2.76	7	2	4	27	3
Jan. 22-23	2.30	neg.	2.35	1	2	1	32	5
Feb. 4-5	5.14	uctn.	.604	7	3	13	99	3
Feb. 6-7	5.27	neg.	1.00	1	1	-	32	3
Feb. 8-9	5.33	uctn.	4.91	1	4	23	18	3
Feb. 10-11	3.74	.935	1.76	4	1	-	18	5
Feb. 12-13	4.07	neg.	3.87	1	1	-	32	4
Feb. 14-15	5.00	neg.	3.40	2	1	-	18	6

Feb. 16-17	3.13	neg.	1.34	2	1	-	32	3
Feb. 18-19	2.80	neg.	5.87	4	1	-	27	3
Feb. 20-21	5.86	neg.	5.63	0	1	-	27	3
Feb. 22-23	4.10	uctn.	2.45	1	1	-	32	2
Feb. 24-25*	4.8	.302	4.48	7	4	1	18	4
Feb. 26-27	4.31	uctn.	2.45	7	4	124	18	3
Feb.28-Mar.1	1.93	neg.	2.76	1	1	-	18	4
Mar. 2-3	2.41	uctn.	.534	1	3	3	36	4
Mar. 4-5	.902	neg.	.850	2	2	1	18	3
Mar. 6-7	3.27	neg.	.756	7	3	34	18	2
Mar. 8-9	2.39	uctn.	2.06	7	4	1234	18	3
Mar. 10-11	2.11	uctn.	.970	7	5	4	99	3
Mar. 14-15	1.44	uctn.	.448	0	1	-	32	4
Mar. 16-17*	2.5	neg.	.80	1	1	-	18	4
Mar. 24-25	2.49	.606	2.51	2	1	-	23	3
Mar. 26-27	2.84	neg.	1.97	4	1	-	99	2
Mar. 28-29	4.89	.293	2.45	2	1	-	18	5
Mar. 30-31	2.67	uctn.	.513	6	5	2	36	4
Apr. 1-2	1.41	.600	1.45	7	2	124	99	2
Apr. 3-4	2.49	1.29	1.02	7	1	-	99	6
Apr. 8-9*	4.4	neg.	.13	2	1	-	36	3
Apr. 14-15*	5.2	uctn.	.50	2	1	-	32	5
Apr. 18-19	5.57	2.84	uctn.	0	1	-	99	2
Apr. 20-21	5.32	3.63	.600	1	1	-	27	4
		*	*	*				
May 13-14	4.03	.592	uctn.	1	2	2	36	5
May 15-16	4.43	4.35	.209	1	1	-	99	3

May 17-18	2.44	2.10	.225	8	4	234	99	3
May 19-20	1.97	1.86	.0719	1	1	-	36	2
May 21-22	2.02	1.73	.0777	1	1	-	99	3
May 23-24	4.89	4.91	.867	1	1	-	23	5
May 25-26	.422	.618	.0914	6	6	14	36	5
May 27-28	.717	.194	.208	6	6	134	05	3
May 29-30	2.46	1.05	.131	1	1	-	36	3
May 31 -June1	2.68	3.67	.666	6	2	3	32	2
June 2-3	2.62	1.54	.433	1	1	-	99	4
June 4-5	2.39	3.72	.372	1	1	-	36	4
June 6-7	1.91	3.83	1.66	6	6	1234	99	2
June 8-9	2.34	7.77	.908	6	2	3	99	2
June 10-11	2.30	2.29	.547	6	3	2	18	4
June 13-14	1.84	3.09	.694	1	1	-	18	3
June 16-17	2.91	5.41	.575	6	2	12	14	4
June 19-20	1.22	7.49	.129	6	2	1	32	4
June 20-21	1.11	3.89	.116	6	4	2	36	3
June 21-22	1.67	5.00	.0871	6	1	-	99	4
June 22-23	4.42	6.67	1.54	6	1	-	36	3
June 23-24	2.97	5.24	.308	6	2	123	18	2
June 24-25	1.76	6.66	.702	1	1	-	18	2
June 25-26	1.52	5.64	.686	2	1	-	18	2
June 26-27	.835	2.01	.750	9	6	24	14	4
June 27-28	.123	2.16	.0899	5	2	1	23	4
June 28-29	.675	2.16	.238	8	3	3	32	5
June 29-30	2.02	6.18	.294	6	2	2	23	3
June 30 -July1	1.66	6.26	.599	8	2	4	23	5

July 1-2	1.58	10.5	.630	8	3	2	14	3
July 2-3	1.64	7.31	2.52	6	4	1	18	3
July 3-4	1.96	2.86	1.10	6	5	4	36	4
July 4-5	1.23	.633	.015	9	6	2	36	8
July 5-6	1.77	3.34	.419	2	1	-	18	3
July 6-7	1.14	2.30	.896	9	4	12	18	5
July 7-8	1.43	4.09	.865	9	4	3	27	4
July 8-9	1.47	2.01	.354	9	6	2	27	4
July 9-10	1.30	4.41	.0112	1	1	-	32	5
July 10-11	.729	4.30	.406	8	3	2	32	4
July 12-13	1.02	5.35	.464	0	1	-	99	3
July 13-14	.973	4.44	2.03	9	4	34	18	5
July 14-16	.598	5.35	2.24	9/1	6/1	2/-	18/18	4/2
July 16-17	.736	3.37	.30	1	1	-	36	4
July 17-18	.368	7.11	.231	1	1	-	99	3
July 18-19	.837	8.28	.411	1	1	-	32	3
July 19-20	.931	3.86	.722	8	4	4	23	4
July 20-21	.431	3.05	.323	1	1	-	99	2
July 21-22	.497	1.46	.355	8	6	34	99	2
July 22-23	.465	1.57	.290	8	4	12	32	2
July 23-25	.357	3.95	1.39	14/1	1/1	-/-	32/18	2/3
July 25-26	.636	4.18	.723	48	4	23	18	2
July 26-27	.598	4.28	1.43	1	1	-	18	3
July 27-28	.650	6.13	1.80	9	2	234	18	2
July 28-29	.615	3.48	.518	8	2	24	99	4
July 29-30	.598	7.13	.371	0	1	-	27	3
July 30-31	.442	5.35	.245	1	1	-	99	3

July 31-Aug. 1	.774	3.40	.356	1	1	-	99	3
Aug. 1-2	.640	4.91	1.74	1	1	-	18	3
Aug. 2-4	.345	6.67	.598	8/1	5/1	3/-	18/99	3/2
Aug. 4-5	.390	5.64	2.38	8	2	4	18	3
Aug. 5-6	.316	1.26	.280	9	4	3	36	3
Aug. 6-7	.216	3.86	.263	1	1	-	99	3
Aug. 7-8	.225	4.93	.406	1	1	-	18	3
Aug. 8-9	.385	3.49	.858	1	3	34	18	4
Aug. 9-10	.454	3.07	.402	9	6	1	99	2
Aug. 10-11	.447	3.68	.774	8	3	34	18	4
Aug. 11-12	.221	1.15	.282	1	1	-	32	4
Aug. 12-13	.291	6.96	.774	6	3	4	99	2
Aug. 13-14	.163	3.30	.645	6	5	12	27	3
Aug. 14-15	.794	6.84	.817	1	1	-	99	4
Aug. 15-16	.349	2.12	1.16	9	5	34	18	5
Aug. 16-17	.277	1.30	.459	8	2	12	32	3
Aug. 17-18	.854	2.73	1.46	9	2	4	14	3
Aug. 18-19	.109	1.14	.466	8	2	1	05	3
Aug. 19-20	uctn.	.373	.307	9	6	234	05	4
Aug. 20-21	.130	.552	.288	4	1	-	05	2
Aug. 21-22	.099	.644	.672	9	5	34	14	3
Aug. 22-23	.0804	.295	.519	9	7	23	23	3
Aug. 23-24	.172	1.08	.388	0	1	-	27	3
Aug. 24-25	.136	.757	.347	8	2	3	18	3
Aug. 25-26	.100	1.85	.408	0	1	-	23	3
Aug. 26-27	.102	.621	.756	9	5	4	18	5
Aug. 27-28	.104	2.56	.882	4	1	-	99	2
Aug. 28-29	.100	.948	.557	9	2	4	99	4

CHAPTER V

ANALYSIS OF DATA AND CONCLUSIONS

In Table IV three significant figures are given for almost all days. (Starred days indicate instrumental or other difficulties widening the error limits indefinitely for these days. However they are included for completeness.) The comments to follow refer to Table IV and histograms included at the thesis' end. A sample of the semilog plot used to arrive at the initial counting rates for the F, T, and R components will be found at the back of this thesis.

Two experimental values, X and R in Table II, establish the error limits on the final figures for airborne concentration. The initial counting rates X can usually be determined to better than two significant figures, about three per cent. The pitot gauge measuring airflow rate could be read with fair certainty only to about one cubic foot per minute in about twenty-five, or about four per cent. Other errors are negligible compared to these, and the total percentage error in an average concentration obtained by this technique is of the order of seven per cent.

Perhaps the most obvious feature of all three components is the large day-to-day variation they exhibit. The immediate suggestion is that this variation is at least partially the result of local meteorological conditions and their variation. A cursory survey of the data on hand shows however that the day-to-day variation of the F component is

much smaller than that of the natural components, which vary over an order of magnitude, as has been previously observed. The F component settles to ground level from an accumulation of nuclear-explosion debris above the tropopause, while the natural components diffuse upward from the ground as gases. The settling process can be regarded as proceeding at a uniform rate, but the diffusion process is strongly influenced by the type of terrain, local winds and vertical mixing. The present findings are thus in accord with these proposed mechanisms.

In presenting a more detailed analysis of the present data with regard to meteorological influences, attention should be drawn to the fact that whereas desultory experimental work of this nature has continued for half a century no satisfactory correlation of weather and airborne activity has ever been achieved. This is not surprising, for the meteorological situation on any given day is a complex interaction of numerous parameters, and the airborne activity is a function of many of them. The installation at Winnipeg has the definite advantage of being situated in a region of relatively flat and unvarying terrain, minimizing the purely geographical aspects of weather as regards its influence on airborne activity, and enhancing the possibility of uncovering true meteorological influences.

Several of these short-term effects have been documented by this investigation. The three histograms at the back of the thesis display the data in a form which reveals both short and long-term trends. The most effective short-term influence on the levels of all three components is the scavenging effect of

heavy snowfall, e. g. some fifteen inches during Feb. 24-27; the levels of all fall rapidly immediately following this precipitation. Rainfall, particularly if it extends over several days, while not as effective as snowfall in sweeping the air clean of activity, causes marked decreases in the R level, e.g. May 25-28, June 6-27, July 4-5, July 8-10, Aug. 5-6, and Aug. 17-20. Most of these reductions are paralleled by similar drops in T levels but it will be noted that the effect on F levels is much less marked. Whereas it is known that the natural activities are adsorbed on aerosols of diameter 0.001 to 0.04 μ (W52), little if anything is known of the nature of the fallout particles as regards charge and size. The ineffectiveness of any scavengers except snow and heavy rain (May 23-26) suggests that fallout may consist of much smaller particles than those carrying the T and R components, possibly even atomic in nature; the smaller particles would have a correspondingly lower cross-section for precipitative scavenging, leading to the results noted.

The T and F activities on a given sample are a more or less representative average over the sampling period; however because of the short (\sim 32-minute) half-life of the R component the R activity on the filter is characteristic only of the few hours prior to cessation of sampling. As this would suggest, the days on which it rained or snowed in this period show drops in the R level. Of the seven days exhibiting the lowest R level only one had measurable precipitation and this occurred in the period mentioned. On three days the winds were variable, on three northerly and on one occasion from the southwest. Wind direction is not therefore an important factor; but with only

two exceptions each of these low days was preceded by a day with relatively heavy precipitation. The lowest measured values of the T component occur on days with rain, particularly thunderstorms; the highest occur predominantly on days free of precipitation, without correlation with wind direction.

Each of the components demonstrates a characteristic long-term variation. Data on hand is of course not yet adequate to establish a definite yearly fluctuation for the natural components, but some reasonable interim conclusions can be drawn. The thoron concentration in the winter months appears almost negligible, a not unexpected development in view of the fact that the heavy snow cover in these months would prove a severe barrier to the 59.5-second half-life thoron gas. When the spring break-up occurred the T component increased more than an order of magnitude, as would therefore be expected.

The radon concentration however was significantly higher in the winter months than in the summer. A possible explanation for this relatively unexpected phenomenon lies in the fact that the low ground-level temperatures in winter cause frequent temperature inversions, which maintain a stable layer of air close to the ground, allowing the radon concentration in a given air mass to reach considerable size before atmospheric disturbances shift it away from the source of the radon. However, in the summer months rapidly ascending thermals create continual turbulence and sweep radon-bearing air masses upward before a substantial concentration of the gas can build up. Since the winter snow cover provides only a token barrier to the longer (3.82-day) half-life radon, this agrees with facts observed,

The F level rises systematically through December and January, remains approximately stable until nearly the end of May, then falls steadily, a true decrease (not noted in the other components' records) which is now (early November) being mentioned by Government agencies; the present study shows the trend continuing beyond their dates, and will be continued until mid-1960 to obtain further information on the important phenomenon of fallout, and correlate it with nuclear tests. (None occurred during the study to date.)

The small-scale convenient technique herein described for simultaneous monitoring of F, T, and R components of airborne radioactivity has as yet received only limited application, in this installation. Many possible lines of investigation suggest themselves, for which the new technique is more or less ideally suited: 1. simultaneous monitoring of the F, T, and R components by samplers at several different heights at the same location, to investigate the instantaneous vertical distributions of the three components; 2. detailed examination of the air at various locations, including indoors with and without air conditioning, below ground level, in open residential and industrial areas, et cetera; 3. short-term sampling (of the order of one hour per filter) on a continuous basis to monitor the diurnal variation of the R component (which would be the dominant component, near equilibrium on such a sample). Other applications are no doubt conceivable; results of these investigations would add materially to the available data on the increasingly interesting phenomena of airborne radioactivity.

PART II

CHAPTER I

INTRODUCTION

Classical experiments before 1900 demonstrated the interaction between a moving charge and a magnetic field, whereby the charge was subjected to a velocity-dependent force perpendicular to the charge's direction of motion. This effect became the basis of one of the first instruments used to investigate the radiations from active nuclei, the fixed-field photographic-recording β -ray spectrograph. If a particle with charge e and mass m describes with velocity v a circular orbit of radius ρ in a plane perpendicular to a magnetic field H , the following relation between magnetic and centripetal forces must hold:

$$H e v = m v^2 / \rho$$

Therefore

$$m v = e H \rho$$

Thus the momentum of the particle is directly proportional to the product of the magnetic field and the radius of the orbit described. If a particle with charge e and momentum unknown traverses such an experimental array, and if the field H and the radius ρ of the resulting orbit can be measured, the momentum of the particle can be determined. If the field H is fixed, particles of different momenta will traverse orbits of different ρ ; if a photographic plate is interposed, the particles of different momenta will strike it at different places, producing a spectrographic record of the momentum distribution.

By 1912 β -rays had been identified as high-energy electrons and von Baeyer, Hahn, and Meitner (V11, V12) had obtained photographic records of the differential magnetic deflection of radiation from natural β -emitters. Danysz (D12, D13) improved their crude design, using defining slits and baffles to select a narrow sheaf of β -rays, and enclosing source, slit, baffles, and photographic plates in a vacuum chamber to reduce air scattering of the electron beam (see Fig. 3). With additional photographic plates perpendicular to the uniform magnetic field of his simple instrument he traced the orbits of electrons from a line source parallel to the field, and proposed that the β -particles be made to travel a full semicircle and impinge approximately perpendicularly upon the detecting photographic plate. This made use of a first-order radial focusing property of this geometry, a consequence of the fact that if a semicircular arc is rotated through a small angle about one end, the other end moves tangentially, as can be seen from the limiting orbits sketched in Fig. 3. If a monoenergetic electron source is used, the electrons traversing the central orbit strike the plate at the largest radius, and those whose orbits diverge initially from the central orbit strike at a slightly smaller radius, producing a line with a clearly-defined high energy edge corresponding to the electrons from the central orbit. This design is thus admirably suited for analysis of a mixture of monoenergetic electron groups, which appear as a collection

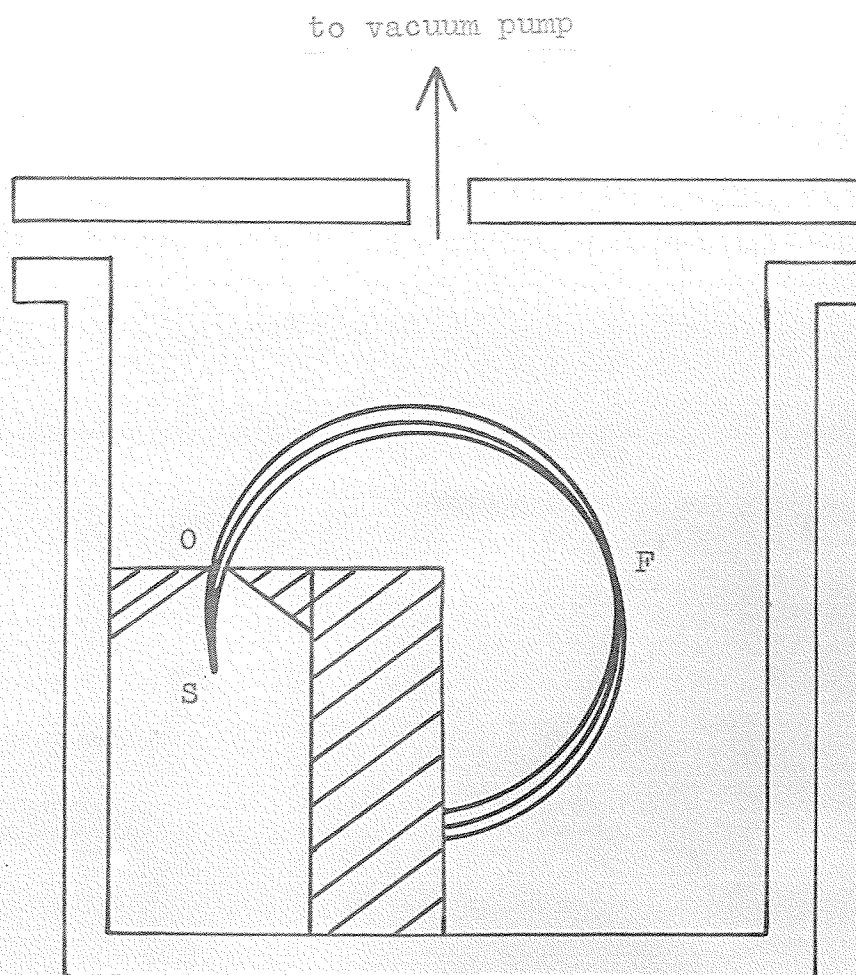


Fig. 3. Danysz' design for an early β -ray spectrograph: S source, O slit, F 180° first-order focus. Diagonal cross-hatching indicates lead shielding. The magnetic field is perpendicular to the plane of the page. (See D12.)

of lines with characteristic positions on the detecting plate.

The earliest spectroscopic analysis of β -radiation, by the above-mentioned and others, notably Rutherford and Robinson (R13) revealed such a line structure, which theoreticians immediately interpreted as analogous to the line structure of optical spectra and arising from energy level structures in the decaying nuclei. However discovery of a continuous component of every β -spectrum led to the assignment of a different origin to the lines in the spectrum. Examination disclosed line-spacing energetically equal to the atomic shell spacing for any given atom. At first it was thought that a monoenergetic electron group or line arose by photoelectric collisions, each involving a nuclear γ -ray and one of its own atomic electrons. Further investigation led to a more subtle interpretation, which suggested that after a β -transition to an excited state some daughter nuclei gave up part or all of their excitation energy not by emission of a γ -ray but by a direct interaction between the nucleus and one of its atomic electrons, which was ejected with an energy E determined by the corresponding γ -ray energy $h\nu$ and the ionization energy W of the shell in question thus:

$$E = h\nu - W$$

Detection of the X-rays emitted during reorganization of the atomic shells after such an interaction supported this theory. Experiments, notably that of Bainbridge et al. (B53)

on technetium, which decays by electron capture, disclosed that varying the chemical combination (changing the orbital wave functions) changed the decay constant; this, as well as instances of electron emission where the "parent" γ -ray is of a multipolarity which would make the transition probability vanishingly small, serves as evidence of a direct nuclear-orbital interaction, christened "internal conversion".

The semicircular focusing method had been in use for fifteen years before an examination of the shape of an individual conversion line from a semicircular machine was undertaken. Wooster (W27) in 1927 offered a semi-empirical method for line-shape analysis. Ten years later Li (L37) presented an exhaustive theoretical description of the conversion-line shape produced by a semicircular machine. Papers by Lawson and Tyler (L40) and Campbell and Kyles (K52) distilled the essentials regarding line-shape from semicircular spectrometers, invaluable for high-resolution work with these machines.

The relative intensities of conversion lines in a given spectrum provide information as to the energy-level spins and parities of the nuclide whose de-excitation gives rise to the lines. The theoretical material involved is beyond the scope of this thesis, but useful references include Rose (R58) Part I, and Siegbahn (S55), Chapter XIV (also written by Rose).

The fixed-field photographic-recording β -ray spectrograph was extensively employed in investigations of the conversion-line spectra of the γ -rays from radionuclides. The development of magnetic-lens β -ray spectrometers and



scintillation spectrometers for γ -rays led to a temporary loss of interest in the fixed-field instrument, but recent years have seen it rise again to prominence in nuclear physics. It is now frequently used in conjunction with a lens-type β -ray spectrometer, since the fixed-field instrument can attain better resolution than any lens-type machine. Furthermore, although the semicircular spectrograph has a relatively low transmission, an entire spectrum is scanned at once and the exposure time can be extended to compensate for the low transmission. Measurement of line intensities with the photographic-recording instrument is not as straightforward as that with a lens-type machine, but results obtained by the former method can be used to supplement and confirm those of the lens-type machine at a higher resolving power. Comments on resolving power of the present machine are included in the appropriate following sections, when optimal conditions and adjustments are discussed.

CHAPTER II

DESCRIPTION OF THE SPECTROGRAPH

I. MAGNET

Several years before the present study was undertaken a group at the University of Manitoba constructed a semicircular β -ray spectrometer of a fixed-orbit design employing a scintillation detector. The magnetic field was provided by a permanent magnet wound with demagnetizing coils, by which the residual field on the magnet could be varied; by varying the field in small steps an entire spectrum could be scanned. The machine was constructed and tested, but difficulties in maintaining stability in the demagnetization process proved insurmountable, and the spectrometer design was abandoned. The various components remained on hand unused until it was decided to utilize the magnet in the construction of a photographic-recording fixed-field β -ray spectrograph. (Initially it was planned also to use the vacuum box from the previous design, but its vacuum properties had deteriorated severely; it was eventually discarded and one of a new design was constructed as described below.)

Necessarily, since the magnet was in final mechanical form at the commencement of this project, discussion here will be confined to a description of this form, with a few additional details drawn from the manufacturer's manual. It is regrettable but possible that these manufacturer's

specifications have a degree of uncertainty in that the history of the magnet involves sea voyages between Britain, Canada, and Australia, and is not fully known. Intentional or accidental alterations may not be accounted for in the information presently on hand.

Plates IV and V show front and rear views of the spectrograph fully assembled. The magnet sat on a concrete pedestal, and the vacuum box fitted snugly between its pole pieces as shown. Also shown are the leads to the demagnetizing coils whose use will be described below. Fig. 4 gives the three elevations of the magnet, showing actual dimensions. Table V gives the manufacturer's listed specifications (subject to the qualification referred to above).

In use, the magnet's field was adjusted to a desired approximate value by brief energizing of the demagnetizing coils. Each of the coils had a resistance of about ten ohms; direct current at a few amps was led from a heavy-duty potentiometer chain in the appropriate direction through the coils in parallel for a few seconds at a time, until fluxmeter measurements in the air gap indicated that the desired field strength had been obtained. Precise knowledge of this field strength was unnecessary, since the spectrograph was to be calibrated at any given field setting by comparing positions of lines of known and unknown $H\rho$ i. e. momentum, on plates from the instrument, as discussed below. The field setting chosen was of course dictated by the $H\rho$

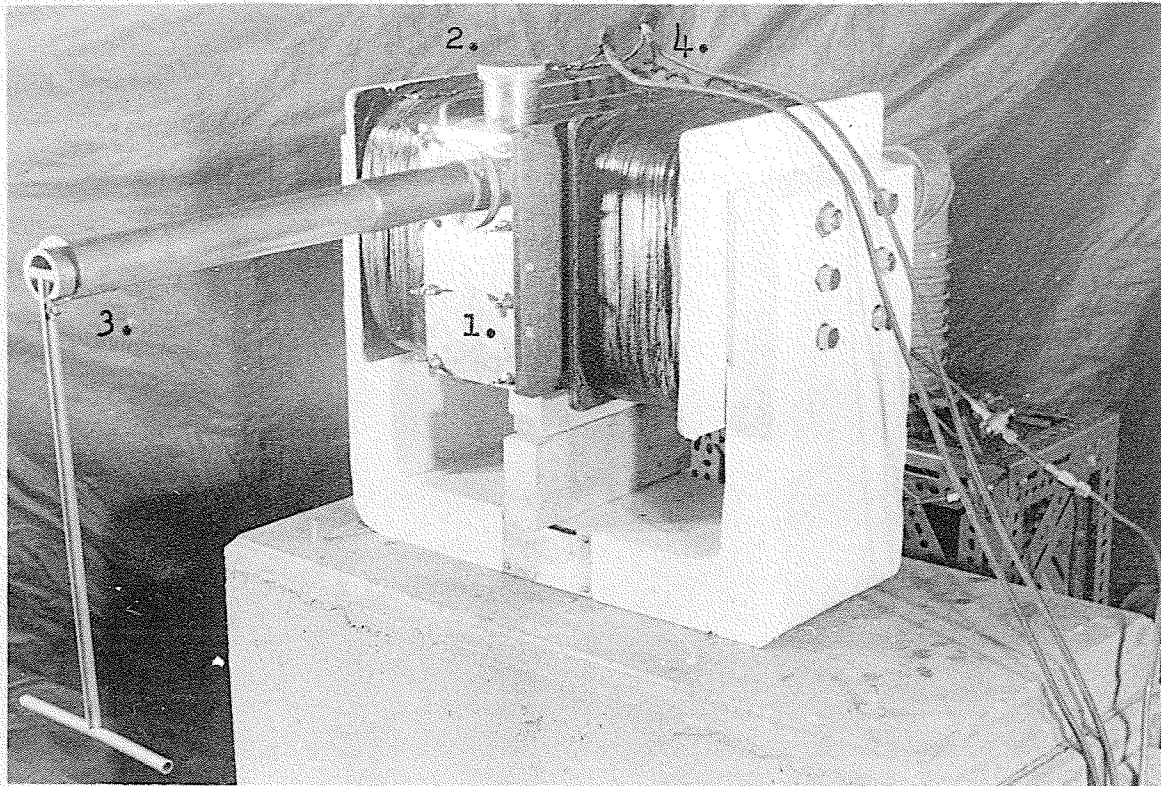


PLATE IV

Spectrograph front view: 1. access panel on vacuum box (note wingnuts); 2. source plug in position; 3. withdrawal mechanism, handle in full-open position (note retaining clip around exposed end of solid cylinder-- see text); 4. leads to demagnetization coils.

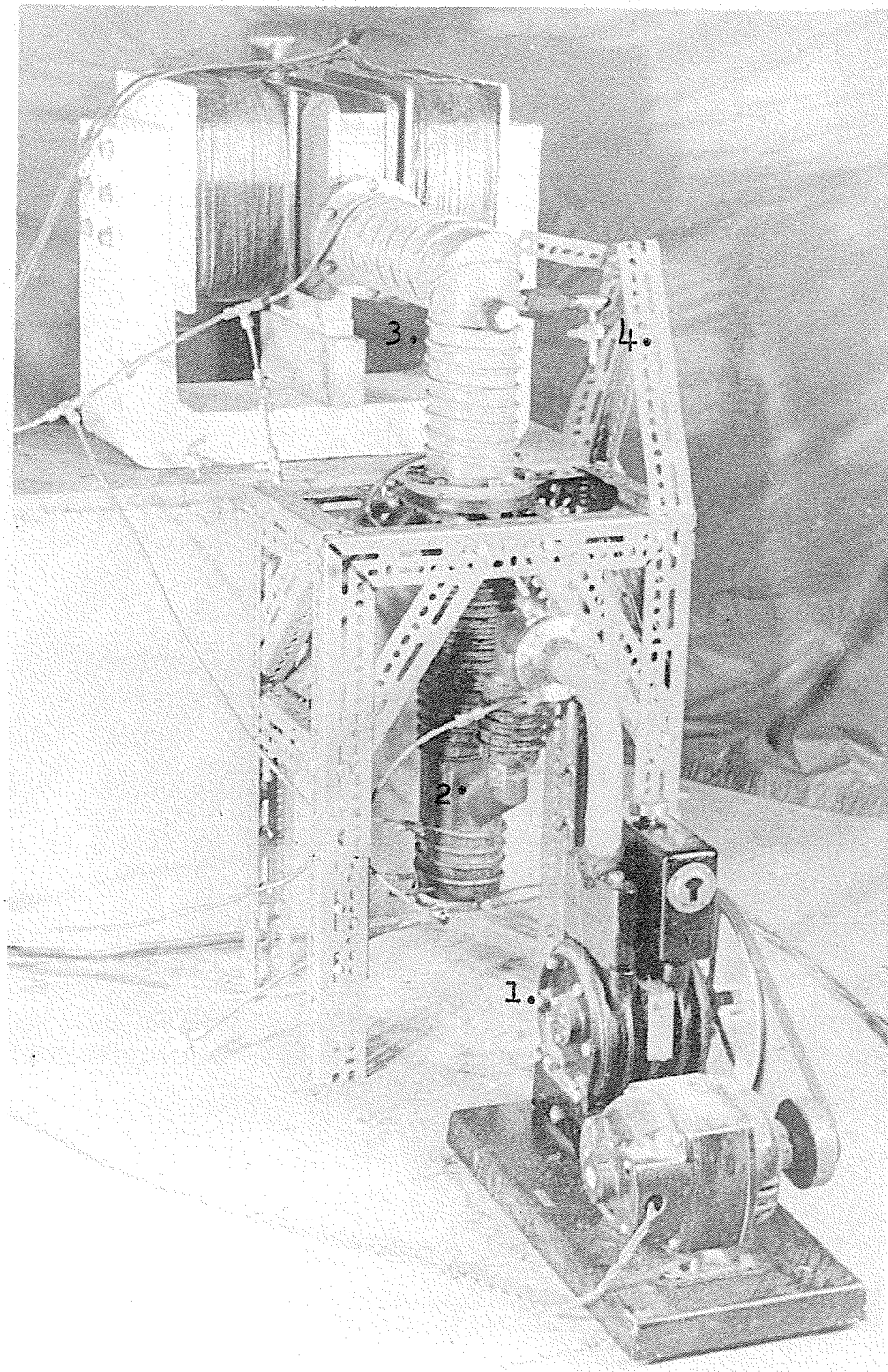
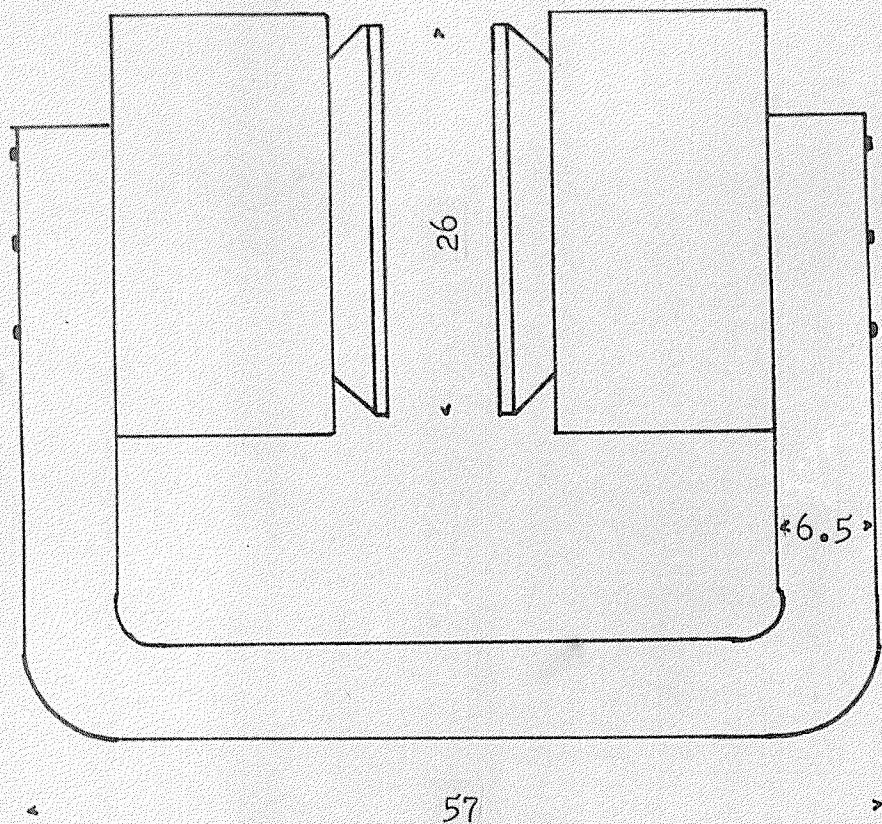
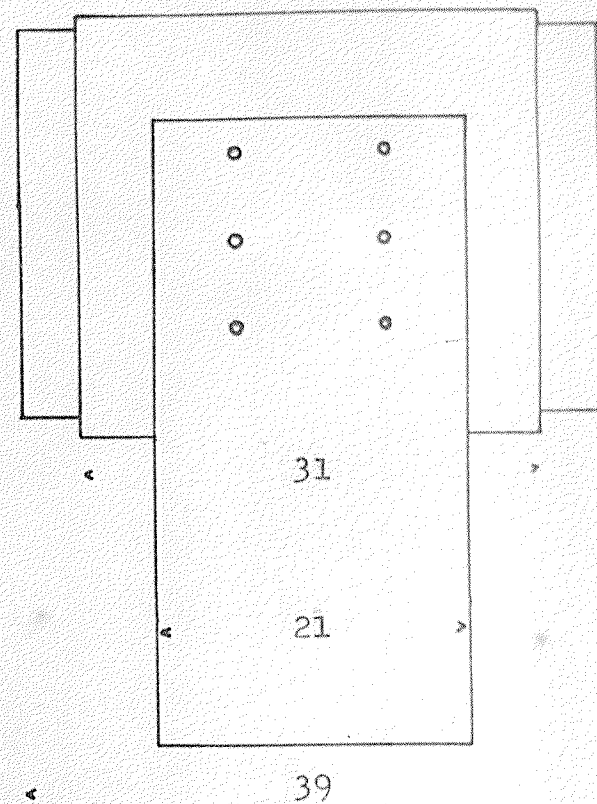


PLATE V

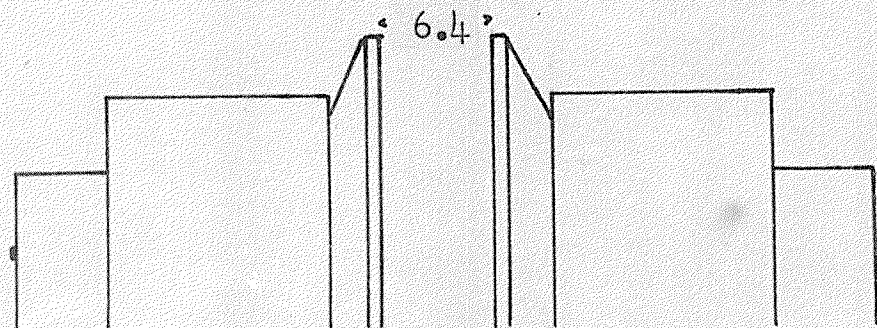
Spectrograph rear view: 1. backing pump; 2. diffusion pump; 3. L-pipe; 4. discharge tube (note air inlet stopcock). Note water jacket tubing.



49



57
15



(All dimensions in centimeters)

Fig. 4. Three elevations of magnet, with actual dimensions indicated. Approximately to scale, with 1 cm. = 5 cms.

47

TABLE V

MANUFACTURER'S SPECIFICATIONS FOR MAGNET

Weight: Armco iron yoke	270 lbs.
Armco iron pole tips	60 lbs.
Alcomax II blocks	100 lbs.
Coils	100 lbs.
Maximum permanent field strength:	
	1600 oersteds
Mean non-uniformity of field in central	
area 12x24 cms.:	2.2 per cent
Coils: each 1440 turns 16 S. W. G. wire	
Bolts: 1/2" non-magnetic stainless steel	
Manufacturer: William Jessop & Sons Ltd.,	
	Sheffield, England

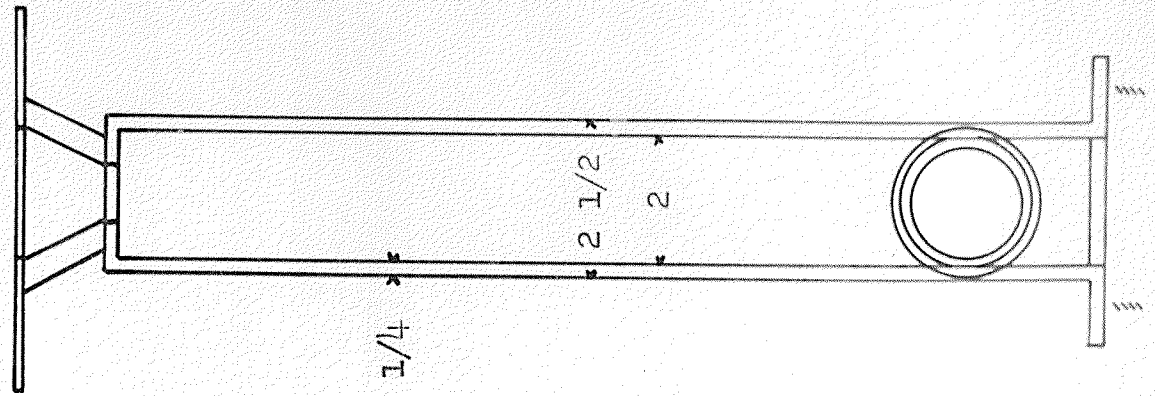
range of interest. Equipment for precise field measurement was unavailable, so the uniformity of the field was not known to better than a few per cent; since therefore no corrections of the Hartree type could be applied, field nonuniformity was considered an indeterminate limiting factor on resolution obtained.

II. VACUUM CHAMBER AND SYSTEM

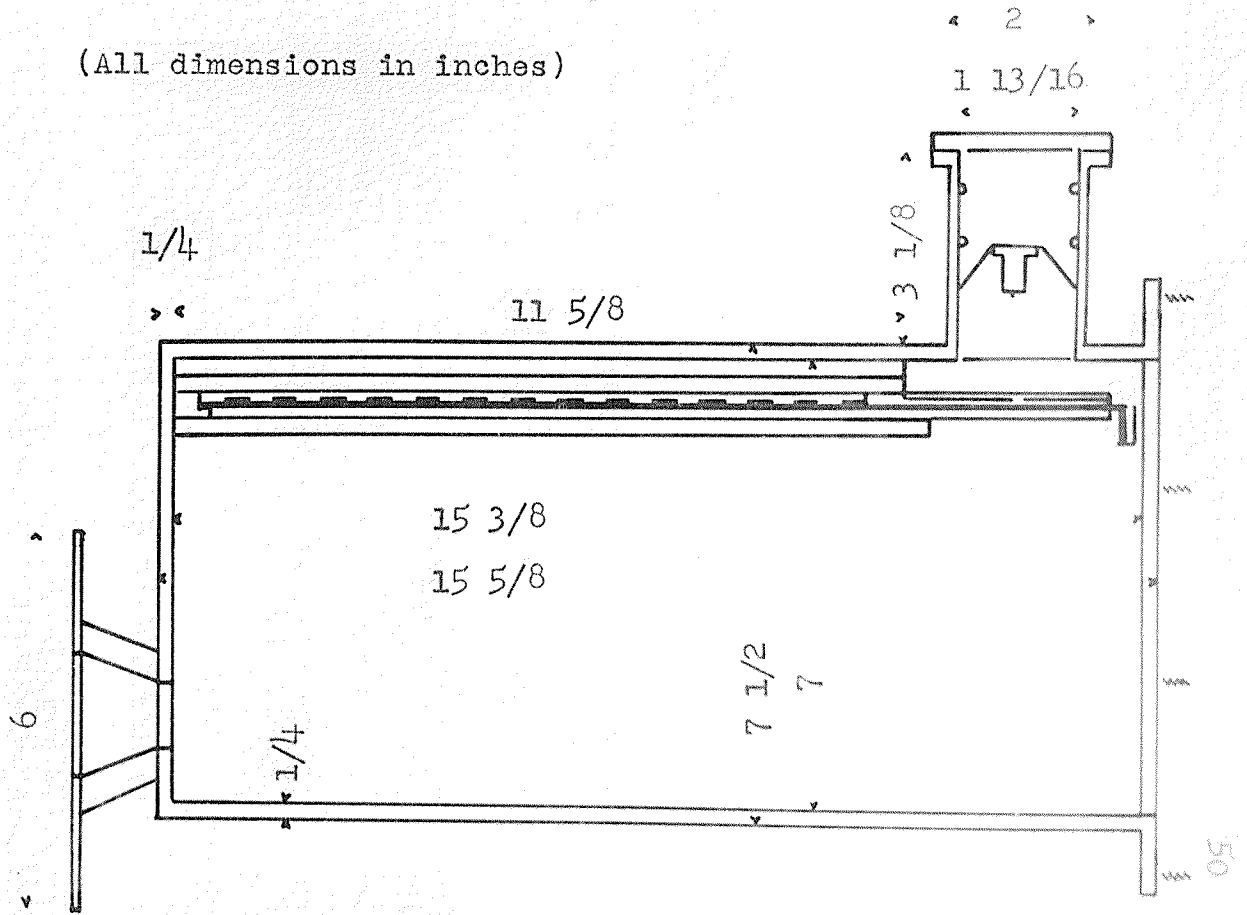
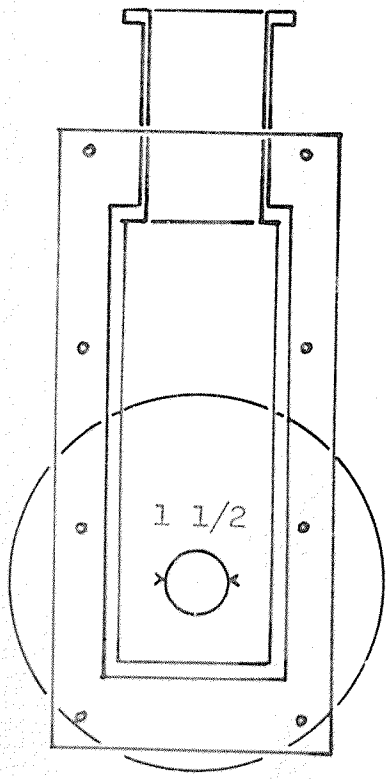
The vacuum system of the spectrograph consisted of a rectangular brass box which fitted between the magnet pole faces and was coupled by an L-shaped pipe to a diffusion pump, Distillation Products model MC275.01, backed by a W. M. Welch Duo-Seal rotary forepump. The arrangement of pumps and L-pipe can be seen in Plate V .

All dimensions of the brass box are indicated in Fig. 5 which shows three elevations of the box, whose internal fittings will be described in a following section. The box was made from sheet brass, silver-soldered at all joints. The access panel was held in place by eight wing-nuts on fixed bolts, and sealed by an O-ring seated in a rectangular well on the panel; these details may be noted in Plate VI . On the other end of the box was an aperture with an annular faceplate, which was bolted to a similar plate on the L-pipe. This joint was sealed by a rubber gasket seated between the faceplates. The lower end of the L-pipe was coupled by a similar joint to the top of the diffusion pump, which was mounted on a Dexion rack as shown.

Fig. 5. Vacuum box, three elevations; approximately to scale, with 1" = 3".



(All dimensions in inches)



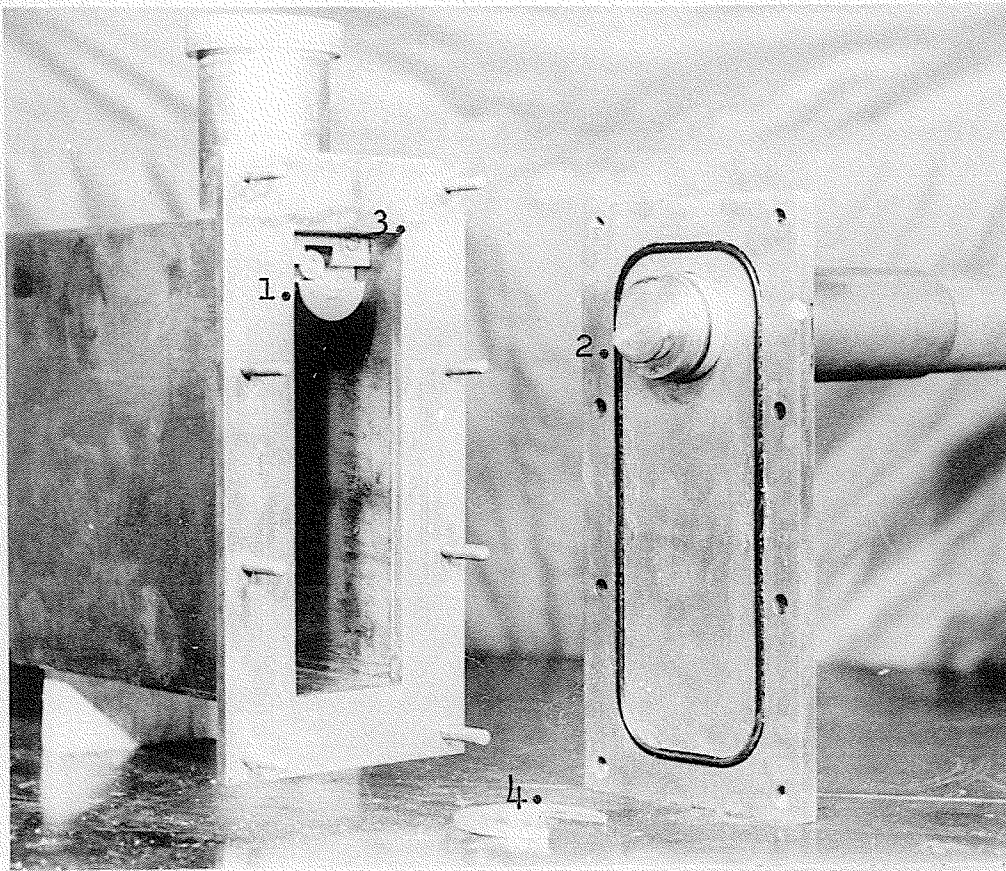


PLATE VI

End of vacuum box with access panel removed: 1. semi-circular trough of coupling (see text); 2. solid semi-circle of coupling (see text); 3. brass yoke retaining plate holder; 4. horseshoe clip (see text). Note solid cylinder of withdrawal mechanism projecting from access panel, with one of its two O-rings visible.

The diffusion pump was coupled to the forepump by a joint with smaller faceplates sealed by an O-ring and connected by a short length of vacuum hose to the forepump as shown. Also visible are the water jackets around L-pipe and diffusion pump, which led to a special outlet and through which cold water was continually circulated when pumping was in progress. An additional jacket allowed quenching of the diffusion pump if fast cooling was desired, by adjustment of the proper valves in the water circuit. All vacuum joints were coated with Apiezon M grease before coupling.

It was felt that precise knowledge of the vacuum level was unnecessary, and that a pressure low enough to allow no discharge in a simple discharge tube would be adequate to minimize air scattering. Accordingly the L-pipe was fitted with such a small discharge tube, visible on the ascending column in Plate V. After pumping was commenced a Tesla-coil high-voltage tester was energized and touched to an electrode projecting beyond the glass envelope; when no further discharge was seen in the tube between the internal end of this electrode and the metal wall of the L-pipe, a sufficiently low air pressure was assumed to exist in the system for operation of the spectrograph.

III. SOURCE ASSEMBLY

Several forms of source have been employed in this type of β -ray spectrograph with varying degrees of success.

Each form has advantages discussed analytically by Li (L37), but simplicity and ready availability led to the choice for this project of a source in the form of a layer of iridium 250 micrograms per square centimeter thick sputtered onto one side of an aluminum wire of circular cross-section and diameter 0.0037 inches by Messrs. Barr & Stroud Ltd. Glasgow.

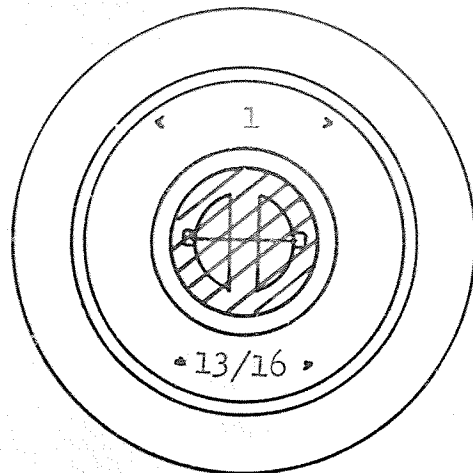
After much thought it was decided to mount this wire in a small holder milled from pure aluminum, as shown in Plate VII and Fig. 6, a method which subsequently proved to have serious shortcomings. One inactive wire was mounted thus and irradiated at a high pile factor location in the Harwell reactor. On the source's return the mount was found to have warped under the acute thermal stress imposed, relaxing the tension on the active wire, which then developed sufficient curvature to limit possible resolution with this source to about one per cent.

A second similar source was prepared and irradiated at Brookhaven at 10^{13} n/cm²/sec. for three weeks; when it arrived broken beyond salvaging the first source was straightened by trial and error and fitted with a small brass collimator (see Plate VII), a satisfactory interim arrangement. The aluminum mount with the active wire was affixed with two screws to a brass plug as shown in Fig. 6. The entire source assembly was then inserted into the cylindrical port on top of the vacuum box. Fig. 5 shows the geometry of the source assembly in operating position. The brass plug was fitted with two O-rings to serve as



PLATE VII

Source mounting plug (upside down with respect to operating position): 1. O-ring seals; 2. aluminum mount (barely visible are heads of mounting bolts); 3. brass collimator (black vertical line visible through hole is space between aluminum supports; barely visible across it is source wire).



(All dimensions in inches)

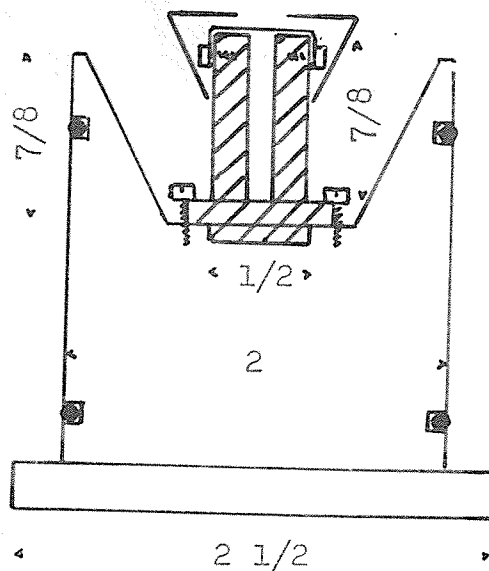


Fig. 6. Source mounting, top and cross-section views; approximately to scale, with 1" - 1". Diagonal crosshatching indicates small aluminum support for active wire, bolted as indicated to the brass plug proper. Note O-ring seals.

vacuum seals. The various dimensions as indicated in Fig. 5 were chosen to give a satisfactory source-slit-plate geometry, and the assembly design assured reproducibility of this geometry. It will be noted that the slit, not the source, was in the plane of the photographic plate; further discussion of this point is included below. Optimal azimuthal position of the brass plug was found by trial and error, so that the lines produced were clearly transverse to the long dimension of the plate; marks were scratched into the flanges of plug and port and aligned to duplicate this azimuthal position for succeeding plates.

IV. PLATE HOLDER AND ASSEMBLY

Two avenues are open to the designer of a semi-circular β -ray spectrograph; the instrument can be intended for use for absolute $H\rho$ measurements or comparative $H\rho$ measurements. In the first case provision must be made for measurement of the magnetic field strength H and for deduction of ρ from the geometry of source, slit, and recorded line. This latter requirement makes it preferable to have source and plate in the same plane. In the second case spectrographic records are made with two different sources, one whose spectrum is known and the other whose spectrum is to be analysed, under the same conditions of field and geometry, which need not however be precisely known. The resulting known and unknown spectra are compared, and the $H\rho$'s of the unknown lines inferred from those of

the known lines. To serve as a baseline for comparison an index which locates each spectrographic record positively with respect to the fixed geometry of the instrument is usually provided.

The present instrument is of this second type. Since absolute geometrical measurements did not need to be made it was accordingly possible to take advantage of the property of the source-slit-plate geometry shown (Fig. 5) which gives a fixed shape to the conversion line no matter what its position on the plate, making comparison of line intensities more straightforward.

The design of the plate holder was essentially simple; it is shown in detail in Fig. 7 . The plate was placed in a shallow well, and a brass cover screwed into place. The plate rested on a rectangular aperture into whose long sides were milled regularly-spaced rectangular notches as seen in Plate VIII. These notches served as the index referred to above, and appeared as a square-cut sawtooth pattern on the edges of each recorded spectrum (see e. g. Plate IX). A 1/8" brass plate sliding smoothly in a channel below the notched aperture served as a shutter.

As the end-view cross-section indicates, the plate holder was shaped to slide snugly into a brass sleeve permanently mounted with solder-sealed screws to the inside top of the vacuum box, as shown in Fig. 5 . After the loaded plate holder was slid into operating position in the sleeve, a small brass yoke was affixed with two screws

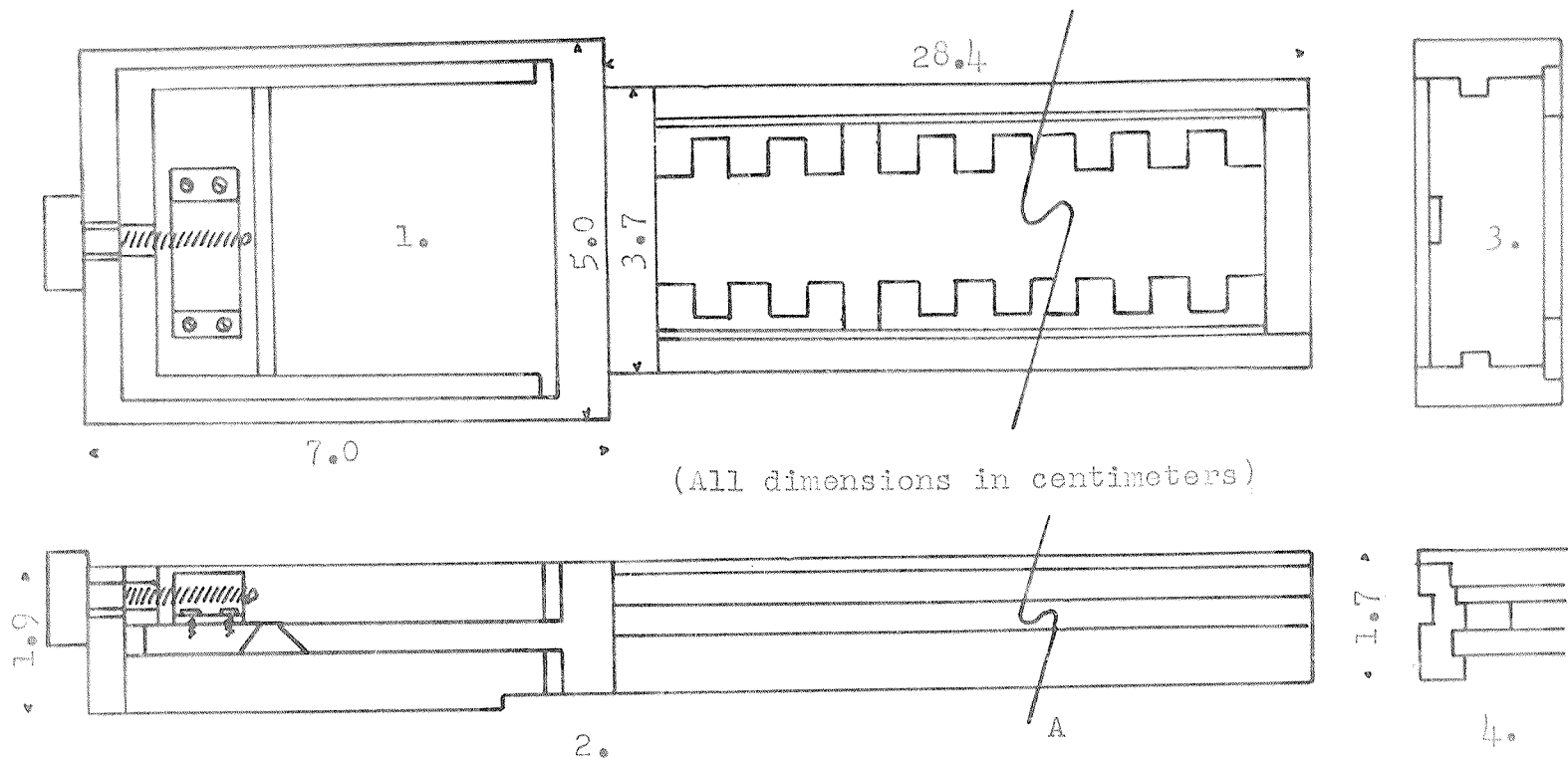


Fig. 7. Plate holder, various views: 1. top: note slit mechanism, with movable jaw on left and fixed jaw on right; note also notch pattern in plate well with cover removed (deep notch every tenth); 2. side: note groove which matches ridge on sleeve in vacuum box; 3. end: note again grooves; note also notch beneath cover, into which screwdriver is inserted to pry off cover; 4. section A: (a) cover; (b) plate; (c) notch pattern; (d) shutter; (e) aperture. Approximately to scale, with 1 cm. = 1 cm.

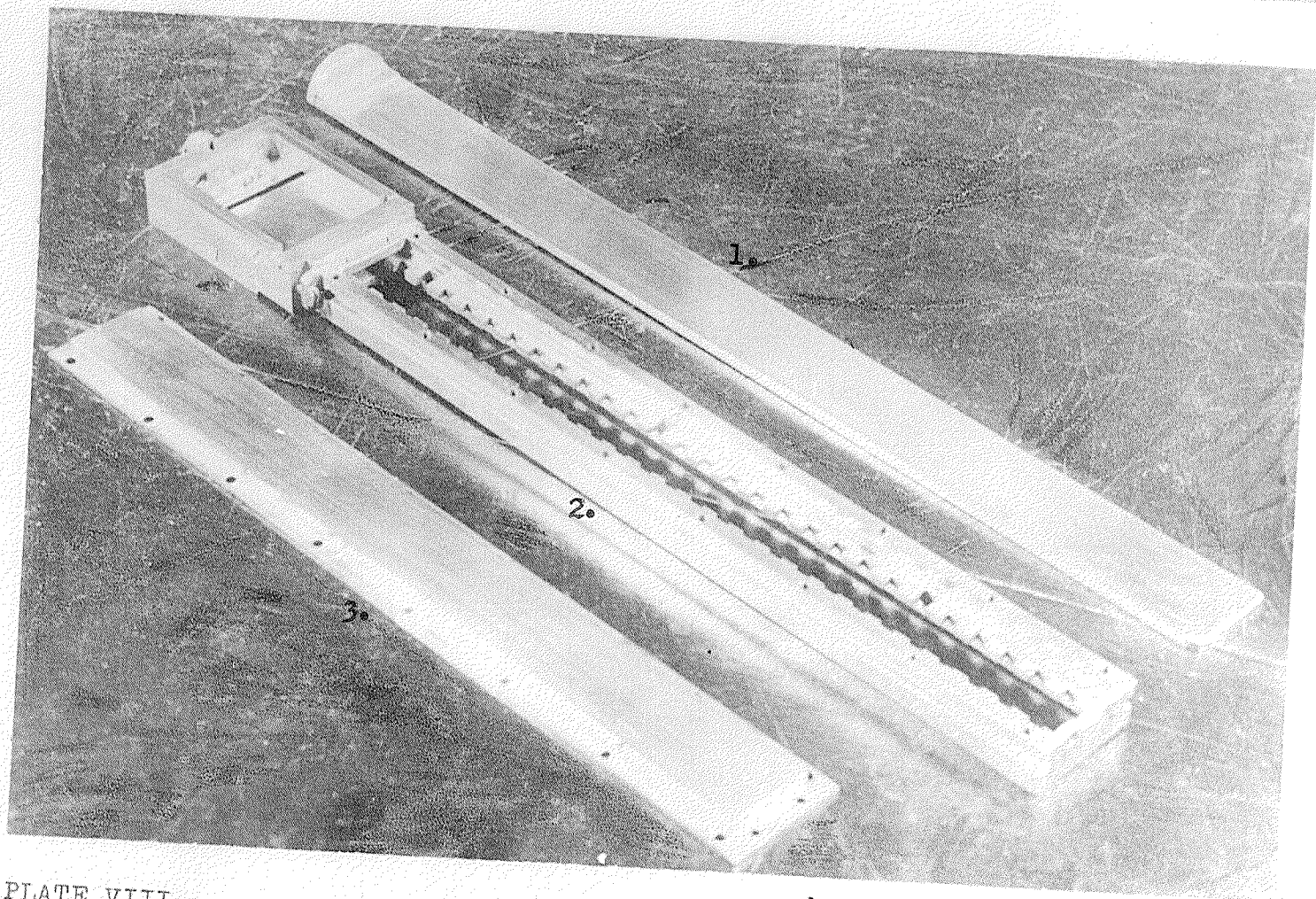


PLATE VIII

Plate holder components: 1. shutter (upside down with respect to main frame); 2. main frame (note notches along sides of plate well; note also slit assembly at upper end, with knurled adjusting screw visible on far end); 3. brass cover (upside down with respect to main frame).

to the end of the sleeve, overlapping the end of the plate holder and locking it in place (see Plate VI).

The slit mechanism was rigidly attached to the end of the plate holder proper, to assure fixed geometry from slit to notches. Its width could be chosen by adjusting the movable jaw parallel to itself by means of a knurled screw projecting beyond the end of the unit. The screw is visible in Plate VIII.

Since the plate was not to be exposed until the vacuum system had been evacuated to operating level, the means whereby the shutter could be opened under vacuum gave rise to much discussion before the present quite satisfactory method evolved. Since the access panel had to be easily removable, and since the shutter was to be withdrawn through a port situated at the upper end of the access panel, it was necessary to incorporate a coupling between the shutter proper and the panel-mounted withdrawal mechanism, which coupling could be engaged under vacuum prior to withdrawal of the the shutter. It was finally decided to accomplish exposure of the plate by withdrawing the shutter into a tubular extension of the vacuum chamber long enough to accommodate the withdrawn shutter. A thin rectangular supporting guide on the extreme outer end of the plate holder, beyond the slit, assured that the shutter would return easily into the closed position after exposure. To withdraw the shutter a short solid brass cylinder riding on two greased O-ring seals was thrust into the long tube

until a solid semicircle projecting beyond its inner end could be meshed by rotation of the solid cylinder through 180° about its axis into a hollow semicircular trough on the outer end of the shutter proper. An extension handle of light brass, hinged for convenience, was used to slide the solid coupling cylinder into place, engage the shutter, and withdraw the coupled unit, exposing the plate. To keep the solid cylinder from being driven back into the long tube by external air pressure while the chamber was evacuated, a horseshoe-shaped piece of thin brass of larger diameter than the long tube was clipped into a groove on the outer end of the solid cylinder. This prevented it from sliding into the tube beyond the groove, which was so positioned as to assure that the shutter would in this position be withdrawn beyond plate and slit and yet remain in the outer supporting guide, to allow closing the shutter without difficulty. The various features described above can be seen in Plates IV and VI and Fig. 5.

CHAPTER III

OPERATION OF THE SPECTROGRAPH

I. PREPARATION OF THE PLATE

The plateholder was originally designed to accommodate glass-backed photographic plates, 10 7/8"x1"x1/16"; however, it was subsequently learned that plates of these dimensions could not be obtained with the desired emulsion, except by special order. After some inquiries and tests it was decided to employ Ilford Ilfex No-Screen X-Ray Film, cut into strips of appropriate size with a paper shear. For brevity such a strip will be referred to as a "plate". All handling of unexposed film was done in total darkness after it was found that unacceptable fogging resulted from any but the briefest exposure even to indirect light from a Wratten 6B safelight. A plate was cut and laid into the well in the opened plateholder. Several strips of paper were laid on top of the plate to serve as packing to hold the plate in position. The top brass cover was pressed into the well and screwed into place. The slit was adjusted to the desired width. The plateholder was slipped into the brass sleeve in the vacuum box, and the small yoke bolted into place, fixing the holder in position.

II. EXPOSURE OF THE PLATE

The access panel was fitted over the bolts on the open end of the vacuum box and fastened tightly in place with eight wingnuts. The source plug was pressed down into the cylindrical port on the end of the top of the vacuum box, and twisted about its vertical axis until the marks mentioned in Chapter II Section III were aligned, bringing the source wire parallel with the magnetic field. The fore-pump and diffusion pump were turned on. Initially tests of vacuum were made as discussed in Chapter II Section II, using a Tesla coil; it later materialized that the energized Tesla coil was contributing spurious pulses to several nearby electronic units, and also fogging exposed plates inside the spectrograph by light from the bright discharge in the vacuum chamber. The Tesla coil was laid aside, since the vacuum level was not critical and since the necessary pumping time had now been determined. When this time had elapsed the shutter was withdrawn as described in Chapter II Section IV.

After the required exposure time had elapsed the shutter was again closed, and the withdrawal mechanism uncoupled and left in the position seen in Plate IV. The diffusion pump was unplugged and quenched; when it had cooled the forepump was turned off and a glass stopcock on a side extension of the discharge tube was opened to bring the interior of the spectrograph to atmospheric pressure. The source plug was removed and set aside. The wingnuts

holding the access panel were removed and the panel lifted off.

III. PROCESSING OF THE PLATE

The yoke was unbolted and the plateholder removed from the sleeve. In the darkroom the top cover of the plateholder was unscrewed and pried out with a screwdriver in a slot milled in the end of the plateholder between the cover and the frame. The plate was lifted out of the well, developed for eight minutes in DuPont Liquid X-Ray Developer, washed for twenty seconds in running water, fixed for ten minutes in DuPont Liquid X-Ray Fixer, and washed for an hour or more in running water. After drying the plate was ready for analysis.

CHAPTER IV

CALIBRATION OF THE SPECTROGRAPH

1. THEORETICAL BACKGROUND

In order to discuss the calibration of the spectrograph it will be necessary first to discuss the analysis of photographic records of conversion lines with respect to relative intensity and resolution, as follows.

Photographic density D as defined as

$$D = \log_{10} \frac{I_0}{I} \quad (1)$$

where I_0 is light transmitted through the unexposed part of the film and I light transmitted through the exposed part.

Silberstein (S23) showed also

$$D = C \log_{10} (\alpha E + 1) \quad (2)$$

where C and α are constants and E is exposure and is proportional to the total number of electrons received at the point in question. (For Ir^{192} a day's exposure results in a decay of the source of one per cent.)

Let $\alpha E = e$, the "electron density". Then

$$\log_{10} \frac{I_0}{I} = C \log_{10} (e + 1) \quad (3)$$

Now consider microphotometer traces of a line and of the sharp blackening edge or step function produced on a plate by an index notch (see Fig. 8 for definitions of symbols to be used). Because different light strengths may have been used for (a) and (b) R_b is not necessarily equal to R_b' nor $R_0 = R_0'$.

However

$$\frac{R_b}{R_0} = \frac{R_b'}{R_0'}$$

So

$$\log_{10} \frac{R_b}{R_0} = \log_{10} \frac{R_b'}{R_0'} = C \log_{10} (e_0 + 1) \quad (4)$$

where e_0 is the electron density of the continuum near the line.



4.



3.



2.



1.

PLATE IX

The four photographic plates analyzed; numbers identify each for purposes of discussion elsewhere.

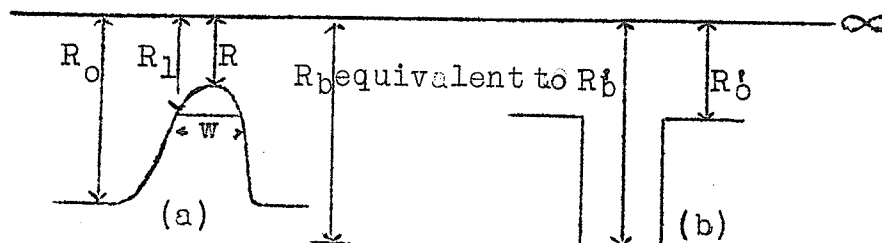


Fig. 8. Microphotometer traces of (a) conversion line and (b) step function: R_0 = deflection corresponding to continuum near line; R = deflection corresponding to peak; R_1 = deflection corresponding to true width at half height; R_b' = deflection corresponding to unexposed part of film; R_0' = deflection corresponding to continuum near step function. (The line at ∞ represents infinite blackening, i. e. no light transmitted.)

* * *

Also
$$\log_{10} \frac{R}{R_b} = C \log_{10} (e + 1) \quad (5)$$

where e is the electron density at the peak. Combining

(4) and (5) gives
$$\begin{aligned} \log_{10} \frac{R_0}{R} &= C \log_{10} \left(\frac{e + 1}{e_0 + 1} \right) \\ &= C \log_{10} \left(\frac{e - e_0}{e_0 + 1} + 1 \right) \\ &= C \log_{10} (\epsilon' + 1) \end{aligned} \quad (6)$$

where $\epsilon' = \frac{e - e_0}{e_0 + 1}$

Thus
$$\log_{10} \frac{R_0}{R_1} = C \log_{10} \left(\frac{\epsilon' + 1}{2} \right) \quad (7)$$

The true relative intensity I of a line is given by

$$I = A \frac{\rho}{\eta}$$

where η is the energy sensitivity of the emulsion, ρ is the solid angle correction factor, and A is the area

under the line of radius ρ . Because the evaluation of A is in some cases rather difficult, it is approximated by the product of the height of the line and its width at half-height, substituting this rectangle for the integrated area of the line. Although the rectangle is eighteen per cent smaller than A for circular wire sources, the ratio of the various rectangles are closely the ratio of the areas of the corresponding lines to within the experimental error (S54).

$$\text{So} \quad I = w \left(e - e_0 \right) \frac{\rho}{\eta} = w \xi' \left(e_0 + 1 \right) \frac{\rho}{\eta} \quad (8)$$

where w is the width of the line at half-height R_1 . Since the relative intensities for the conversion lines of Ir¹⁹² have been determined elsewhere, equation (8) can be used to plot a curve for η as a function of the energies of the lines in a given spectrum, effectively calibrating the photographic plate as to the dependence of its sensitivity on the energy of the β -particle striking it.

Before (8) can be employed values of ξ' and w must be determined, using equation (6). The first requirement is a value of C , obtained as follows. Experimental values of R'_b/R'_0 at the same points on plates exposed different lengths of time are taken. Now $D = C \log_{10} (\alpha E + 1)$ and

$$D = \log_{10} \frac{I_b}{I_0} = \log \frac{R'_b}{R'_0} = C \log_{10} (\alpha E + 1)$$

For the first plate therefore

$$\frac{R'_b}{R'_0} = (\alpha t_1 + 1)^C = p$$

where t_1 is the time of exposure, and α a constant with the

appropriate units. For the second plate

$$\frac{R'_2}{R'_0} = \left[\alpha (0.99)^d t_2 + 1 \right]^C = q$$

where d equals the number of days between the exposure of the first and second plates, to correct for source decay.

Let $t'_2 = (0.99)^d t_2$, the effective exposure time. Then

$$(\alpha t_1 + 1)^C = p$$

$$(\alpha t'_2 + 1)^C = q$$

Then $\log p = C \log (\alpha t_1 + 1)$ (9)

$$\log q = C \log (\alpha t'_2 + 1)$$

and $\frac{\log p}{\log q} = \frac{\log (\alpha t_1 + 1)}{\log (\alpha t'_2 + 1)} = m$

so $\alpha t_1 + 1 = (\alpha t'_2 + 1)^m$ (10)

where m is a decimal fraction which can be determined from the microphotometer trace. The author is indebted to Prof. S. M. Neamtan of the Department of Mathematical Physics at the University of Manitoba for the following numerical method of solving equation (10) for α . Let $x = \alpha t_1$ and $k = t'_2/t_1$. Equation (10) becomes $1 + x = (1 + kx)^m$, with $0 < m < 1$, $k > 1$, and $mk > 1$. The root sought satisfies the inequality

$$\frac{1}{(mk)^{\frac{1-m}{k}} - 1} < x < (k^{\frac{1}{1-m}} - 1)$$

and will ordinarily lie closer to the above upper bound.

To approximate to the root use the iterative relation

$$x_{r+1} = (1 + kx_r)^m - 1$$

Starting with some value of x_0 near the upper bound, successive values x_1, x_2, x_3 et cetera can be calculated until a value x_r is found such that $x_{r+1} = x_r$. This is the desired root.

Solving then for α in (10) allows determination of C in (9); different pairs of plates can be used to get several values of C , whose mean can be used as the required constant in (6). With R'_b/R'_0 from experimental data (measured near the line of interest), equation (4) leads to

$$\frac{R_b}{R'_0} = \frac{R'_b}{R'_0} = a_1 = (e_0 + 1)^C$$

and so
$$\sqrt[C]{a_1} = e_0 + 1$$

Taking $\frac{R_0}{R}$ from the data, equation (6) leads to

$$\frac{R_0}{R} = a_2 = (\epsilon' + 1)^C$$

and
$$\epsilon' + 1 = \sqrt[C]{a_2} \quad \text{or} \quad \epsilon' = \sqrt[C]{a_2} - 1$$

Now, knowing ϵ' it is possible to get R_1 from equation (7)

thus
$$\frac{R_0}{R_1} = \left(\frac{\epsilon'}{2} + 1\right)^C$$

$$R_1 = R_0 \left(\frac{\epsilon'}{2} + 1\right)^{-C}$$

Knowing R_1 it is then possible to measure w from the data, in arbitrary units.

The only value now required before (8) can be solved for η is ρ for the line of interest. In Fig. 9 distances x and d are not known with any great accuracy; it is however possible to measure d_1 and d_2 with satisfactory accuracy from a recorded spectrum and its microphotometer trace. Since the $H\rho$ values of the recorded lines are known from other work, it is possible to set up equations from which the ρ values of the various lines can be determined. Let

$$\begin{aligned} H\rho_1 &= k_1 & \rho_2 &= \rho_1 \frac{k_2}{k_1} \\ H\rho_2 &= k_2 & \rho_3 &= \rho_1 \frac{k_3}{k_1} \\ H\rho_3 &= k_3 & & \end{aligned} \quad (11)$$

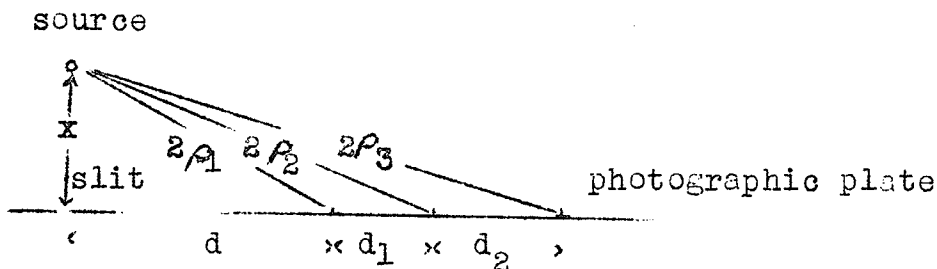


Fig. 9. Geometry of the source-slit-plate arrangement, indicating three conversion lines with radii ρ_1, ρ_2, ρ_3 , between which the spacings d_1 and d_2 can be measured.

* * *

Using the Pythagoras theorem gives

$$4\rho_1^2 = x^2 + d^2$$

$$4\rho_2^2 = x^2 + (d + d_1)^2$$

$$4\rho_3^2 = x^2 + (d + d_1 + d_2)^2$$

Combining yields $4(\rho_2^2 - \rho_1^2) = 2dd_1 + d_1^2$

and $4(\rho_3^2 - \rho_1^2) = 2dd_1 + 2dd_2 + 2d_1d_2 + d_1^2 + d_2^2$

from which $4\left[\frac{k_3^2}{k_1^2} - 1\right]\rho_1^2 = 2d_1d_2 + d_1^2 + d_2^2 +$

$$2(d_1 + d_2) \left\{ \frac{4\rho_1^2 \left[\frac{k_2^2}{k_1^2} - 1 \right] - d_1^2}{2d_1} \right\}$$

This equation can be solved for ρ_1 in terms of known or measurable values for the other parameters, and all other required radii can be obtained from ratios of their known $H\rho$'s such as equations (11).

The application of this theory to practical analysis of photographic records of conversion lines will be outlined in the following section, as it is used to effect a calibration of the present instrument.

2. CALIBRATION PROCEDURES

After many trial exposures were made as described in Chapter III using the source described on page 53, the four spectrum plates pictured actual size in Plate IX were selected, taken to Ottawa, and processed on a Leeds and Northrup recording microphotometer belonging to the Pure Chemistry section of the National Research Council. Each plate was scanned end to end six times, once along the notches and five times along the continuum by different parallel paths. A sample of one of these traces and a sample plate can be found at the back of the thesis. The microphotometer traces were then analyzed as follows, to calibrate the spectrograph and the film employed.

The simplest calibration to be made was that of the index notches (page 57) with respect to electron momentum $H\phi$. The trace along the notches was taken, and the average distance between successive sharp (high-energy) edges was measured. Since this distance along the trace corresponded to one centimeter on the plate, it was then possible to measure distances from a given notch to the peaks of the various lines on the trace, calculate their actual spacing on the plate, and plot a graph of distance from a given notch versus $H\phi$ (Fig. 10). If now an unknown spectrum were recorded with the same magnetic field, the positions of the lines could be converted directly to their $H\phi$ -values by use of this graph. Table VI gives the resolution (full width at half height divided by momentum value of the line) for the K-conversion line of the 316 Kev γ -ray.

Fig. 10. Calibration of the notches with respect to H_p ; the points shown are plotted at measured positions of the lines indicated, using H_p values from Johns and Nablo (J54).

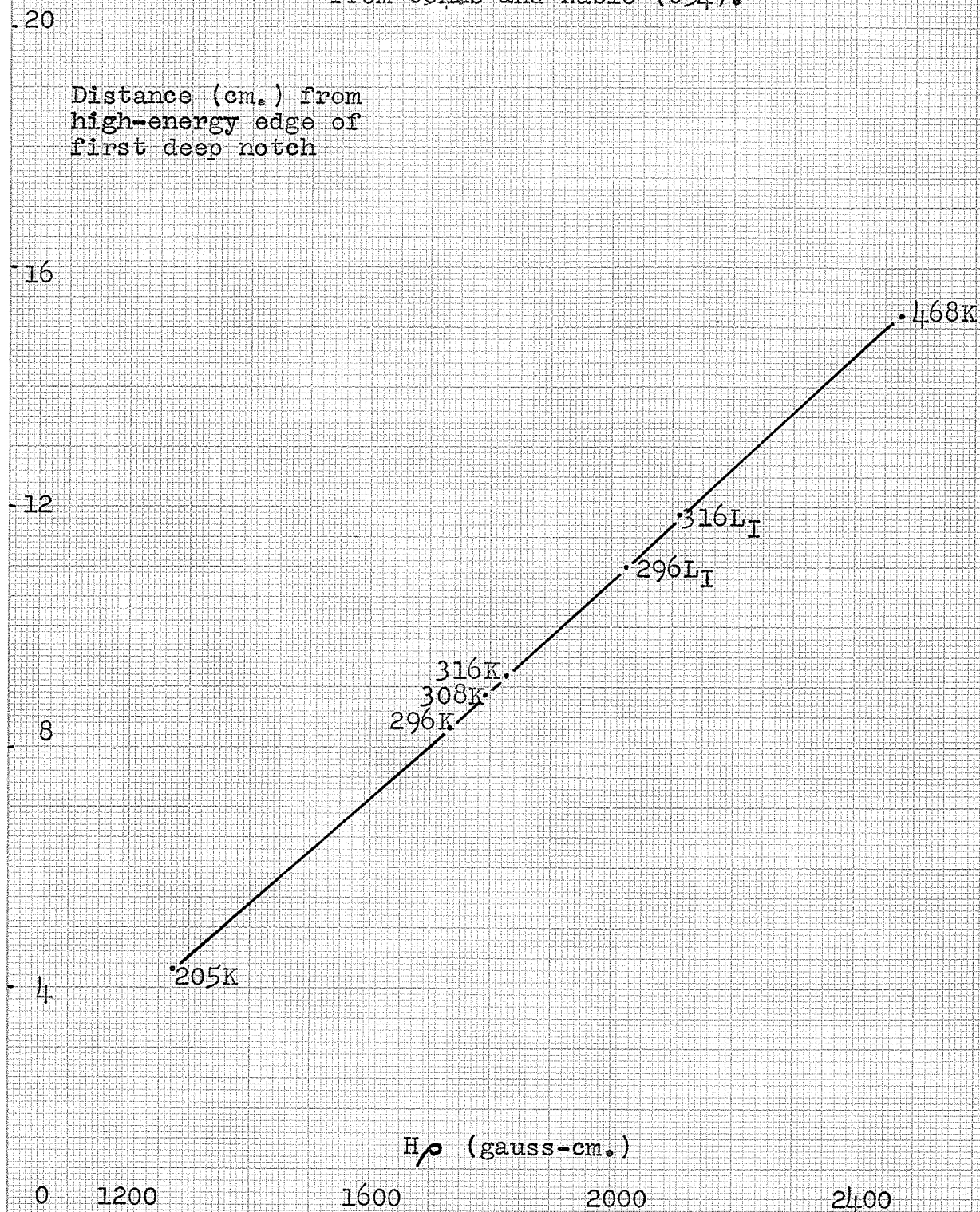


TABLE VI

PERFORMANCE OF THE SPECTROGRAPH

Plate Number	Slit Width	Exposure Time	Resolution
1	2.28 mm.	117 hours	.55%
2	1.58 mm.	48 hours	.41%
3	0.95 mm.	60 hours	.41%
4	2.28 mm.	40 hours	.39%

These values indicate the performance of the spectrograph as demonstrated in its records of the K-conversion line of the 316 Kev γ -ray in Ir¹⁹².

The more intricate calibration procedure for the photo plates, involving the intensities of the conversion lines, employed the analytic techniques detailed in section 1 above. First, using the method outlined on pages 68-70 and three pairings of the chosen plates, an average value of the constant C was obtained. The three trials and the resulting constants

are shown here:	Plates 1&2--	$\alpha = 0.0132$	$C = 2.45$
	Plates 1&3--	$\alpha = 0.0182$	$C = 2.08$
	Plates 1&4--	$\alpha = 0.0126$	$C = 2.70$
			Average C = 2.41

Table VII gives the electron energies and momenta for the five conversion lines of Ir¹⁹² used in this work. Table VIII gives absolute conversion line intensities with the references from which they have been taken. Using the method of pages 70-71 the ρ -values of the lines were calculated, as listed here:

205K line--	$\rho = 5.84$ cms.
296K line--	$\rho = 7.94$ cms.
308K line--	$\rho = 8.22$ cms.
316K line--	$\rho = 8.38$ cms.
468K line--	$\rho = 11.35$ cms.

Table IX gives the experimental values for $\log R_0/R$ and $\log R'_0/R'_0$ and the mean $\log R_0/R$ for the four plates examined. Antilogging yielded R'_0/R'_0 and the procedure described in the first paragraph of page 70 was carried out, yielding the factors w , ξ' , and $(e_0 + 1)$ in equation (8) page 68. With these values for w , ξ' , $(e_0 + 1)$, and ρ for each line, plus the known relative intensity I from Table VIII, equation (8) was rewritten

$$\eta = w\xi'(e_0 + 1)\frac{\rho}{I}$$

TABLE VII

ENERGIES AND MOMENTA OF Ir¹⁹²

CONVERSION LINES USED IN THIS WORK

E_{γ} (Kev)	E of K-Line (Kev)	Momentum H_{γ} (gauss-cm.)
205.4	127.0	1274
295.8	217.4	1732
308.4	230.0	1791
316.5	238.1	1827
467.8	389.4	2476

All values from Johns and Nablo (J54).

TABLE VIII

ABSOLUTE INTENSITIES OF Ir¹⁹²

CONVERSION LINES USED IN THIS WORK

E_{γ} (Kev)	Absolute Intensity of K-Line x 10 ³
205.4	4.15
295.8	16
308.4	15
316.5	33.8
467.8	9.1

The values for intensity here given represent the average of values given by Bashilov (B52), Baggerley (B55), and unpublished work of Kyles and Campbell, and Connor and Fairweather.

TABLE IX

MICROPHOTOMETER DATA

Line	log R_e/R					Mean	log R_b'/R'_0
	1	2	3	4	5		
<u>PLATE 1</u>							
468K	.135	.130	.13	.14	.140	.135	.335
316K	uc*	.51	.65	uc	uc	.58	.975
308K	.37	.30	.38	.40	.40	.37	1.025
296K	.37	.32	.37	.42	.38	.37	1.045
<u>PLATE 2</u>							
468K	.05	.04	.055	.055	.055	.051	.115
316K	.348	.34	.34	.34	.335	.340	.355
308K	.14	.14	.14	.135	.145	.140	.37
296K	.155	.145	.145	.14	.14	.145	.375
205K	.055	.055	.035	.04	.045	.046	.435
<u>PLATE 3</u>							
468K	.035	.025	.040	.05	.040	.038	.085
316K	.285	.295	.275	.275	.29	.284	.285
308K	.12	.13	.130	.13	.12	.126	.30
296K	.13	.145	.144	.120	.125	.133	.31
205K	.065	.042	.033	.045	.043	.045	.355
<u>PLATE 4</u>							
468K	.060	.050	.053	.055	.05	.054	.115
316K	.435	.42	.44	.45	.435	.436	.405
308K	.175	.18	.20	.185	.17	.182	.43
296K	.19	.19	.195	.20	.20	.195	.44
205K	.05	.08	.05	.06	.05	.058	.53

*indicates value uncertain.

and used to calculate η for each line on the chosen plate. Table X gives the consolidated data for each of the four plates. Note the line giving " η' ". This is a corrected value of η , when the finite thickness of the source is taken into account. The source used in this work was 250 micrograms per square centimeter in thickness. Investigations in Edinburgh using similar sputtered sources had revealed that the low energy portion of the Ir β -spectrum and its conversion lines were attenuated by source absorption effects. An empirical correction function was determined by Fairweather for a source 440 micrograms per square centimeter in thickness (thesis, I. L. Fairweather, University of Edinburgh 1958, page 62 et seq.). Pro-rating this function for 250 micrograms per square centimeter yields the following correction factors which when multiplied by η correct η for source thickness. This corrected value is shown in Table X as η' . The correction factors are shown here:

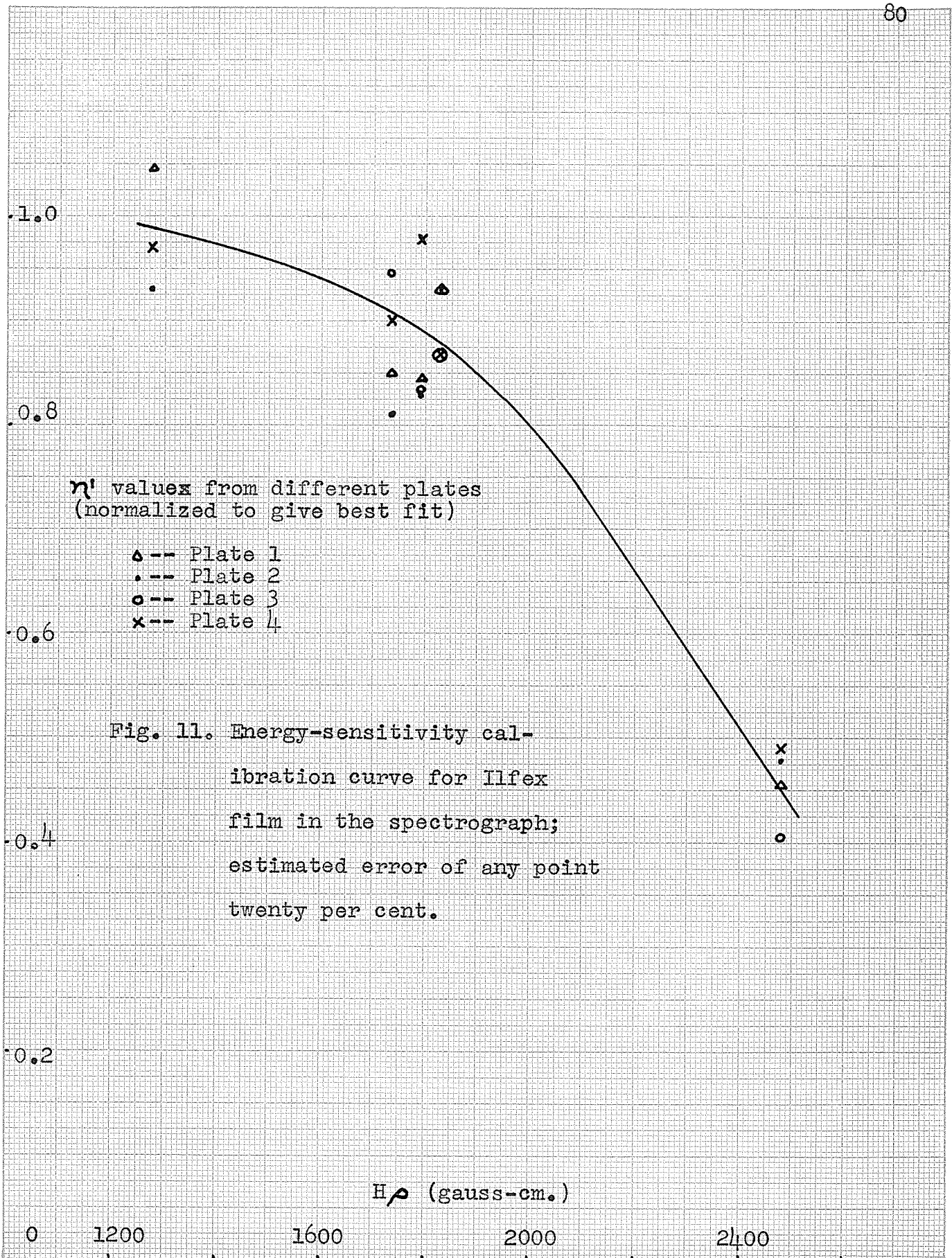
Line	205K	296K	308K	316K	468K
Factor	1.308	0.96	0.95	0.94	0.88

The graphs of η' against $H\beta$ values for the lines, as determined from the four plates of different exposures, should differ only by a constant factor from one another. The values of η' have therefore been normalized together to yield the best curve through all four sets of data, by plotting all four sets of data on semilog paper and moving each by a vertical distance to give best overlap. The resulting graph is Fig. 11. For most films η' has a maximum at about $H\beta = 1000$, corresponding to momenta of electrons with range equal to emulsion thickness.

TABLE X

CONSOLIDATED DATA

Line	$(\epsilon_0 + 1)$	ϵ'	$w \times 10^2$	ρ	$I \times 10^3$	η	η'
<u>PLATE 1</u>							
468K	1.377	0.138	10.0	11.35	9.1	0.237	0.210
316K	2.541	0.742	10.5	8.38	33.8	0.491	0.461
308K	2.667	0.424	7.5	8.22	15	0.465	0.442
296K	2.716	0.424	9.0	7.94	16	0.514	0.495
<u>PLATE 2</u>							
468K	1.116	0.050	8.0	11.35	9.1	0.557	0.49
316K	1.403	0.384	8.0	8.38	33.8	1.07	0.935
308K	1.424	0.143	7.0	8.22	15	0.781	0.823
296K	1.432	0.149	8.0	7.94	16	0.847	0.816
205K	1.514	0.045	7.5	5.84	4.15	0.721	0.944
<u>PLATE 3</u>							
468K	1.085	0.037	8.0	11.35	9.1	0.4	0.352
316K	1.314	0.312	7.5	8.38	33.8	0.766	0.72
308K	1.332	0.128	7.5	8.22	15	0.70	0.665
296K	1.346	0.136	7.5	7.94	16	0.681	0.655
205K	1.405	0.044	7.0	5.84	4.15	0.61	0.795
<u>PLATE 4</u>							
468K	1.116	0.053	11.0	11.35	9.1	0.815	0.715
316K	1.474	0.517	7.0	8.38	33.8	1.32	1.240
308K	1.509	0.196	9.0	8.22	15	1.455	1.380
296K	1.523	0.205	8.0	7.94	16	1.245	1.195
205K	1.660	0.057	8.0	5.84	4.15	1.065	1.39



CHAPTER V

CONCLUSIONS

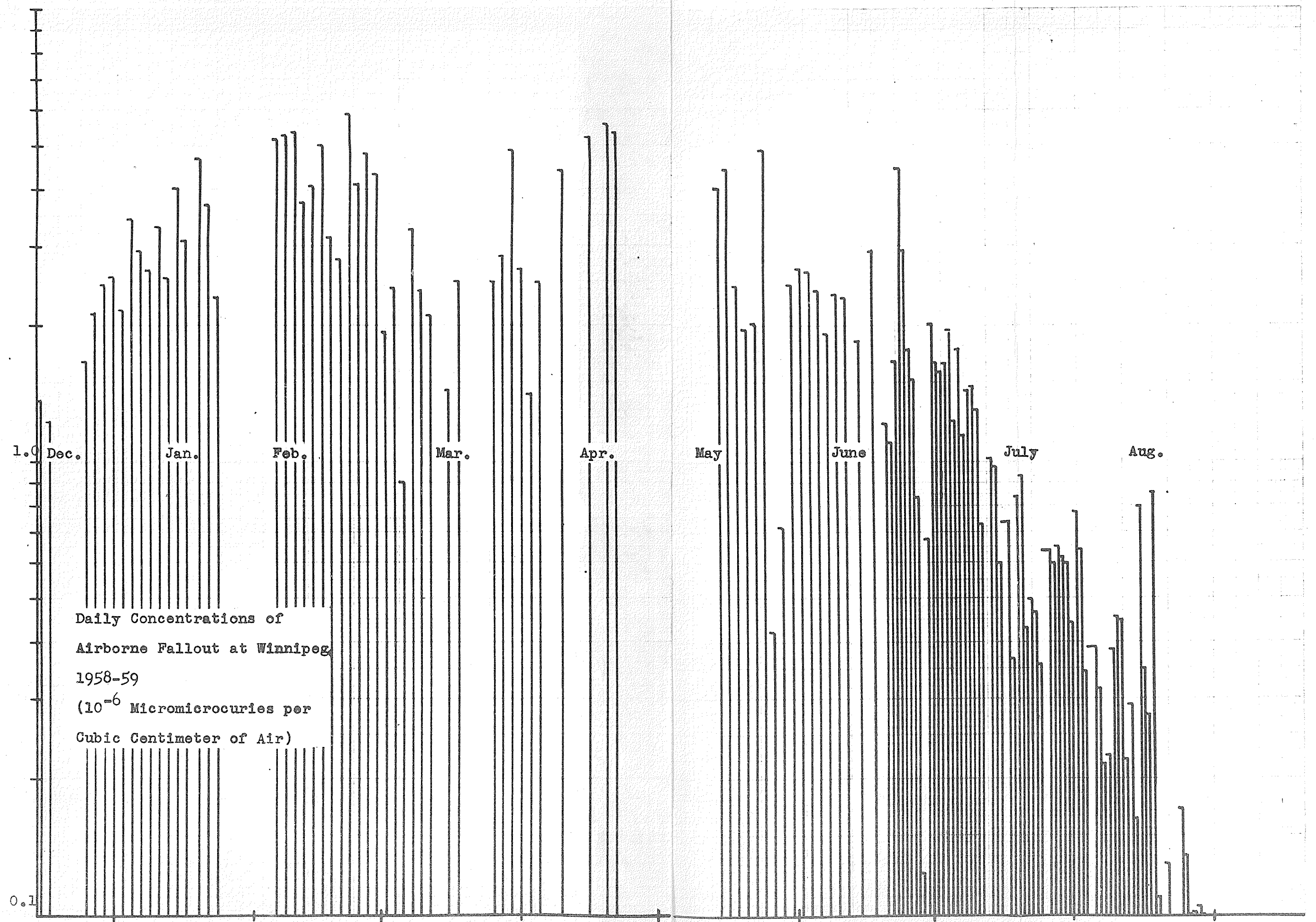
The calibration described in the previous chapter also yielded values for the resolution achieved by the instrument, in terms of true width at half-height of a given line as a percentage of the $H\alpha$ -value for the line. These figures for the resolution achieved with the settings used for the different plates are listed in Table VII. It must be emphasized at this point however that the present performance of the spectrograph is considerably below its potential capabilities. It will be recalled that the data used herein was taken using a source of relatively low quality as regards both mechanical form (straightness et cetera) and microphysical characteristics. The comparatively low specific activity of Ir^{192} necessitated a thick (0.25mg/cm^2) layer of source on the supporting wire, militating further against good energy resolution of the lines. A future intention is to employ a source of thorium active deposit plated on a straight support wire; this material has such a high specific activity it can be used successfully in a layer of effectively infinitesimal thickness, eliminating the line broadening due to the lowered energy of those particles which must traverse the thick source to reach its surface and escape.

As can be seen from the sample microphotometer trace at the back, the graininess of the film used in this work

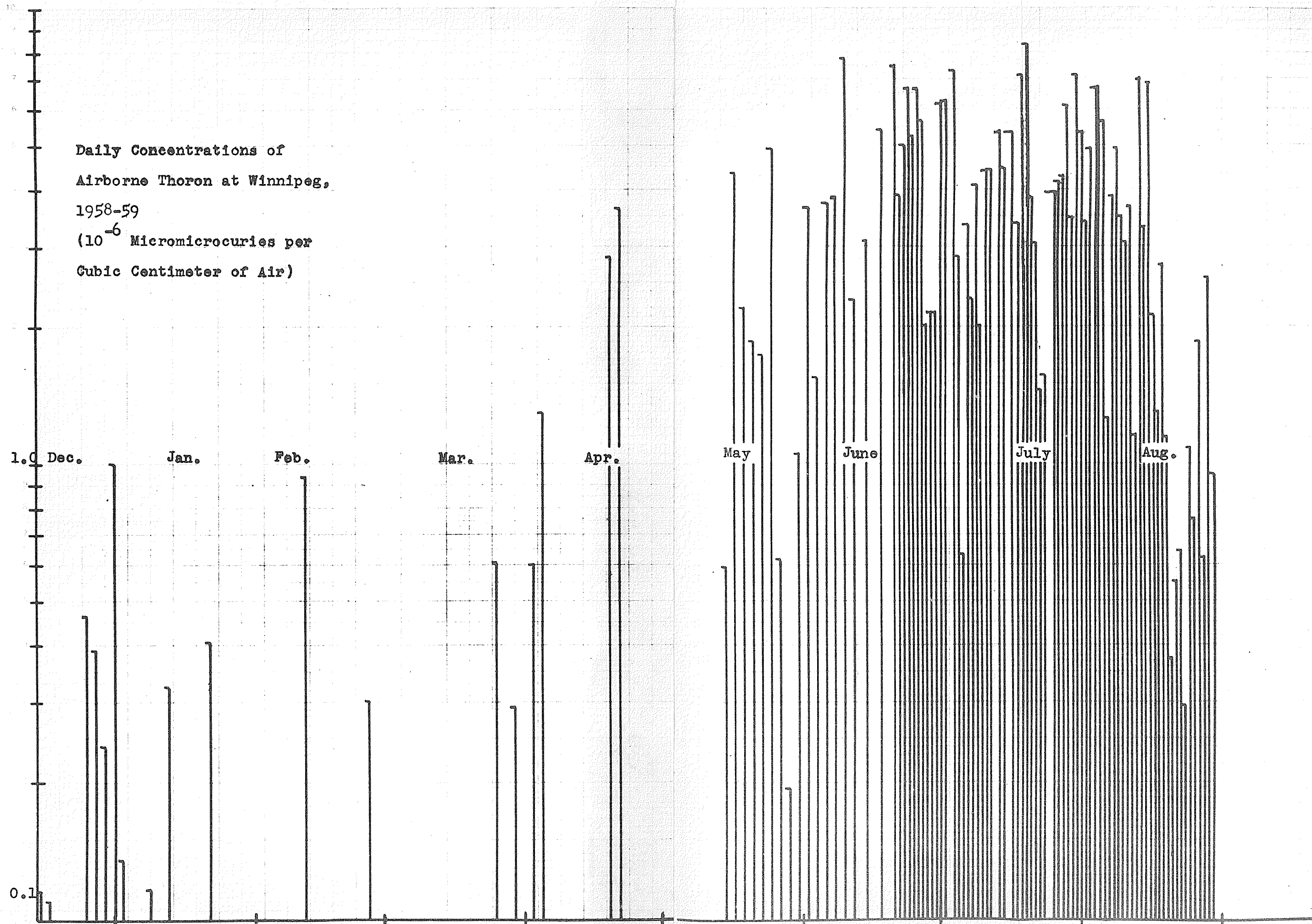
is so considerable as to obscure low-intensity lines and distort even those of relatively high intensity. X-ray film has been used almost exclusively as the recording agent in this type of spectrograph in previously reported work and it seemed not unreasonable to attempt to use Ilford Ilfex for it is a widely-used X-ray film. However an attempt must be made to find an emulsion sufficiently fine-grained to minimize these difficulties. The graininess of the present film would have been detected earlier had a microphotometer been available locally, and the attempt would have been made to obtain fine-grain film, although this is not the customary grade for X-ray emulsions.

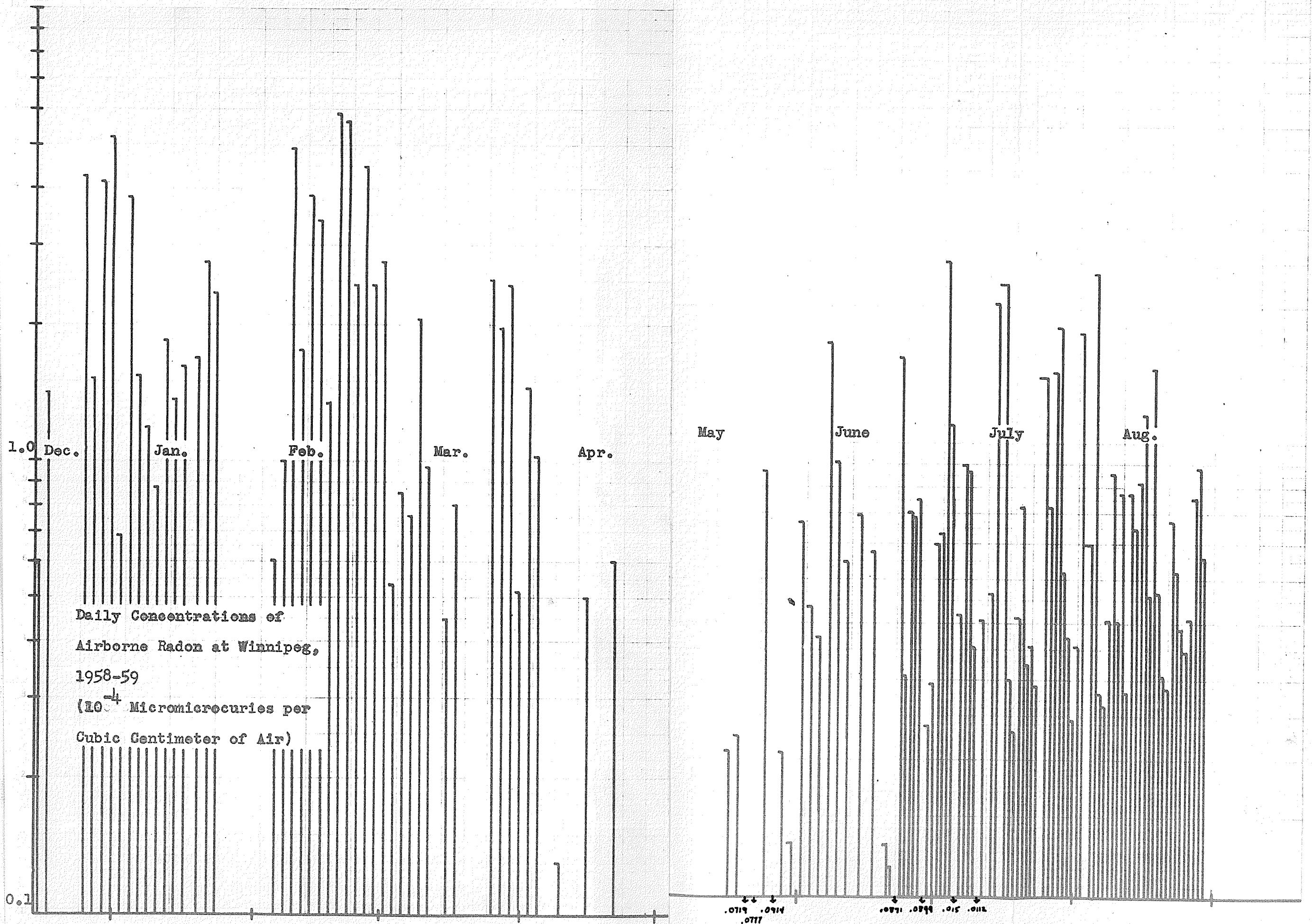
BIBLIOGRAPHY

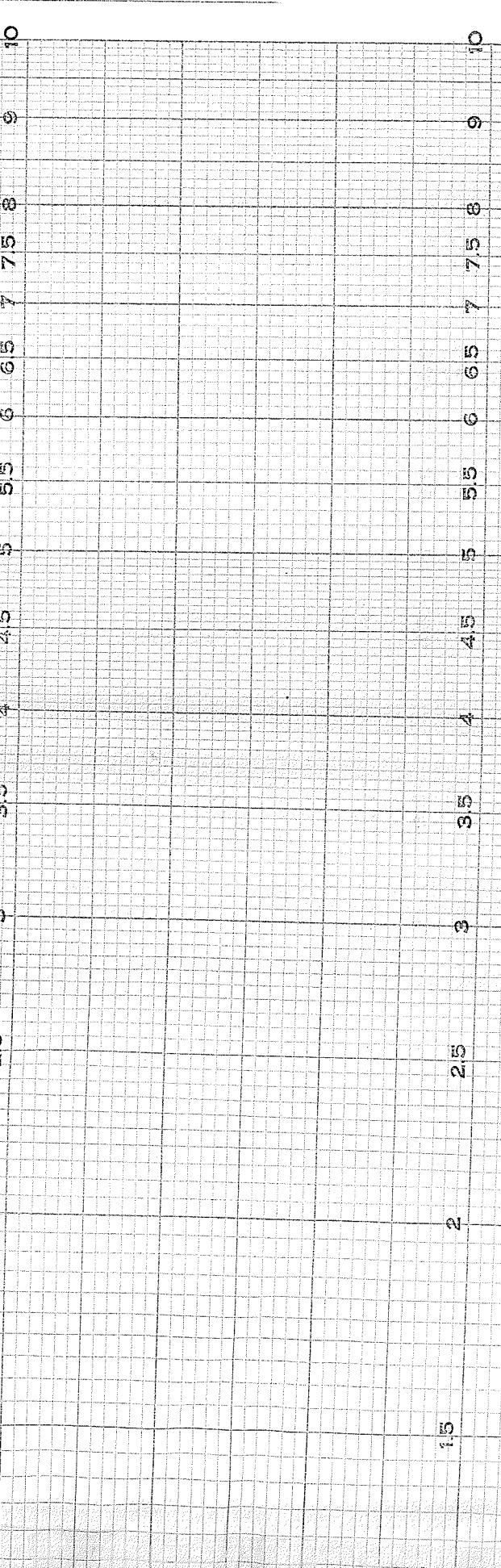
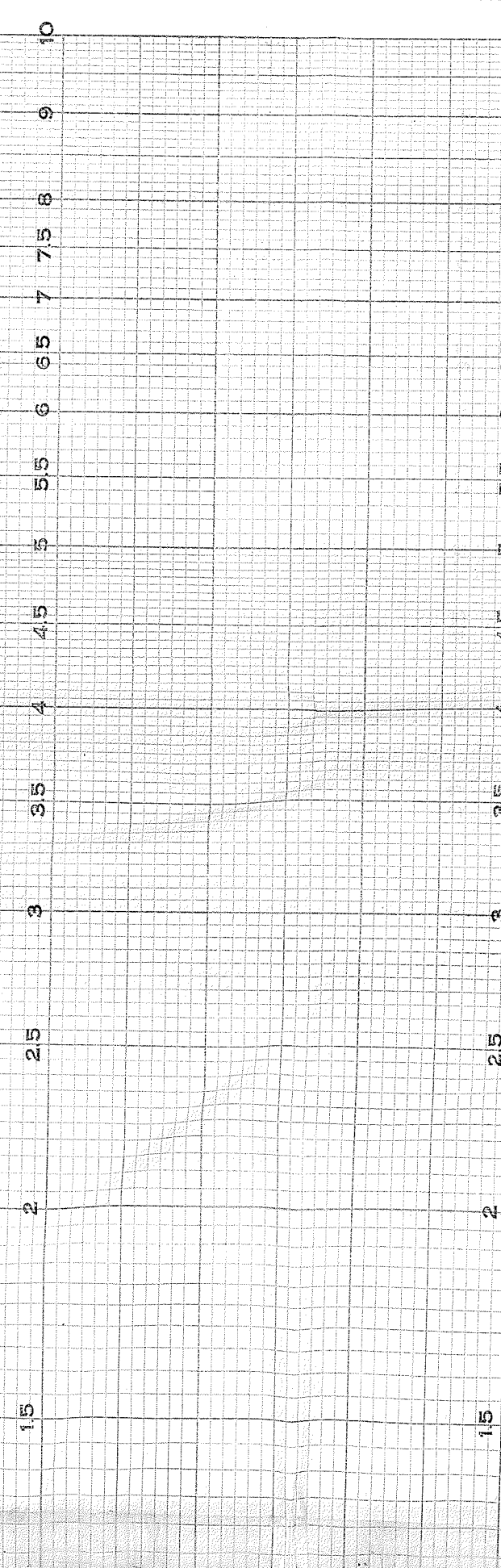
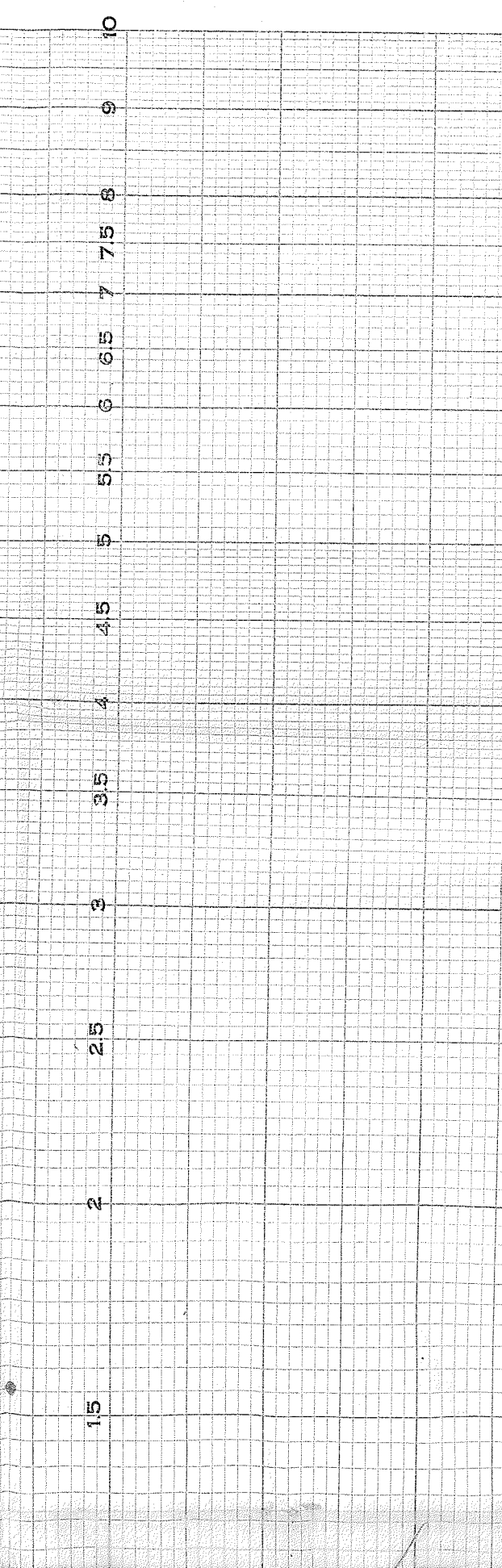
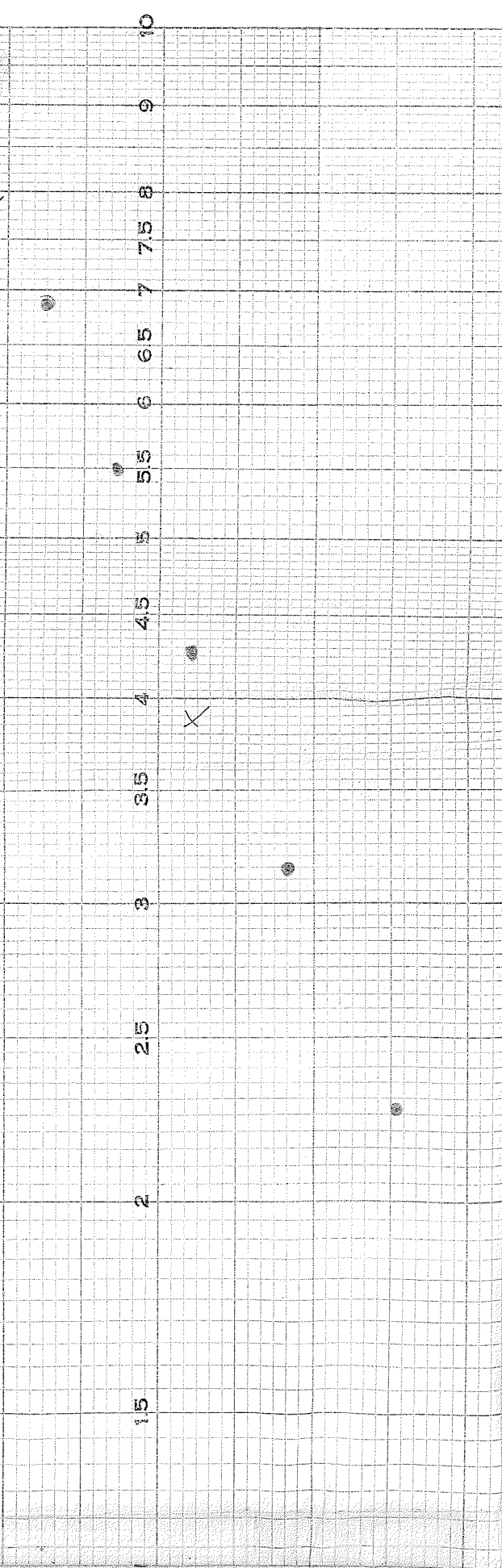
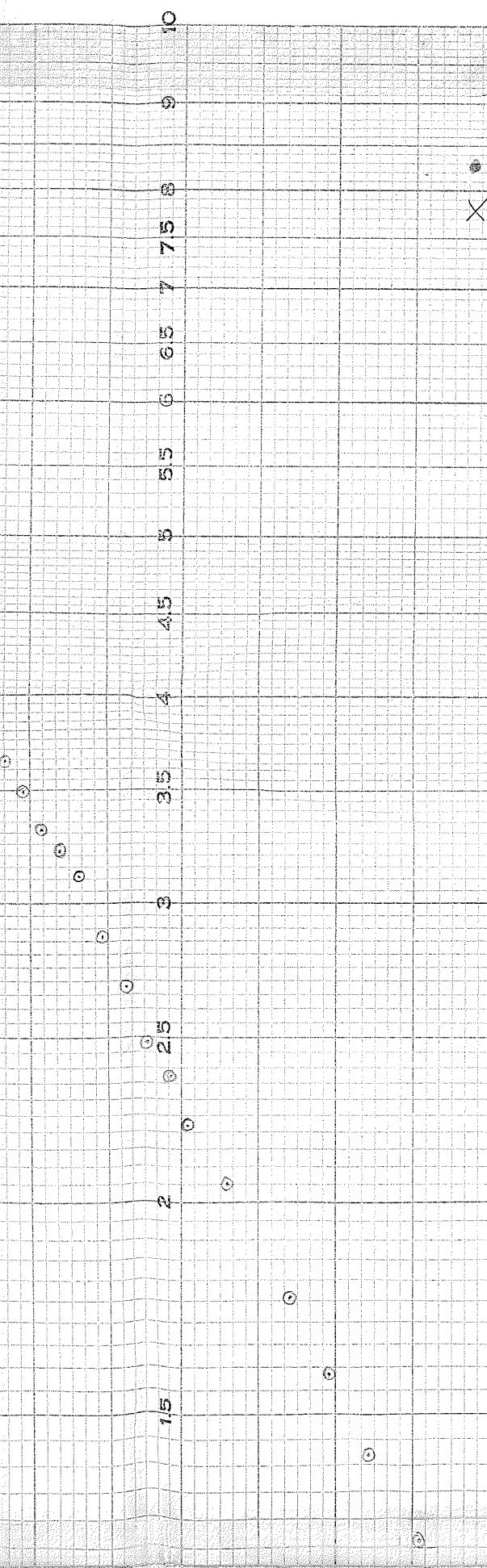
- V11: von Baeyer, Hahn, and Meitner, Phys. Zeit. 12, 273,
378 (1911)
- D12: Danysz, J., Le Radium 9, 1 (1912)
- V12: von Baeyer, Hahn, and Meitner, Phys. Zeit. 13, 264 (1912)
- D13: Danysz, J., Le Radium 10, 4 (1913)
- R13: Rutherford, E. and H. Robinson, Phil. Mag. 26, 717 (1913)
- S23: Silberstein, L. Phil. Mag. 45, 1062 (1923)
- W27: Wooster, W. and C. D. Ellis, Proc. Roy. Soc. A114, 266,
729 (1927)
- L37: Li, K. T. Proc. Cambridge Phil. Soc. 33, 164 (1937)
- F39: Flammersfeld, Z. Physik 114, 227 (1939)
- L40: Lawson, J. L. and A. W. Tyler, Rev. Sci. Inst. 11, 6
(1940)
- B52: Bashilov, A. A. et al. Izvest. Akad. Nauk S. S. R.
Ser. Fiz. 16, 264 (1952)
- K52: Kyles, J. and C. G. Campbell, Proc. Phys. Soc. 66,
911 (1952)
- W52: Wilkening, M. H., Rev. Sci. Inst. 23, 13 (1952)
- B53: Bainbridge, K. T. et al., Phys. Rev. 90, 430 (1953)
- J54: Johns, M. W. and S. Nablo, Phys. Rev. 96, 1599 (1954)
- S54: Slatis, H. Arkiv f. Fysik 8, 441 (1954)
- B55: Baggerley, L. L. et al. Phys. Rev. 100, 1364 (1955)
- S55: Beta- and Gamma-Ray Spectroscopy, edited by K. Siegbahn, North-Holland Publishing Company, Amsterdam
(1955)
- R58: Internal Conversion Coefficients, by M. E. Rose, North-Holland Publishing Company, Amsterdam (1958)



Daily Concentrations of
Airborne Thoron at Winnipeg,
1958-59
(10^{-6} Micromicrocuries per
Cubic Centimeter of Air)







15
2
2.5
3
3.5
4
4.5
5
5.5
6
6.5
7
7.5
8
9
10

15
2
2.5
3
3.5
4
4.5
5
5.5
6
6.5
7
7.5
8
9
10

15
2
2.5
3
3.5
4
4.5
5
5.5
6
6.5
7
7.5
8
9
10

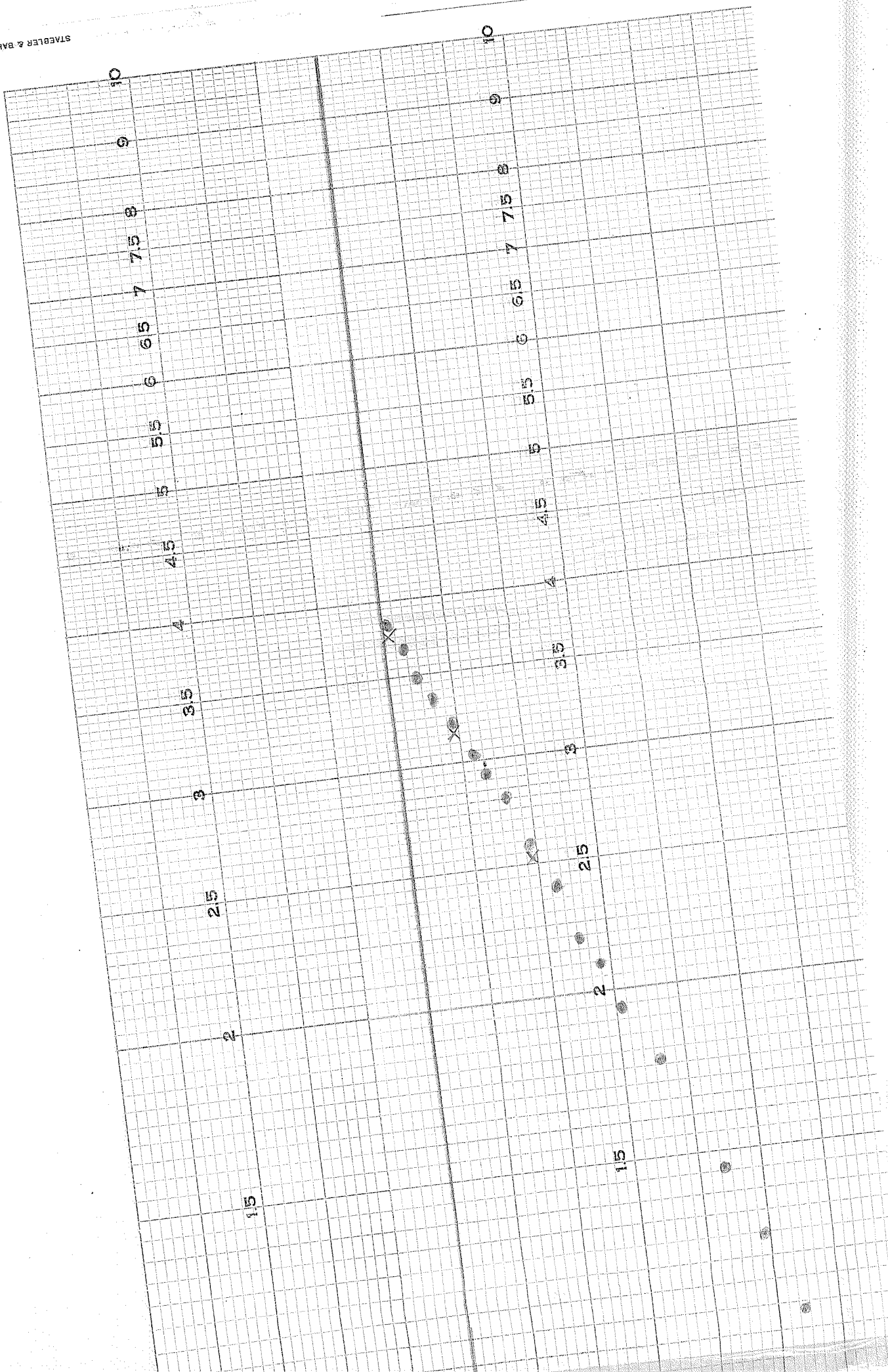
15
2
2.5
3
3.5
4
4.5
5
5.5
6
6.5
7
7.5
8
9
10

15
2
2.5
3
3.5
4
4.5
5
5.5
6
6.5
7
7.5
8
9
10

15
2
2.5
3
3.5
4
4.5
5
5.5
6
6.5
7
7.5
8
9
10

STAEBLER & BAK

CHART NO. RG B-52



15
2
25
3
35
4
45
5
55
6
65
7
75
8
9
10

15
2
25
3
35
4
45
5
55
6
65
7
75
8
9
10

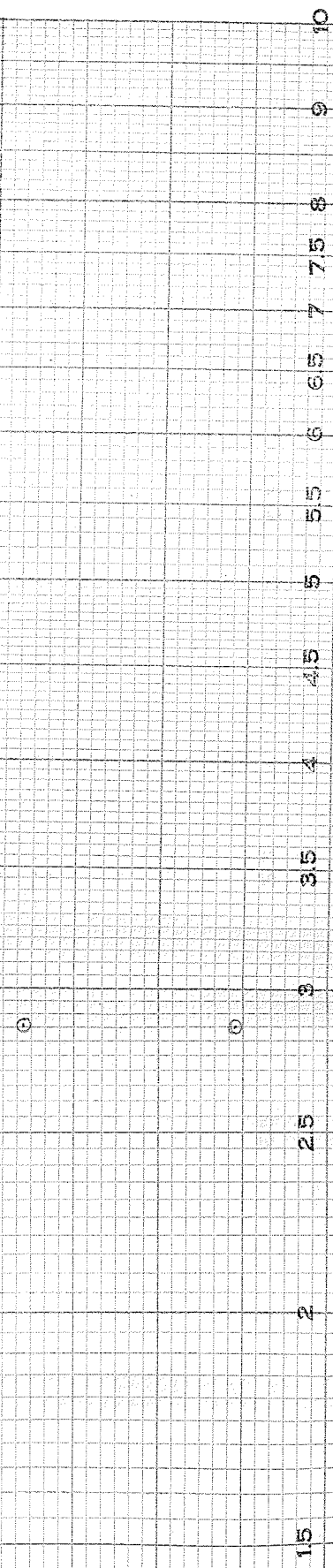
15
2
25
3
35
4
45
5
55
6
65
7
75
8
9
10

15
2
25
3
35
4
45
5
55
6
65
7
75
8
9
10

15
2
25
3
35
4
45
5
55
6
65
7
75
8
9
10

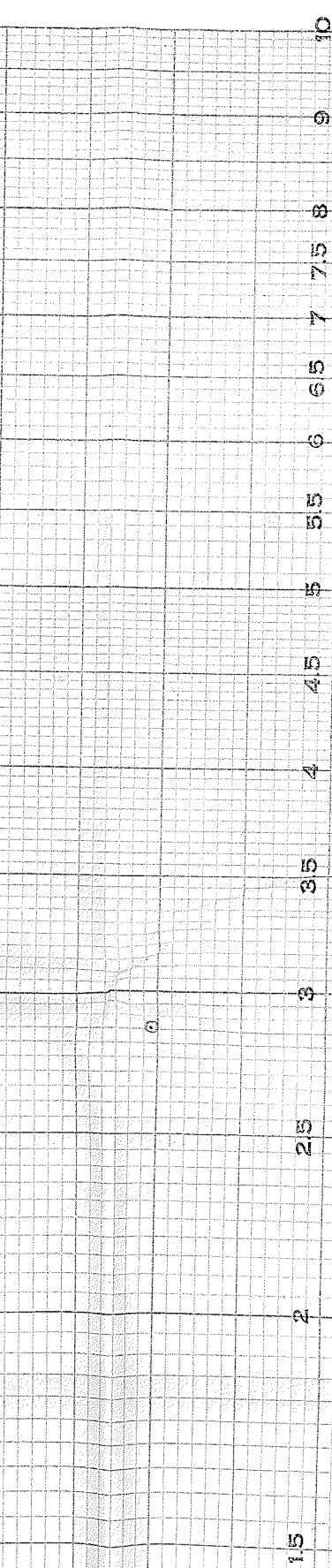
15
2
25
3
35
4
45
5
55
6
65
7
75
8
9
10

15 2 25 3 3.5 4 4.5 5 5.5 6 6.5 7 7.5 8 9 10

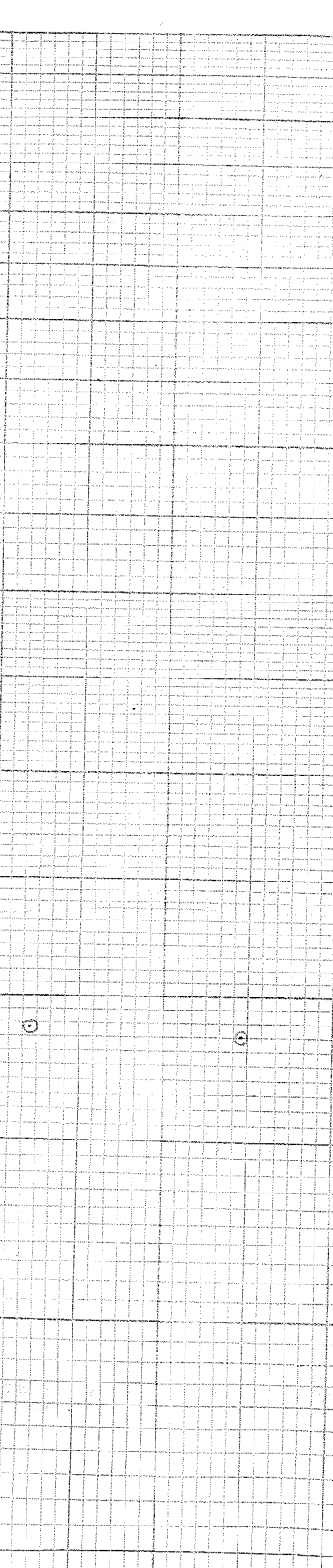


STAEBLER & BAKER LTD. CHART NO. RG 8-52

15 2 25 3 3.5 4 4.5 5 5.5 6 6.5 7 7.5 8 9 10

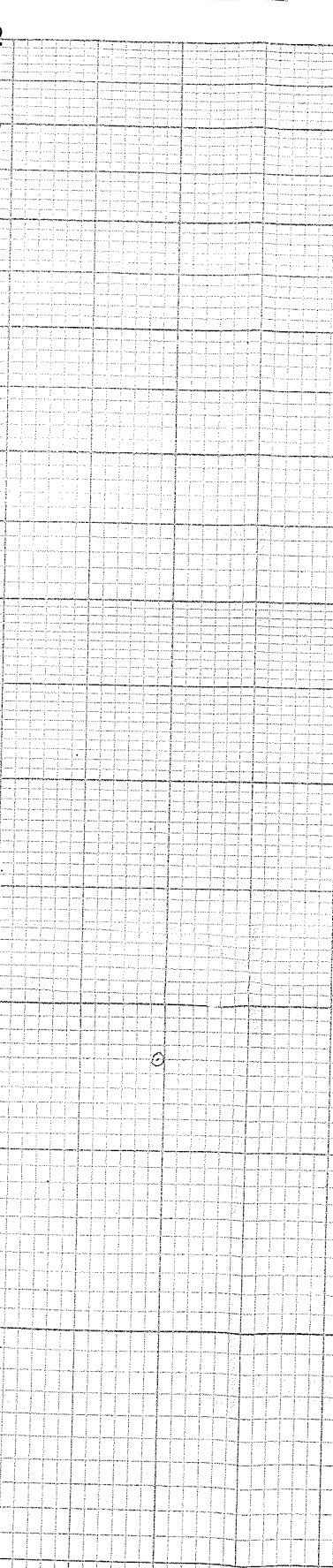


15 2 25 3 3.5 4 4.5 5 5.5 6 6.5 7 7.5 8 9 10



STAEBLER & BAKER LTD. CHART NO. RG 8-52

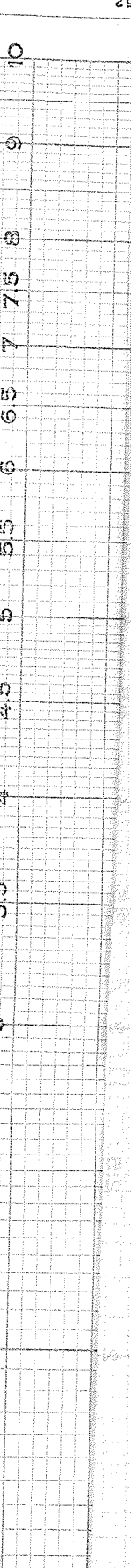
15 2 25 3 3.5 4 4.5 5 5.5 6 6.5 7 7.5 8 9 10

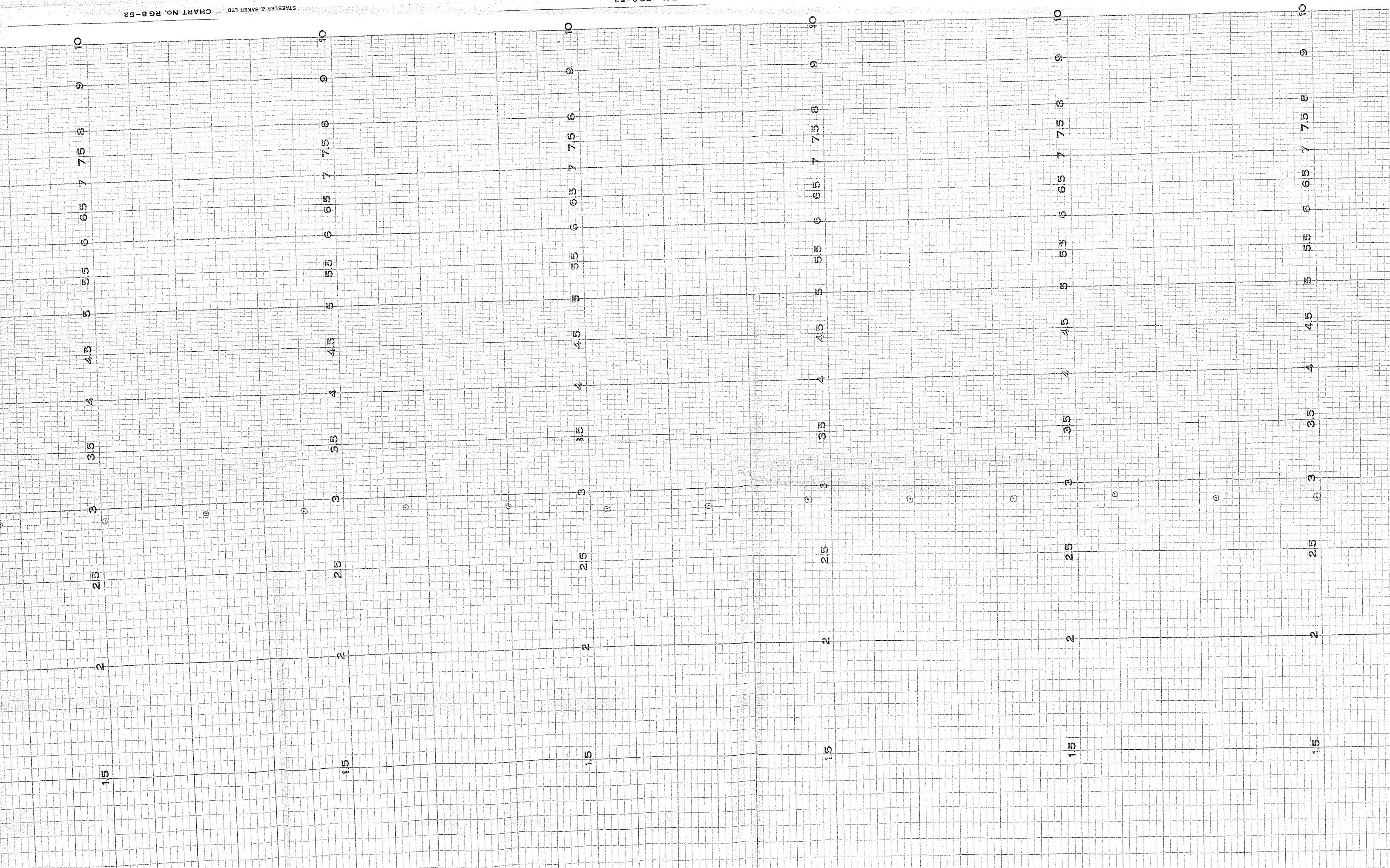


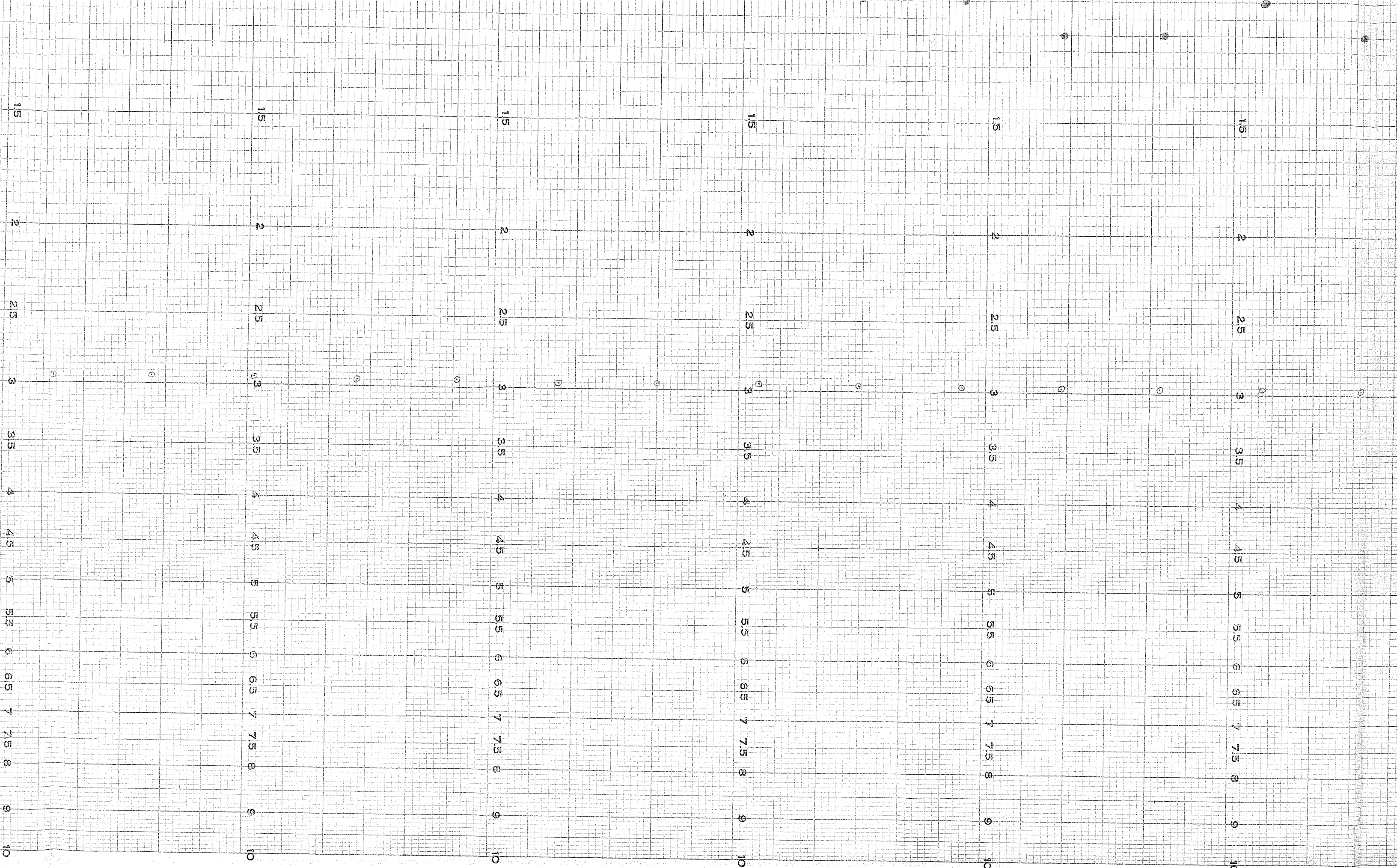
15 2 25 3 3.5 4 4.5 5 5.5 6 6.5 7 7.5 8 9 10



15 2 25 3 3.5 4 4.5 5 5.5 6 6.5 7 7.5 8 9 10







1.5
2
2.5
3
3.5
4
4.5
5
5.5
6
6.5
7
7.5
8
9
10

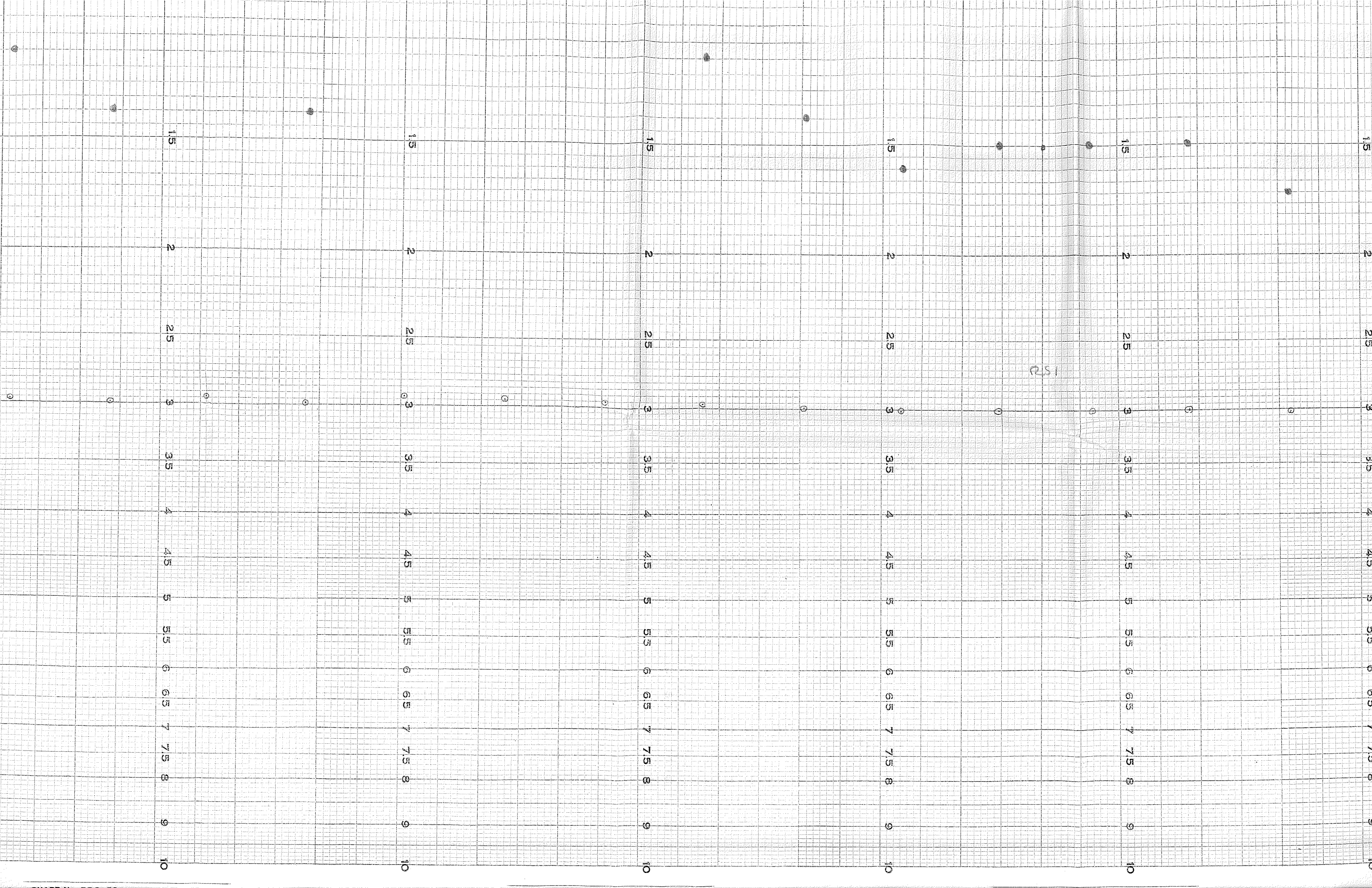
1.5
2
2.5
3
3.5
4
4.5
5
5.5
6
6.5
7
7.5
8
9
10

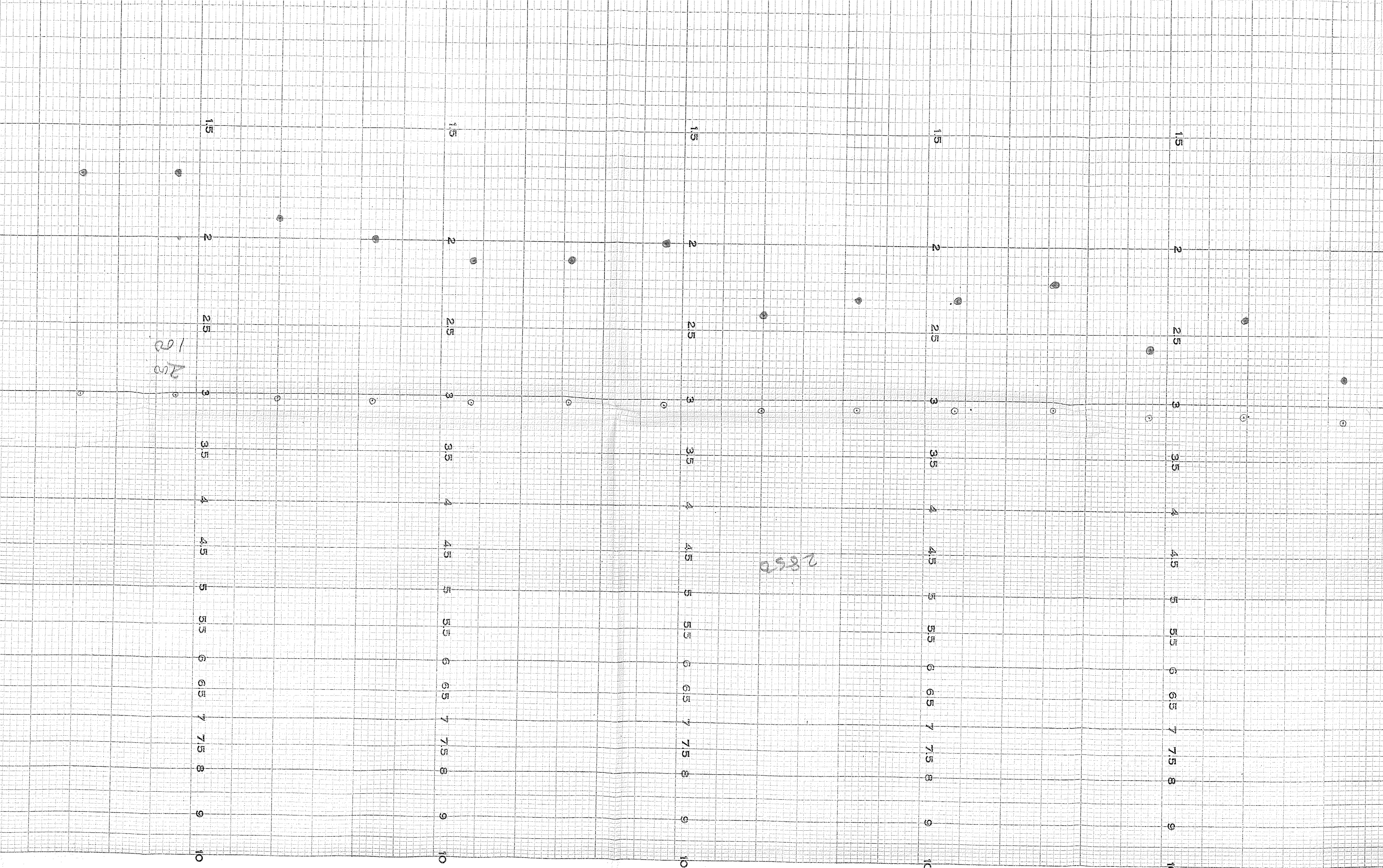
1.5
2
2.5
3
3.5
4
4.5
5
5.5
6
6.5
7
7.5
8
9
10

1.5
2
2.5
3
3.5
4
4.5
5
5.5
6
6.5
7
7.5
8
9
10

1.5
2
2.5
3
3.5
4
4.5
5
5.5
6
6.5
7
7.5
8
9
10

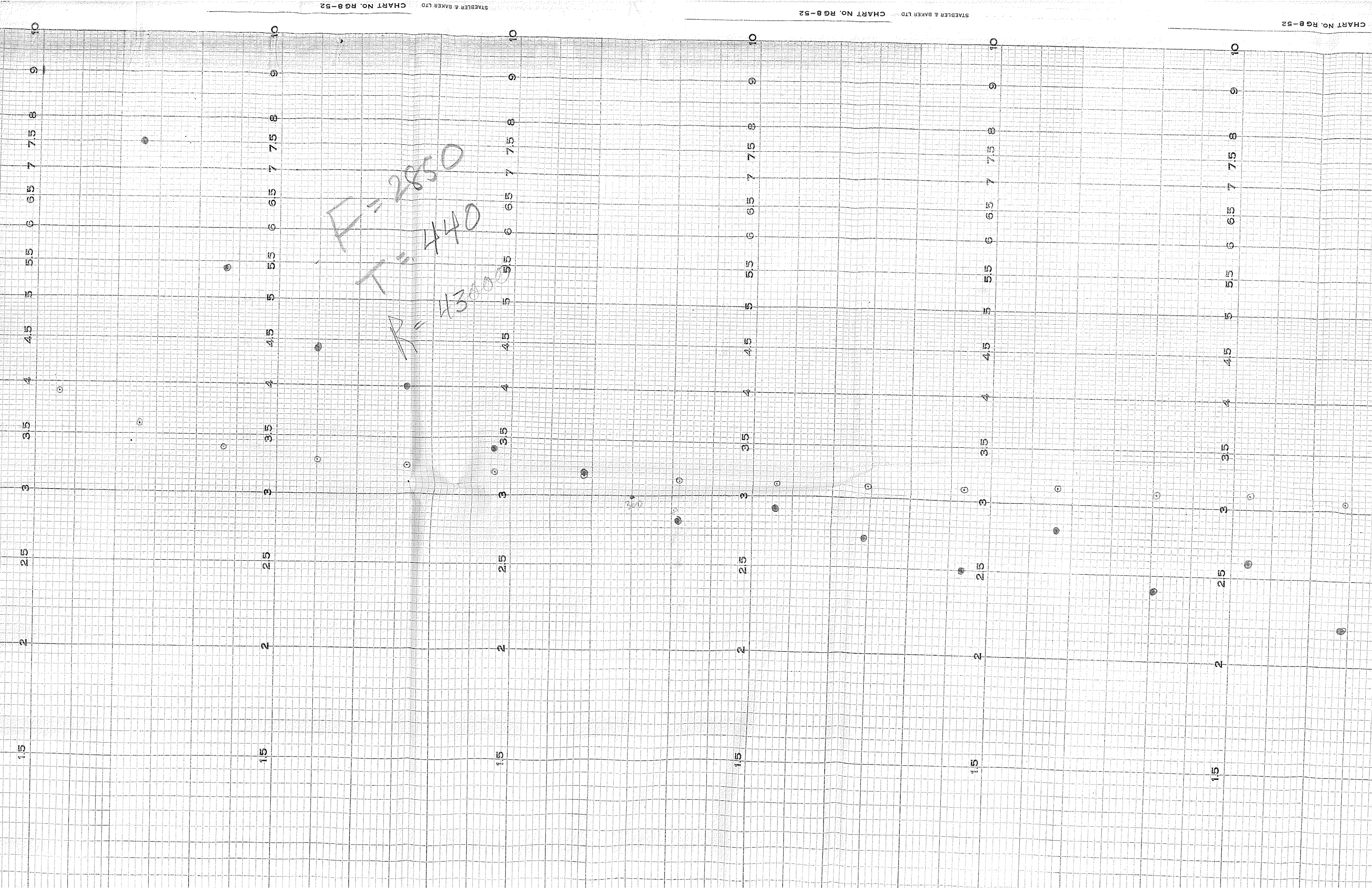
1.5
2
2.5
3
3.5
4
4.5
5
5.5
6
6.5
7
7.5
8
9
10





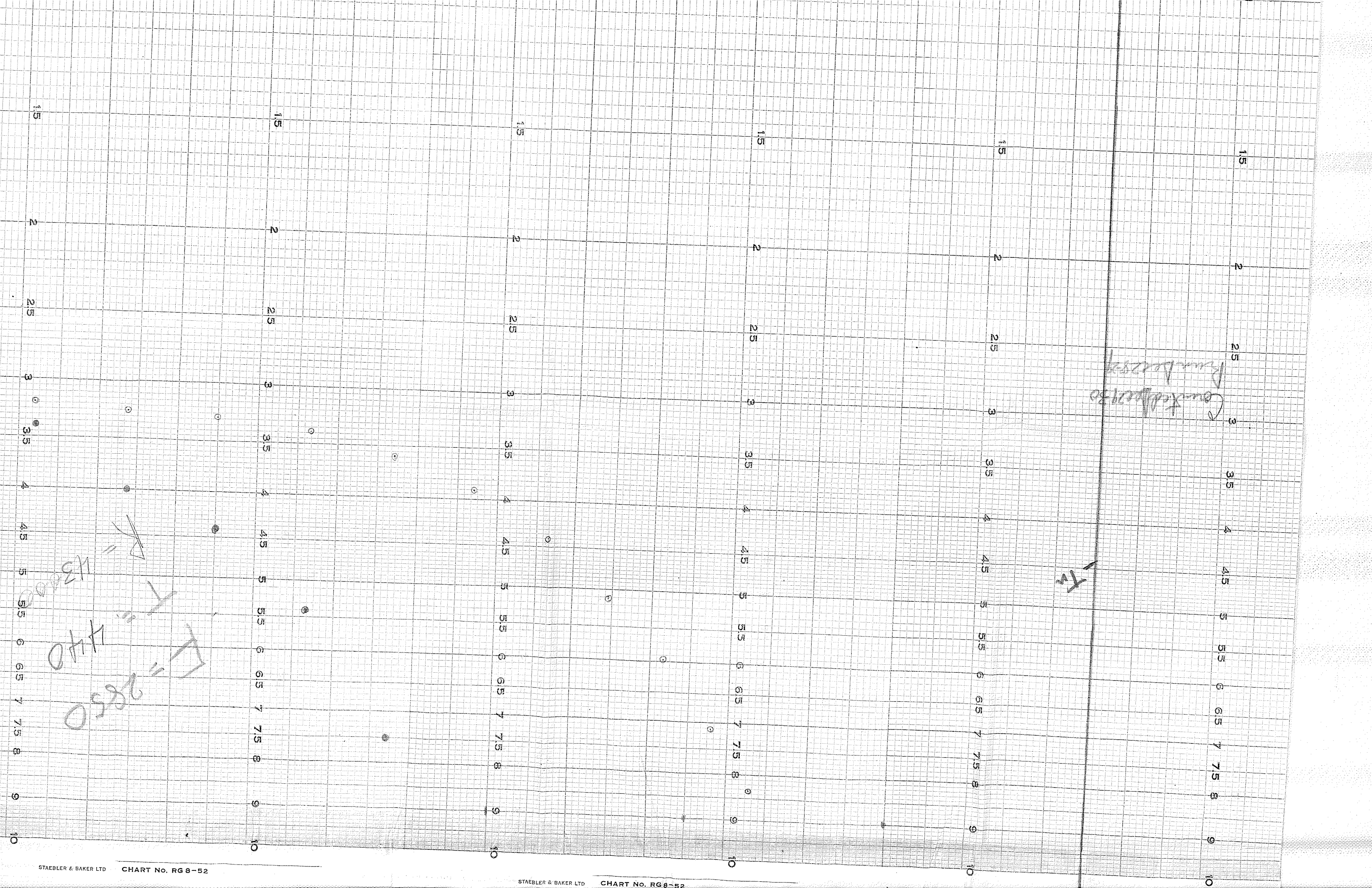
100
200

2850



$\Gamma = 2850$
 $\tau = 440$
 $R = 4300$

28



15

2

2.5

3

3.5

4

4.5

5

5.5

6

6.5

7

7.5

8

9

10

Countdown 130
Run 12200

13

15

2

2.5

3

3.5

4

4.5

5

5.5

6

6.5

7

7.5

8

9

10

15

2

2.5

3

3.5

4

4.5

5

5.5

6

6.5

7

7.5

8

9

10

15

2

2.5

3

3.5

4

4.5

5

5.5

6

6.5

7

7.5

8

9

10

15

2

2.5

3

3.5

4

4.5

5

5.5

6

6.5

7

7.5

8

9

10

15

2

2.5

3

3.5

4

4.5

5

5.5

6

6.5

7

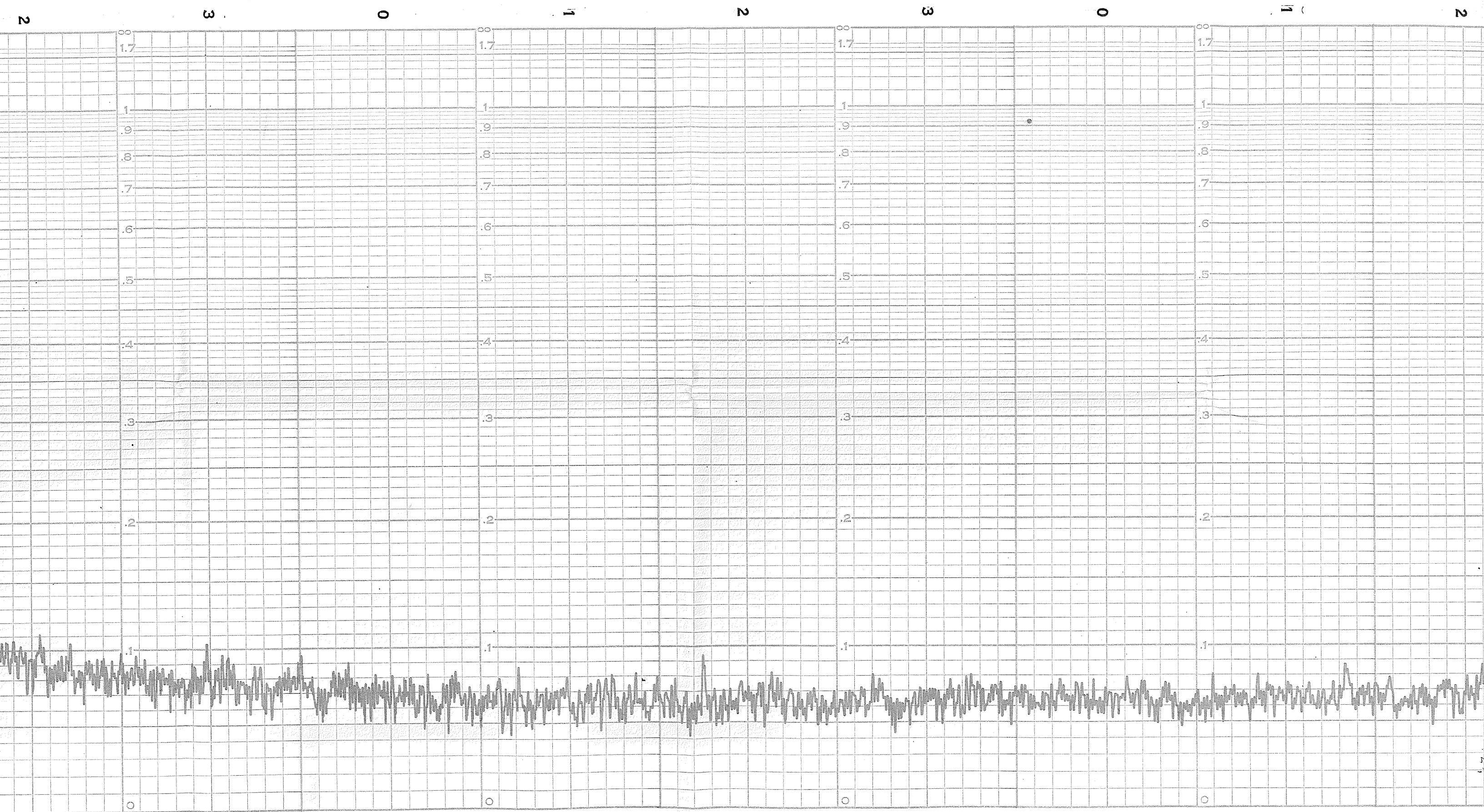
7.5

8

9

10

13300
140
2850



0

1

2

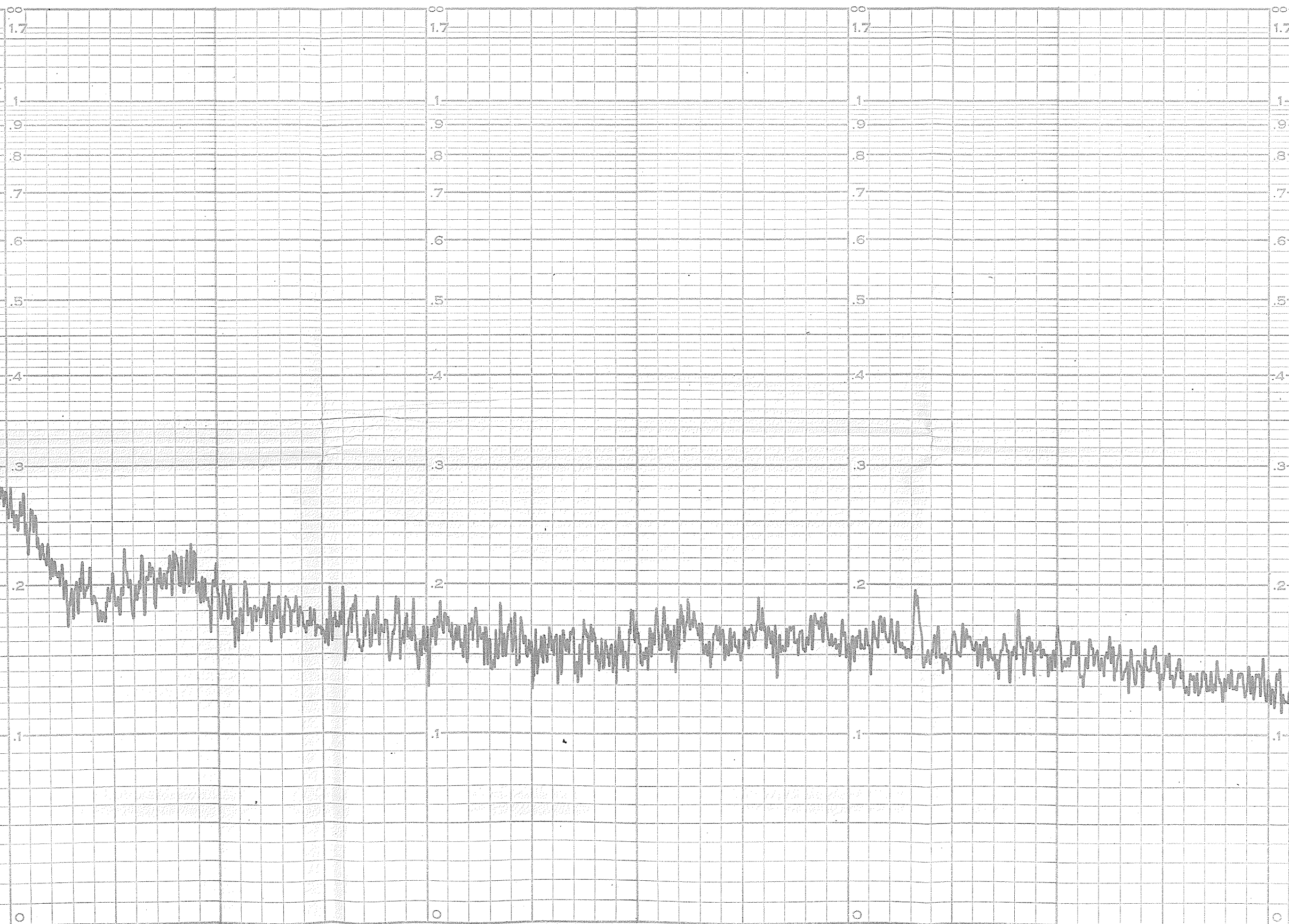
3

0

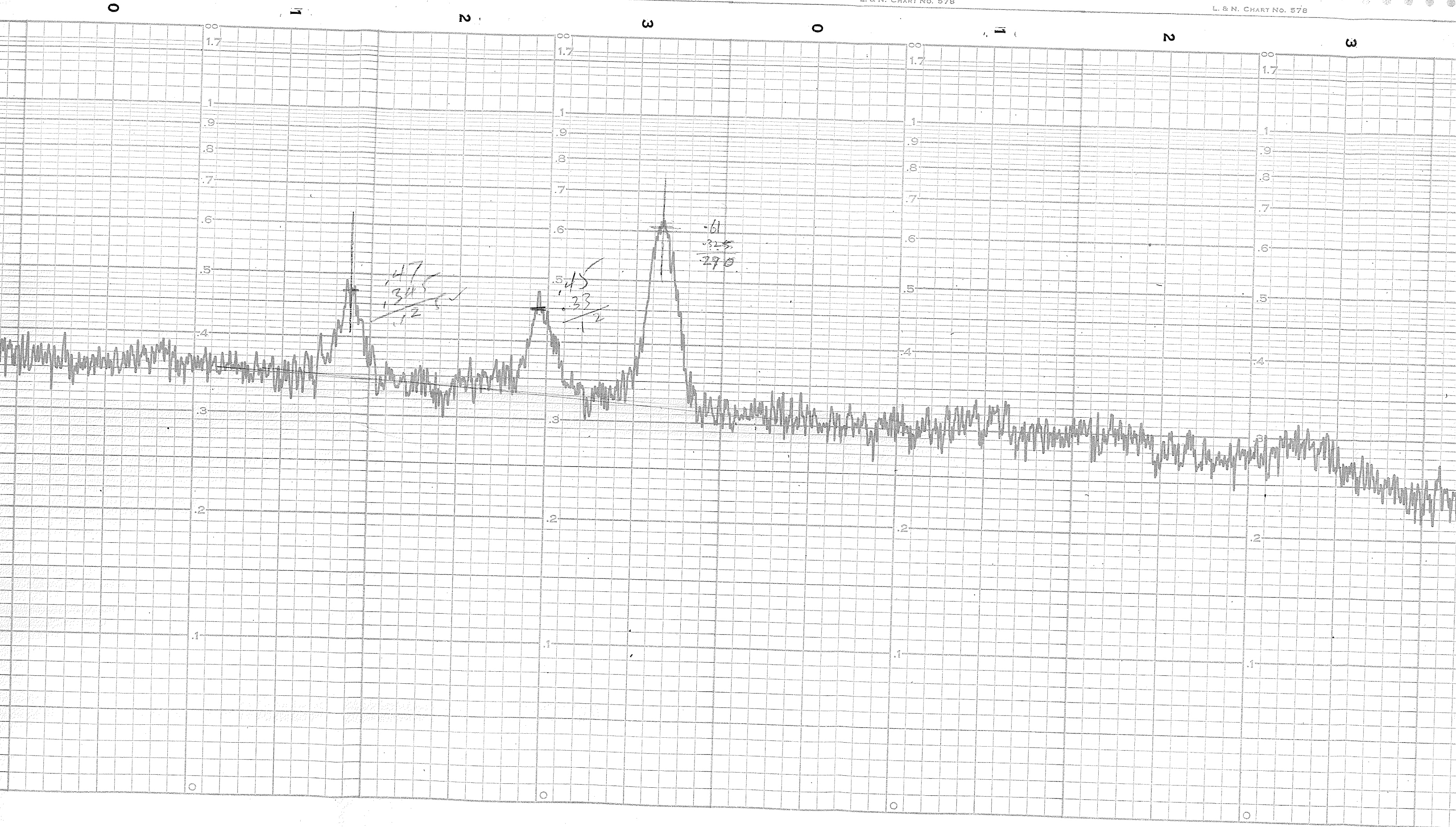
1

2

3



16
12
1.04



3

0

1

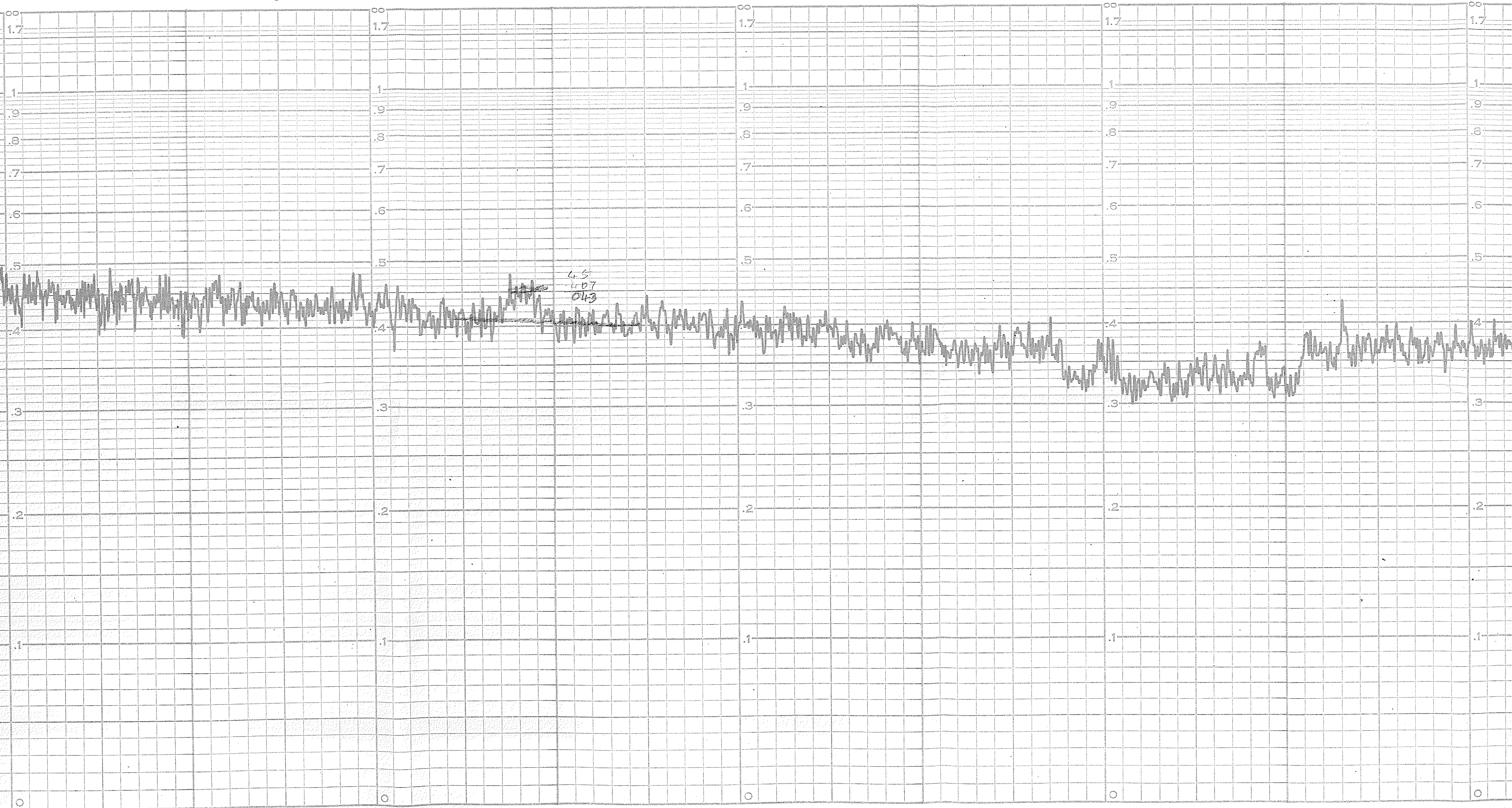
2

3

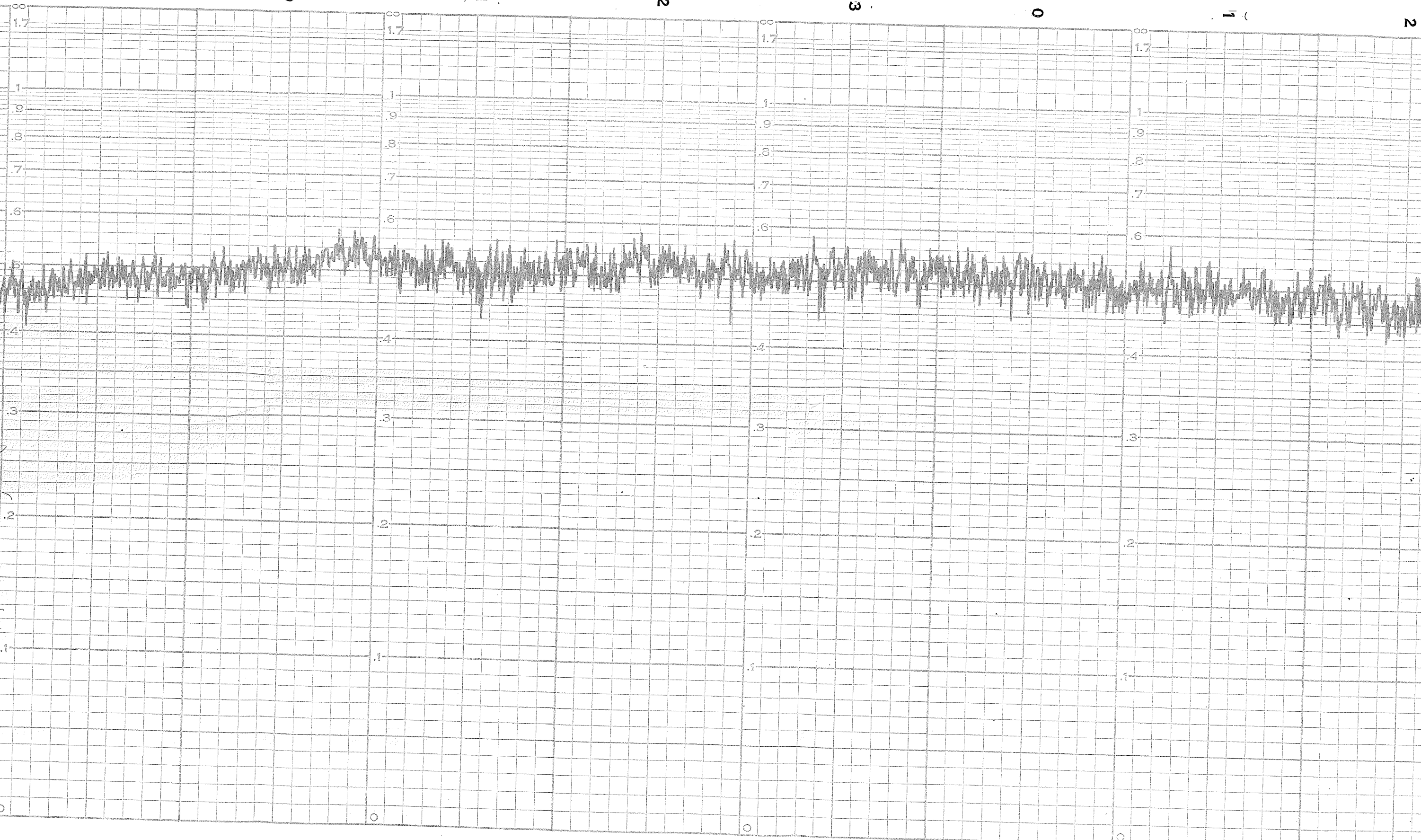
0

1

2



3 0 1 2 3 0 1 2



Handwritten notes:
 1. 1.7
 1.6
 1.5
 1.4
 1.3
 1.2
 1.1
 1.0
 0.9
 0.8
 0.7
 0.6
 0.5
 0.4
 0.3
 0.2
 0.1
 0